INSTITUTO SUPERIOR DE ENGENHARIA DE LISBOA

Área Departamental de Engenharia de Electrónica e Telecomunicações e de Computadores

Millimeter Waves propagation challenges on 5G

Mariana Teresa Amaro Daniel Ferreira

Licenciada

Dissertação para obtenção do Grau de Mestre
em Engenharia Eletrónica e de Telecomunicações

Orientador : Prof. Doutor Pedro Renato Tavares Pinho

Júri:

Presidente: Prof. Doutor António Serrador

Vogais: Prof. Doutor António Luís Topa
Prof. Doutor Pedro Renato Tavares Pinho

February, 2021

INSTITUTO SUPERIOR DE ENGENHARIA DE LISBOA

Área Departamental de Engenharia de Electrónica e Telecomunicações e de Computadores

Millimeter Waves propagation challenges on 5G

Mariana Teresa Amaro Daniel Ferreira

Licenciada

Dissertação para obtenção do Grau de Mestre
em Engenharia Eletrónica e de Telecomunicações

Orientador : Prof. Doutor Pedro Renato Tavares Pinho

Júri:

Presidente: Prof. Doutor António Serrador

Vogais: Prof. Doutor António Luís Topa
Prof. Doutor Pedro Renato Tavares Pinho

February, 2021

Acknowledgments

First I would like to thank my thesis supervisor, Professor Pedro Renato Tavares Pinho for all his guidance, suggestions and teachings throughout the writing of this dissertation. My sincere thank you.

I would also like to thank Instituto de Telecomunicações (IT) for the support and conditions provided during the writing of this work.

I also want to leave my sincere thank to my family, specially my parents, Anabela and João for their unconditional support. Finally, I would like to thank my boyfriend, Sérgio, for the encouragement throughout all the years of study and for supporting me and listening to me when fatigue seemed to take the best of me when writing this dissertation.

Abstract

The 5G is known for being a technology that aims to agregate concepts and technologies to leverage the capacity and coverage of a mobile network. One of the most revolutionary aspects of 5G is the use of higher frequencies to overcome the few available bandwidth on the sub-6 GHz band. Hence, 5G will be making use of frequencies above the 6 GHz, namely the band between 30 and 300 GHz, the millimeter waves, which allow to allocate larger bandwidths.

This dissertation presents the main challenges that millimeter waves induce on propagation. The diverse loss mechanisms are analyzed and the propagation models, that enables the quantification of those losses, are also studied. It is also presented link budgets for different environments, which aim to evaluate the variation of throughput regarding the radio channel characteristics. Finally, the link budgets results and the verified changes on the capacity contribute to calculate the elements number of an antenna array necessary to ensure that capacity.

Concluding that to achieve a 2 Gbps capacity, using a 28 GHz frequency and 0.5 GHz of bandwidth, a 32 element array is needed. In order to achieve a capacity of 10 Gbps the array would need to be compound of 1.5 million elements, which is no a viable solution. One way to overcome this constraint is to extend the bandwidth to 1.5 GHz simplifying the antenna into a 415 element array.

Keywords: 5G, millimeter waves, frequency, bandwidth, beamforming, attenuation.

Resumo

O 5G é conhecido por ser uma tecnologia que pretende agregar conceitos e tecnologias para alavancar a capacidade e cobertura de uma rede movel. Um dos aspectos mais revolucionários do 5G é a utilização de frequências mais elevadas, para colmatar a pouca largura de banda disponivel na banda sub-6 GHz. O 5G fará assim uso de frequências acima dos 6 GHz,nomeadamente entre os 30 e os 300 GHz (ondas milimétricas) que permitem alocar larguras de banda superiores.

Esta dissertação apresenta os principais desafios que a banda de ondas milimétricas introduz na propagação. São estudados os diversos mecanismos que provocam atenuação e os modelos de propagação existentes para a quantificação dessas perdas. São apresentados os *link budgets* para diferentes ambientes que visam avaliar de que forma é que o débito binário é modificado em função das caracteristicas do canal rádio. Por fim, com base no dimensionamento dos *link budgets* e na variação do débito binário, foi possivel cálcular o número de elementos de um agregado de antenas necessário para assegurar esse débito binário.

Concluiu-se que para assegurar um débito binário de 2 Gbps, utilizando uma frequência de 28 GHz e uma largura de banda de 0.5 GHz, é necessário um agregado com cerca de 32 elementos. Para atingir 10 Gbps o agregado de antenas teria de ser constituido por cerca de 1.5 milhões de elementos, não sendo uma solução viável. Uma das formas de viabilizar a solução será utilizar 1.5 GHz de largura de banda, traduzindo-se num agregado com cerca de 415 elementos, bem mais realista.

Palavras-chave: 5G, ondas milimétricas, frequência, largura de banda, *beamforming*, atenuação.

Contents

List of Figures

List of Tables

Acronyms

2G	Second Generation. 1
3G	Third Generation. 1
3GPP	3rd Generation Partnership Project. 2
4G	Fourth Generation. 1
5G	Fifth Generation. 2
5G NR	5G New Radio. 12
ADC	Analogue-to-Digital-Conversion. 16
AF	Array Factor. 63
AR	Augmented Reality. 2
BS	Base Station. 16
C-RAN	Cloud Radio Access Network. 10
CSI	Channel State information. 16
DAC	Digital-to-Analogue-Conversion. 16
DAS	Distributed Antenna System. 14
EIRP	Effective Isotropic Radiated Power. 60, 70
eMBB	Enhanced mobile broadband. 2
FFT	Fast Fourier Transform. 9
FWA	Fixed wireless access. 2
HetNet	Heterogeneous Network. 4
IMT-2020	International Mobile Telecommunications - 2020. 2
InH	Indoor Hotspot. 51
IoT	Internet of Things. 2
ITU-R	International Telecommunication Union - Recommendation Sector. 2
LoS	Line of Sight. 14

LTE Long Term Evolution. 1
MBAs Multibeam Antennas. 16
MBPAAs Multibeam Phased-Array Antennas. 17
METIS Mobile and wireless communications Enablers for the Twenty–twenty Information Society. 31
MIMO Multiple Input Multiple Output. 3
mmMAGIC Millimeter-Wave Based Mobile Radio Access Network for 5G Integrated Communications. 31
mMTC Massive machine-type communications. 2
mmWaves Millimeter Waves. 12, 13
MPC Multipath Component. 38
NLoS Non-Line of Sight. 13
O2I Outdoor-to-Indoor. 29
OFDM Orthogonal Frequency-Division Multiplexing. 9
PA Power Amplifier. 16
PLE Path Loss Exponent. 32
PMBAs Passive Multibeam Antennas. 17
RAN Radio Access Network. 10
RF Radio Frequency. 16
RMa Rural Macrocell. 46
RRM Radio Resource Management. 10
SISO Single Input Single Output. 18
SNR Signal-to-Noise Ratio. 16, 60
TTI Transmission Time Interval. 9
UCA Uniform Circular Array. 66
UE User Equipment. 16
UHF Ultra High Frequency. 27
ULA Uniform Linear Array. 63
UMa Urban Macrocell. 33, 41
UMi Urban Microcell. 33
UPA Uniform Planar Array. 66
URLLC Ultra-reliable and low latency communications. 2
VHF Very High Frequency. 27
VR Virtual Reality. 2
WRC-15 World Radiocomunnication Conference in 2015. 57

1

Introduction

This chapter presents a brief contextualization of this dissertation. The relevant points that leads to the development of this thesis are introduced on section 1.1, followed by the objectives that should be accomplished during the writing of this work, on section 1.2. On section 1.3 is presented a brief view of the chapter organization of this dissertation. Finally on section 1.4 it is presented the contributions provided by this work.

1.1 Motivation

The first mobile generation was introduced in the early 80s and has a simple voice service, based on analog transmission. The Second Generation (2G) appeared in the 90s, and the main difference between the first and second generation is that the second one upgraded the transmission technology from analog to digital, and with the Internet's growth the Circuit Switching (CS) was replaced with the Packet switching (PS) [1]. Since then the mobile technology has suffered a great evolution, passing to the Third Generation (3G), where the data rates were boosted up to 7.2 Mbps [2] and then evolved to the 3.5G and 3.75G. The first release of the Fourth Generation (4G), also known as Long Term Evolution (LTE), was in 2009 and had a boost of performance, achieving almost 10 times faster speed compared with 3G. Based on history, it can be said that the mobile technologies suffer a revolution every ten years, trying to overcome the escalating

demand of data speed and lesser times of response.

The Fifth Generation (5G) is the ultimate mobile generation that aims to achieve ultra-fast connectivity and low latency through the use of multiple technologies. The 5G will also help to unleash massive Internet of Things (IoT) ecosystems, self-driving cars, machine-to-machine communications for industry automation, Virtual Reality (VR) and Augmented Reality (AR).

As in the prior evolution of the mobile technologies. 5G is introducing significant improvements to the communications when compared with the preceding technologies. The 5G networks are currently being standardized by the 3GPP alongside with several trial deployments. The International Mobile Telecommunications - 2020 (IMT-2020) contains the full list of requirements and methodologies that will help evaluate the future and ongoing deployment of 5G networks. The IMT-2020 was addressed by the ITU-R, superseding IMT-Advanced related to the 4G and imposing interoperability with both IMT-Advanced and IMT-2000 (3G).

Figure 1.1 demonstrates how many times the data rate of a 5G system increases compared with a 4G network. The user experienced data rate is expected to be 10 times above of the latest technology, the spectrum efficiency should be 3 times more and latency should diminish 10 times. Also, the 5G networks promises to achieve a maximum of a 20 Gbit/s.

The IMT-2020 has also defined some usage scenarios to help supporting 5G networks deployment:

1. Enhanced mobile broadband (eMBB): This is like what we have nowadays but boosted in performance, including a peak of download of 20 Gbps to help support the increased consumption of multimedia contents as video, as well as emerging services as AR and VR;

2. Ultra-reliable and low latency communications (URLLC): Including very low values of latency and high availability, reliability and security;

3. Massive machine-type communications (mMTC): The ability to support at least one million IoT connections per Km^2 with very long battery life and wide coverage outdoor and as indoor;

4. Fixed wireless access (FWA): The ability to provide fiber-like performance to homes and businesses [3].

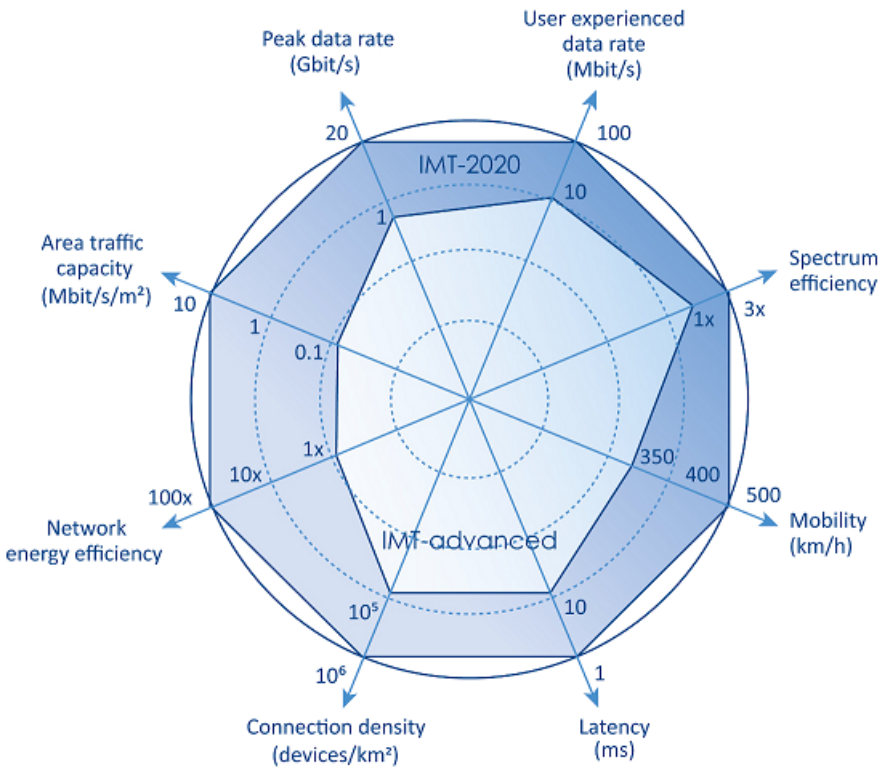

Figure 1.1: Minimum requirement for future communication systems, [4]

In order to meet the above requirements of 5G, there are some key challenges that still need to be addressed. For instance, the spectrum availability, the need of a new air interface, ultra-dense deployment and extensive capacity, are some examples of the challenges that need to be addressed.

The spectrum availability is a matter that needs to be discussed as the frequency band and the microwave band used by the former technologies are starting to be saturated. This is why the 5G can be deployed in multiple frequency bands. The solution can pass by using the millimeter waves band, a frequency band between 30 and 300 GHz that contains large blocks of free space to allocate 5G users. There are also higher frequencies that can help achieving the so requested ultra fast bit-rates.

However, the standards imposed by the 5G implies major changes on propagation characteristics, because mmWaves are easily obstructed. This band is known by the higher attenuation factors and shadow effects that must be overcame with different approaches, like using massive Multiple Input Multiple Output (MIMO) solutions instead of the traditional techniques as tri-sectored sites. Making use of antenna arrays and beamforming are also key changes of this technology, pairing up antenna elements that can go from a few dozens to a couple

of hundreds of elements, creating narrow and longer beams, with higher gains to overcome the signal decay due to obstructions.

This change on the telecommunication paradigm will introduce severe changes to the mobile networks. The changes will pass by refactored antenna designs and new concepts to be used on the deployment of this new technology, such as mmWaves, massive MIMO, new radio interface, Heterogeneous Network (HetNet), etc...

1.2 Objectives

The main purpose of this dissertation is to present an overview of the challenges that millimeter waves can face on a 5G perspective, and understanding the propagation characteristics of millimeter waves and how it can affect the signal quality and the link itself.

This dissertation will focus on some of the attenuation sources such as free space loss, the atmospheric attenuation due to gases, rain attenuation, presence of vegetation and material penetration to name a few known influential factors.

Analyzing and comparing the several propagation models existing for the higher frequencies for the different environments, is a key part of the study to be able to calculate an accurate link budget.

Ultimately, the main goal is to dimension the number of antenna elements of an array that is capable of achieving several Gigabit-per-second of throughput. Understand how the number of elements of an antenna array will change when altering network characteristics such as cell size and bandwidth, when trying to achieve a higher data rate. Finishing with a discussion of the solutions that can be employed to make it a feasible solution for a 5G communication.

1.3 Document Organization

The present dissertation is organized as follow:

- **Chapter 2** discusses the state of the art about 5G and mmWaves, introducing the main changes on the mobile communication systems and discussing the different solutions that can help the deployment of this new technologies;

- **Chapter 3** analyzes the different attenuation sources of the mmWaves band and discuss the performance of the different path loss models depending on the environment;
- **Chapter 4** presents different link budget calculation showing how network variables like link distance, bandwidth and frequency can influence the capacity of the link, and then introduce the antenna arrays and calculates the needed antenna elements to achieve a data rate of the link budgets;
- **Chapter 5** concludes the dissertation, presenting the acknowledged points and discussing the future work.

1.4 Contributions

This dissertation has accomplished the following:

- Calculation of the several losses suffered by a link that uses a higher frequency;
- Calculation of different link budgets using mmWaves band frequencies making use of the most suitable path loss models;
- Gain and size analysis of the antenna array dimensioned to achieve multiple Gigabit-per-second data rates.

Part of the work presented in this dissertation, namely the antenna array design presented on chapter 4, resulted in a scientific paper already accepted in the 2021 Telecoms Conference (ConfTELE) [5].

2

5G and mmWaves technologies

The aim of this thesis is to explore and present the limitations introduced by the newly mobile technology, the 5G, that will make use of the millimeter waves band. With that said this chapter presents a view of the 5G cellular systems as a promising opportunity of mobile evolution and how the millimeter waves can be a solution to overcome the current bandwidth crunch.

This chapter is divided into 2 sections: section 2.1 introduce the technology 5G, comparing it with the former ones and present the major advantages of this telecommunication system. The second section reviews the latest studies about the millimeter waves communication systems.

2.1 5G Cellular Systems

The 5G is a promising "all in one" solution that aims for fulfilling the escalating demand for new services and ultra connectivity between different types of devices. 5G will be responsible for enabling the connectivity on devices such as traffic lights, vehicles, medical devices, electricity systems and list goes on, bringing new business opportunities and helping reform Industrial and Transportation area, while contributing for a greener footprint with higher energy efficiency. The listed advantages will be part of the scenarios that 5G should cover, which should be envisaged mainly through eMBB, URLLC and mMTC as in figure 2.1. Table

2.1 shows the minimal performance requirements and which use case to evaluate it.

KPI	Key Use Case	Values
Peak Data Rate	eMBB	DL: 20 Gbps, UL: 10 Gbps
Peak Spectral Efficiency	eMBB	DL: 30 bps/Hz, UL: 15 bps/Hz
User Experienced Data Rate	eMBB	DL: 100 Mbps, UL: 50 Mbps (Dense Urban)
5% User Spectral Efficiency	eMBB	DL: 0.3 bps/Hz, UL: 0.21 bps/Hz (Indoor Hotspot); DL: 0.225 bps/Hz, UL: 0.15 bps/Hz (Dense Urban); DL: 0.12 bps/Hz, UL: 0.045 bps/Hz (Rural)
Average Spectral Efficiency	eMBB	DL: 9 bps/Hz/TRxP, UL: 6.75 bps/Hz/TRxP (Indoor Hotspot); DL: 7.8 bps/Hz/TRxP, UL: 5.4 bps/Hz/TRxP (Dense Urban); DL: 3.3 bps/Hz/TRxP, UL: 1.6 bps/Hz/TRxP (Rural)
Area Traffic Capacity	eMBB	DL: 10 Mbps/m^2 (Indoor Hotspot)
User Plane Latency	eMBB, URLLC	4 ms for eMBB and 1 ms for URLLC
Control Plane Latency	eMBB, URLLC	20 ms for eMBB and URLLC
Connection Density	mMTC	1,000,000 devices/Km^2
Energy Efficiency	eMBB	Capability to support high sleep ratio and long sleep duration to enable low energy consumption when there is no data
Reliability	URLLC	1-10-5 success probability of transmitting a layer 2 protocol data unit of 32 bytes within 1 ms in channel quality of coverage edge
Mobility	eMBB	Up to 500 Km/h
Mobility Interruption Time	eMBB, URLLC	0 ms
Bandwidth	eMBB	At least 100 MHz; Up to 1 GHz for operation in higher frequency bands (e.g., above 6 GHz)

Table 2.1: Minimum performance requirements [6]

On the spectrum side, 5G will be deployed on the legacy bands, the sub-6 GHz band, referred as the microwave band, and in higher bands of frequency like millimeter waves band, which will unburden the constrains on bandwidth and capacity that exist on the lower frequency band. Table 2.2 demonstrates which bands the 5G and the preceding generations are deployed in or being considered to, showing also the new amount of available bandwidth 5G will make use of. Figure 2.2 shows a possible distribution of the considered bands around the world.

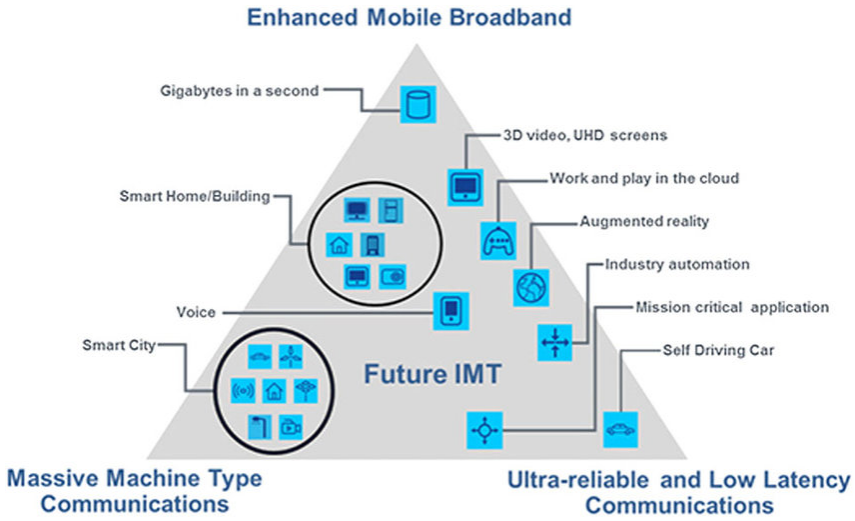

Figure 2.1: Usage scenarios [6]

In order to meet the presented requirements 5G will make use of some radio access solutions. One of the key changes of this technology will be the new air interface, the 5G NR. In similarity to prior generations, 5G NR is based on Orthogonal Frequency-Division Multiplexing (OFDM), as it is an efficient enabler of various services multiplexed for the eMMB scenario. OFDM will also allow coexisting with other waveforms and multi access schemes for connecting IoT devices and enabling mission-critical control communications [9].

One of the major differences between LTE and 5G NR will be the use of scalable OFDM numerology to enable diverse spectrum bands. Instead of having fixed OFDM numerology of 15 KHz spacing between subcarriers, 5G NR will scale the OFDM subcarrier spacing to keep up with the channel widths, since 5G will use millimeter waves that have wider channel widths, instead of the typical LTE carrier bandwidth that can go up to 20 MHz only. The scalable OFDM solution will support better processing of the Fast Fourier Transform (FFT) so that doesn't increase exponentially, also allowing efficient multiplex of services with different bandwidths. This solution will also allow aggregating millimeter waves and sub-6 GHz carriers in order to have a higher performance and robust connectivity [9].

In the other hand 5G NR will also differ on the time domain, applying some scalability on latencies to allow supporting the shorter latencies 5G promises. LTE supports a fixed Transmission Time Interval (TTI) of 1ms. 5G NR will implment a flexible frame structure that scales the TTI up and down, down to microseconds, depending on the specific service requirements [9].

Band	Generation	Frequency (GHz)	Frequency Range (GHz)	Bandwidth (GHz)
Sub-6 GHz	2G	0.8	0.791-0.862	0.071
		0.9	0.880-0.959	0.079
	3G	1.8	1.710-1.880	0.17
	4G	2.1	1.920-2.169	0.249
		2.6	2.500-2.690	0.19
	5G	0.6	0.470-0.694	0.224
		0.7	0.694-0.790	0.096
		1.5	1.427-1.518	0.091
		3.5	3.300-3.800	0.5
		4.7	4.500-4.990	0.49
		5.6	5.500-5.700	0.2
mm Wave	5G	23	22.55-23.55	1.0
		28	27.50-31.23	3.73
		38	38.6-40.0	1.4
		40	40.5-42.5	2.0
		46	45.5-46.9	1.4
		47	47.2-48.2	1.0
		49	48.2-50.2	2.0
		73	71-76	5.0
		83	81-86	5.0
		93	92-95	3.0

Table 2.2: Frequencies bands used by Mobile generations [7]

5G NR also introduces the self-contained integrated subframes to enable different types of subframes to multiplex new services in future, as shown on figure 2.3. It also allows forward compatibility with future features to be deployed in the same frequency due to the capacity of having blank subframes and blank frequency resources. The self-contained subframe is a key enabler to new antenna techniques like massive MIMO, through a more accurate and timely knowledge of downlink channel enables the uplink sounding references signals to be used for download channel estimating, in order to evaluate the link quality and make the necessary beamforming adjustments in a more efficient way.

On the architecture side of the Radio Access Network (RAN), 5G aims to be heterogeneous, where macrocells and ultra-dense small cells (microcells, metrocells, picocells and femtocells) should coexist. 5G RAN will adopt a flexible centralized processing for efficient Radio Resource Management (RRM), cost-effective and performance-optimizing network in an architecture that is referred to as Cloud Radio Access Network (C-RAN) [7]. In this the base station is split into the Remote Radio Unit (RRU) and Baseband Unit (BBU). The RRU is located at the base station site and the BBU is centralised in a data centre facility. The communication between the two units is known as the fronthaul, and is done via a common public radio interface (CPRI), while the backhaul refers to the communication between the BBU and the core network where the telephone network and the Internet are, as on figure 2.4 (b). On legacy networks the fronthaul have

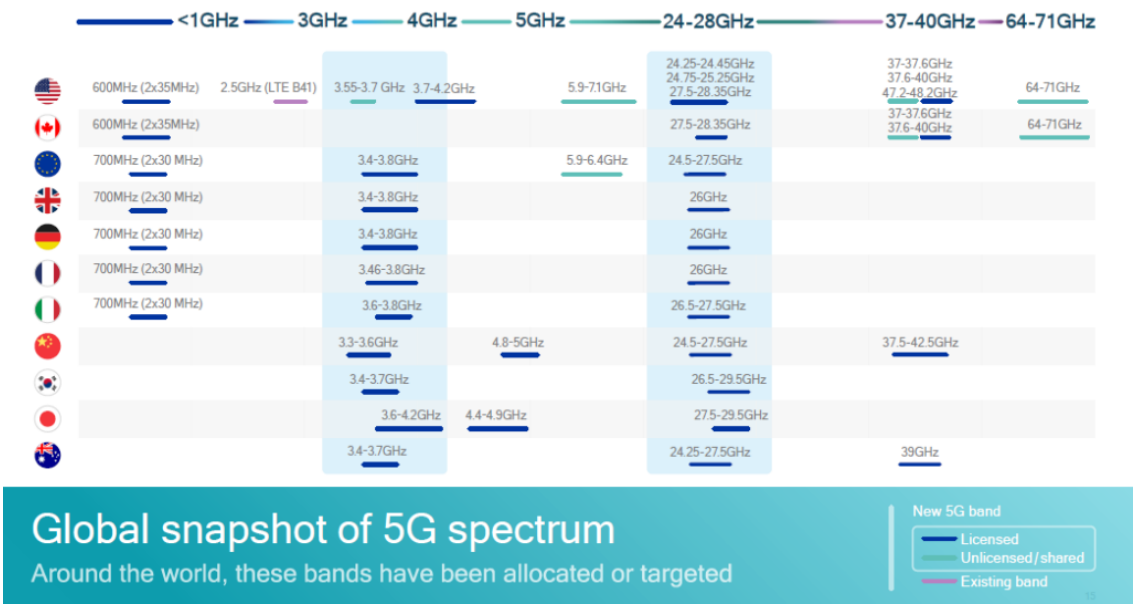

Figure 2.2: 5G Frequency allocation global world[8]

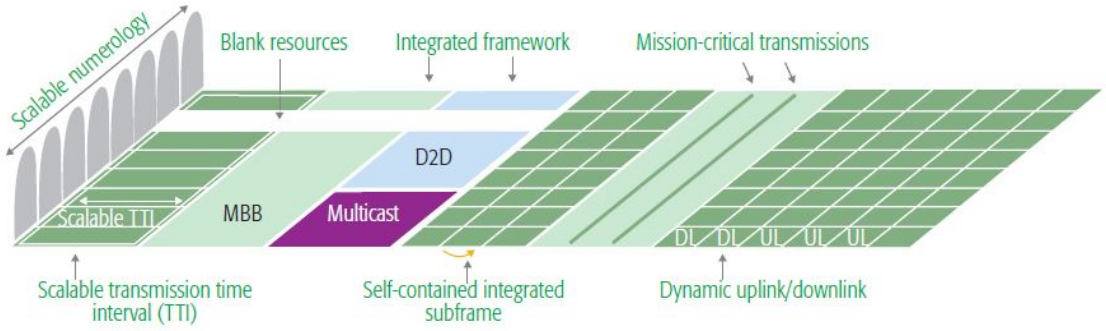

Figure 2.3: 5G NR frame structure [9]

favored a wire connection like optical fiber, the radio-over-fiber (D-RoF) connection.

On 5G HetNets it is not a viable solution due to not being flexible, scalable nor cost-effective. This is because only spots with existing fiber access would be used or it would mean that a ultra dense fiber deployment would be needed to feed the small cells [7]. For this reason the need of wireless solutions have been rising, which makes millimeter waves a good candidate due to its promising capabilities for supporting flexible beamforming, and providing high spatial multiplexing and diversity gains. It also shows potentials for lower cost (with regards to components), higher capacity, lesser interference (due to smaller cell sizes and narrower beams) and smaller antenna form factor [7].

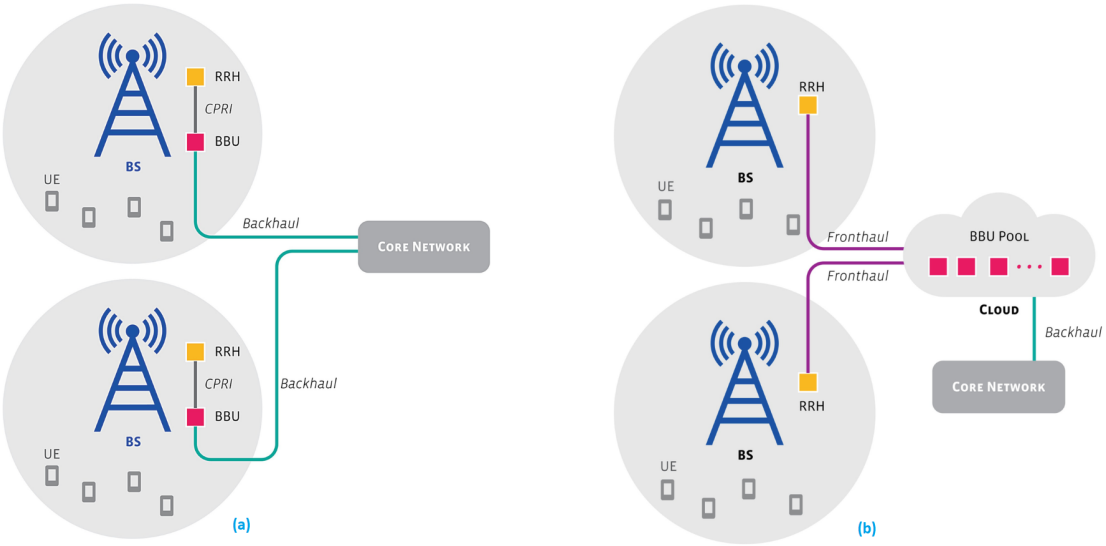

Figure 2.4: RAN architectures, (a) traditional Distributed Radio Access Network (D-RAN); (b) Cloud Radio Access Network (C-RAN) [10]

The above concepts will contribute to 5G mobile systems to be available to the mobile communication business on the year of 2020 despite the fact of still being exploring the best solutions to achieve the extraordinary expectations.

2.2 Millimeter Waves Communications

The mmWaves ranges from 30 to 300 GHz, which is designated as Extremely High Frequency (EHF) band.The band between 3 to 30 GHz is labelled as Super High Frequency (SHF). Whereas EHF and SHF bands have propagation characteristics very identical, the 3–300 GHz spectrum is simultaneously included on the therm mmWave band with their wavelengths ranging from 1 to 100 mm [11].

As discussed before the millimeter waves band is a crucial part of the mobile communications evolution. The fact that the band of frequencies below the 6 GHz is starting to be overloaded with the other cellular technologies, and as 5G requires as much as free bandwidth as possible, the millimeter wave band is the emergent solution. Part of it is still unexploited and has large blocks of bandwidth available that are attractive for the requirement of extremely wide channel widths (hundreds of MHz) of 5G NR technology [9].

The Millimeter Waves have substantial differences to microwaves when speaking about propagation impacting the overall systems. And as the existing cellular

technologies are deployed on the microwaves band where there are a vast knowledge, including a various surveys on the best approaches and multiple measurements campaigns, the same is not applicable to mmWaves hence the urgency of exploring this frequency spectrum. The most notorious of the discrepancies of both bands are the suffered attenuation.

It's possible to calculate the impact of the multiple loss causes, such as the free space loss. Through Friis equation it's expected the attenuation value to increase with the increment of the carrier frequency, however this only happens for antennas with constant gain over frequency. If the system uses antennas with constant aperture then the path loss caused by free space can even decrease with the increment of frequency [12],[13].

Some of the gases present on atmosphere can also be detrimental for the link, as oxygen or water vapour particles that can cause signal absorption due to molecular resonance processes [12], imposing almost 15 dB/Km of attenuation [11]. Therefore the regions of the spectrum affected by this are not viable solutions for wide range outdoor systems.

The atmospheric phenomenon of raining can also affect the viability of the link since the wavelength of Millimeter Waves (mmWaves) frequencies are similar to the size of raindrops, causing sever signal scattering [11]. The rain attenuation is known as specific attenuation due to rain

The presence of vegetation can compromise the signal by introducing extra attenuation to the path loss, therefore if the radio wave travels in foliated environments like forest ambiences, that can be categorized in 3 cases: a tree, a line or multiple lines of trees and a forest [14], so the link can suffer several ways of decay effects such as reflection, diffraction and multipath dispersion [15], that can contribute to form a Non-Line of Sight (NLoS) connection.

The mmWaves also have a different behavior when penetrating on materials compared to the microwaves due to the short wavelength, introducing a sever loss to the propagation, preventing the signal to reach indoor users. Although there isn't a developed model yet to trace the behavior of higher frequencies, there are some surveys on measurements, that tried to quantify the loss of the signal when passing through the most common building materials, such as brick, glass, concrete, etc.. the following table 2.3 shows some of the measurements carried out for some carrier frequencies.

It's possible to say that by increasing the thickness the material, the signal

Material	Thick. (cm)	Penetration loss (dB)			
		sub 2.5 GHz	28 GHz	40 GHz	60 GHz
Concrete	10	17.7	34.1	175	–
Brick wall	10	–	28.3	178	–
Drywall	2.5	5.4	6.8	–	6
Whiteboard	1.9	0.5	–	–	9.6
Wood	0.7	5.4	–	3.5	–
Chip wood	1.6	–	–	0.6	–
Mortar	10	–	–	160	–
Clear Glass	0.3	6.4	3.9	2.5	3.6
Mesh Glass	0.3	7.7	–	–	10.2
Tinted glass	0.38	–	24.5	–	–

Table 2.3: Penetration Loss at mm-wave for specific material, source:[11]

is severely absorbed resulting in large losses, contributing for the need of heterogeneous networks to be possible to cover clogged environments, using other wireless alternatives.

The multiple sources of loss on mmWaves can be diminished by reducing the cell radius, meaning smaller cells, supporting the need of massive dense deployments used on 5G. This architecture can, in another way, increase the spectral efficiency and resource reuse on the areas.

One of the solutions to overcome the severe losses and achieve Line of Sight (LoS) is by employing high directional antennas with high gain, such as array antennas with high gain elements, powered by beamforming techniques.

There are some techniques that can help achieving the coverage and capacity requirements, such as Distributed Antenna System (DAS) or cooperative multi-hop relaying [16].

Instead of using a single large antenna array to cover a single wider cell, the DAS concept introduces the use of multiple smaller antenna arrays to cover small cells in dense urban areas where obstacles can weaken the signal. Therefore networks can benefit from deploying smaller cells antenna architecture, like distribute 16 antenna arrays of 4x4 elements instead of deploying a unique antenna array of 16X16 to cover the same area, promoting LoS and more availability of channel [16], figure2.5 is a diagram of the two systems.

DAS is a good option for dense urban regions where the link can experience multiple static blockages as buildings. On the other hand cooperative multi-hop relaying technique is a better solution for mobile obstacles as vehicles or even the user movement, because takes advantage on the multi-hop NLoS transmissions.

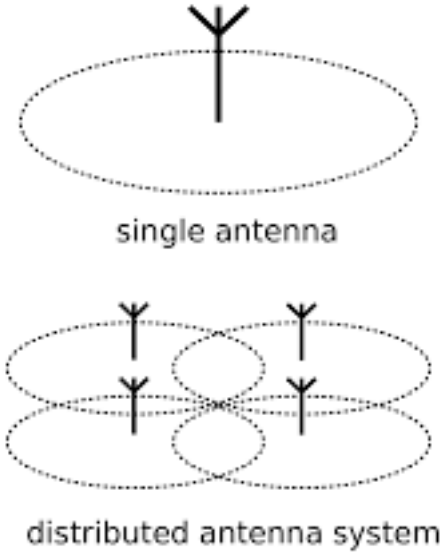

Figure 2.5: Distributed Antenna System vs single antenna system, source: wikipedia

Hence, deploying relays increases the possibility of finding a alternative rout for the connection when a node is being obstructed [16].

When designing an antenna for mmWaves system, the antenna array is the inevitable option and these can be categorized in many ways depending on the design parameters, such as geometrical configuration, electrical architecture, feeding mechanism, etc [17]. When speaking of geometrical configuration the array can be ranked as linear or planar, when the design parameter is the beamforming architecture, antenna arrays can be subdivided in analog, digital or hybrid, etc...

The linear array compound of isotropic elements have a wide pattern on the perpendicular plane of the array axis, and a narrow pattern in same plane of the array axis.

Planar arrays have elements, equally spaced, distributed on a plane and not only on an axis, and can be subdivided in rectangular/square or circular, this layout helps on beam steering in both azimuth and elevation planes [17].

The gain of an antenna is directly proportional to its area, meaning the two dimensional arrays will have higher gain compared with the linear array, which makes the planar arrays a better solution for the mm-waves communication.

There are multiple beamforming techniques to achieve a narrow and directional beam. Precoding or beamforming schemes can usually be classified into

three: digital precoding, analog beamforming, and hybrid (analog-digital) precoding. The analog beamforming has the downside of only be applicable to single-user systems, employing a single stream. This is used to control the phases of signals with the single data stream in order to achieve optimal antenna array gain and an effective SNR. With perfect knowledge of the Channel State information (CSI) available at both the Base Station (BS) and the User Equipment (UE), the analog beamformer employs N antennas at the BS with only one Radio Frequency (RF) chain to send a single data stream to a terminal with M antennas and only one RF chain too [7]. Although it have less degrees of freedom and being less flexible is also much cheaper compared

The digital precoding technique can control both the phase and amplitude of the signals to be emitted, has the possibility of being employed in both single and multi-user systems. Multiple streams are accomplished by the use of a dedicated RF chain by antenna, meaning that each antenna branch requires a Power Amplifier (PA) stage, Digital-to-Analogue-Conversion (DAC) and an Analogue-to-Digital-Conversion (ADC) stage. These are the most expensive parts of the transceiver and the IFFT/FFT stage, making such a design very expensive to implement, increasing the power consumption and complexity of the signal processing [11], making it an impractical solution for the mmWaves massive MIMO systems. On the other hand the analog beamformer is an effective way of producing high beamforming gains, although it have less degrees of freedom and being less flexible, is also much cheaper and simple to implement.

The hybrid precoder scheme is a tradeoff between performance/simplicity in analogue beamforming and flexibility in digital beamforming. In hybrid beamforming analogue processing is performed over a group of RF chains in each transceiver, and then digital processing is performed over all transceivers, as observable in figure 2.6. This architecture have a significant reduction of the number of RF chains and DACs/ADCs stages, in order to lower the implementation cost and consumption power, being a promising solution to massive MIMO systems [11] [7].

All the elements listed above contributes for the massive usage of millimeter waves on wireless technologies, the Multibeam Antennas (MBAs) is an complementary approach to multiuser streaming, capable of produce multiple independent directional beams [19], increasing the capacity of mmWaves networks.

The existing MBAs approaches are the following:

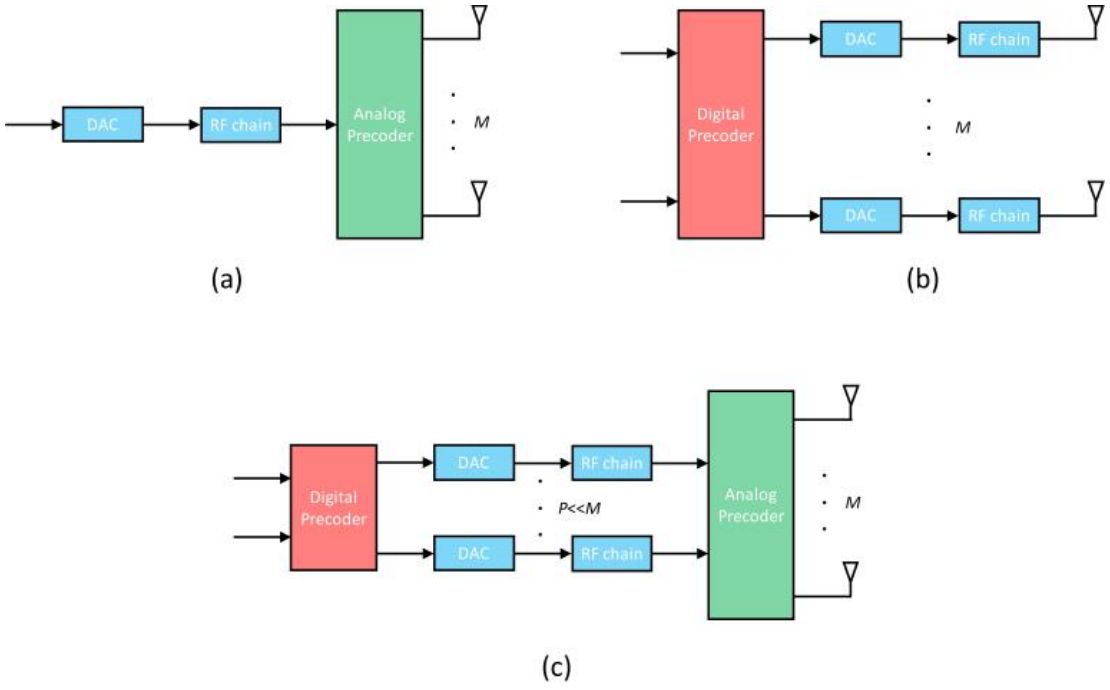

Figure 2.6: Beamforming architectures (a) analog beamforming, (b) fully-digital beamforming and (c) hybrid beamforming [18]

Passive Multibeam Antennas (PMBAs) are MBAs that reach the beamforming on the Radio Frequency (RF) domain. Composed by finite number of strongly isolated input ports, with single transceiver that controls a unique beam. The multibeams are produce by a shared aperture that should cover a angular range, but have the downside of having fixed directions after the system is built. These can be divided in 3 sub-classes.

- Reflector-based PMBAs: this uses a reflector-based quasi-optics component;
- PMBAs based on lenses;
- PMBAs based on beamforming circuits: these are fitted into a single substract with an array of antennas, making it a more flexible approach [19].

There is another type of MBAs, the Multibeam Phased-Array Antennas (MBPAAs), instead of having predefined number of beams, as the PMBAs, these have agile beams, that can be passive or active. The phase-shifting can be at radio frequency band, intermediate frequency or baseband. The most common are the radio frequency phase-shifting, and the most power efficient are the active ones. The MBPAAs that use analog intermediate frequency phase-shifting or baseband

phase-shifting, have lower cost implementations but are limited to narrowband operation [19].

There's a third type of multibeam antennas, the Digital Multibeam Antennas, that obtain digital beamforming at baseband, becoming more robust to failure [19].

It's possible to say that PMBAs are not the most suitable for mobile communications, because the beams are not adaptable to user movement. The MBPAAs although it have a more flexibility to change beam direction need a larger number of phase shifters, and as in 5G systems is expected to use a larger number of antenna elements it would turn into a bulky and complex system. The digital approach is the most promising solution for massive MIMO, due to its simplicity, but has the downside of still having a high power consumption [19].

Another key concept of 5G is the employment of massive MIMO. Through the use of larger antenna arrays, the link's spectrum efficiency and energy efficiency, robustness and reliability can be significantly improved [1], because it can accommodate multiple co-channel users simultaneously [11].

MIMO techniques are an upgrade of the Single Input Single Output (SISO) systems, these only employ a single antenna at both terminals, BS and UE, while MIMO employs multiple antennas at both , achieving higher capacity and reliability then SISO. MIMO's diversity gains increases with the number of independent channels between transmitter and receiver, and the maximum achievable multiplexing gain is the minimum number of antenna elements at both terminals. Original MIMO cannot offer both maximum multiplexing and diversity gain. However massive MIMO has the opportunity to achieve it due to the use of a larger number of antennas [7].

The channel capacity of SISO is dependent on increasing the system SNR or bandwidth, on the other hand, MIMO systems increases the channel capacity by increasing the number of antennas, it should be noted that this increase is not linear and is limited. It also means increasing the costs of deployment, processing complexity and has space constraints on the mobile terminals. The advantaged of massive MIMO the linear increase of capacity with the increase of antennas on BS or UE, and the space constraint is overcame with the use of higher frequencies, due to the decrease of antennas' aperture [7].

Massive MIMO is an obvious beneficial technique to compensate path loss and increase channel capacity, however still have some downsides, namely large

channel estimations, pilot contamination and the need of development of commercial and scalable solutions for heterogeneous network deployments [11][7].

The millimeter waves are a promising solution for the high rates needs of 5G technology, however still face some challenges that are being addressed with the rising of new techniques.

3

Propagation Characteristics and models

In first instance, this chapter presents an overview of the main environment effects on millimeter waves, namely how the propagation in free space changes over the increase of the frequency, the atmospheric attenuation and how different gases affect higher frequencies, the power loss induced by rain, vegetation attenuation and material penetration. In a second section are studied some propagation models, which are needed to predict and simulate the air interface in different scenarios, hence this section presents a comparative overview of the existing models studied by several organizations, with the aim of developing an accurately way to estimate the losses during propagation for a wide frequency range of the millimeter-waves, focusing on the band between 0.5 and 100 GHz.

3.1 Propagation Characteristics

The aim of this section is to introduce the main propagation characteristics of the mmWaves by making some comparisons with the microwaves band. Understand how the environment can influence higher frequencies and how to quantify the signal power variations.

3.1.1 Free Space Loss

The free space loss is the loss associated to the propagation of energy between two end points without any obstacle or reflecting surfaces and it is given by equation 3.1, where c is the speed light constant, d the link distance and f the frequency carrier value.

$$\begin{aligned} FSL_{[dB]} &= 20log_{10}\left(\frac{4\pi df}{c}\right) \\ FSL_{[dB]} &= 92.44 + 20log_{10}(d_{[Km]}) + 20log_{10}(f_{[GHz]}) \end{aligned} \tag{3.1}$$

Figure 3.1 demonstrates the free space loss evolution over frequency considering a 1 Km link ($d = 1Km$). As expected the attenuation increases with frequency showing an that a link of 1 Km distance and using a 30 GHz frequency will loss 20 dB more then a link using 3 GHz as carrier. On figure 3.2 is possible to observe that the free space loss is also proportional to the inter-distance between the transmitter and receiver.

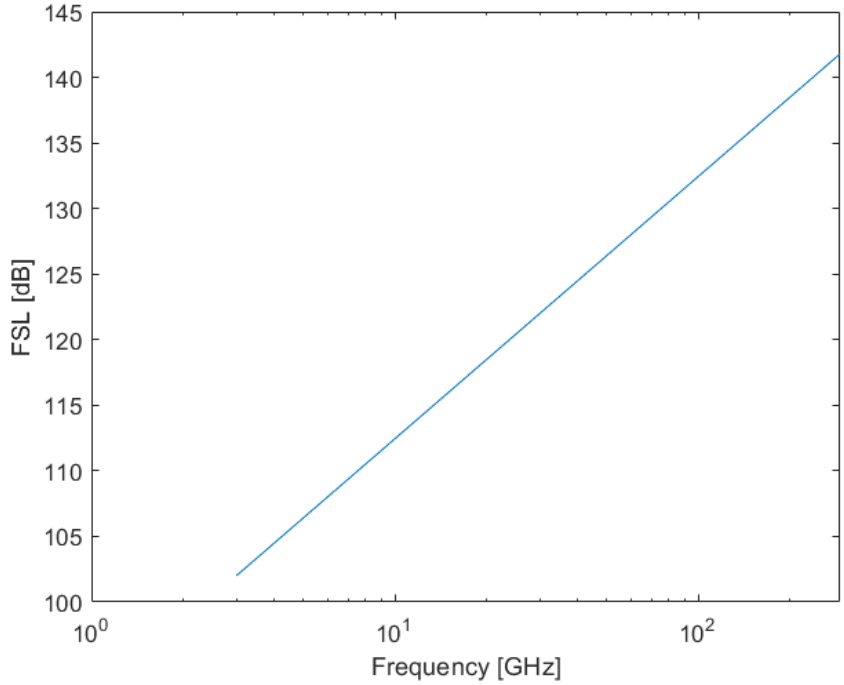

Figure 3.1: Free Space loss over frequency for a 1 Km inter-distance.

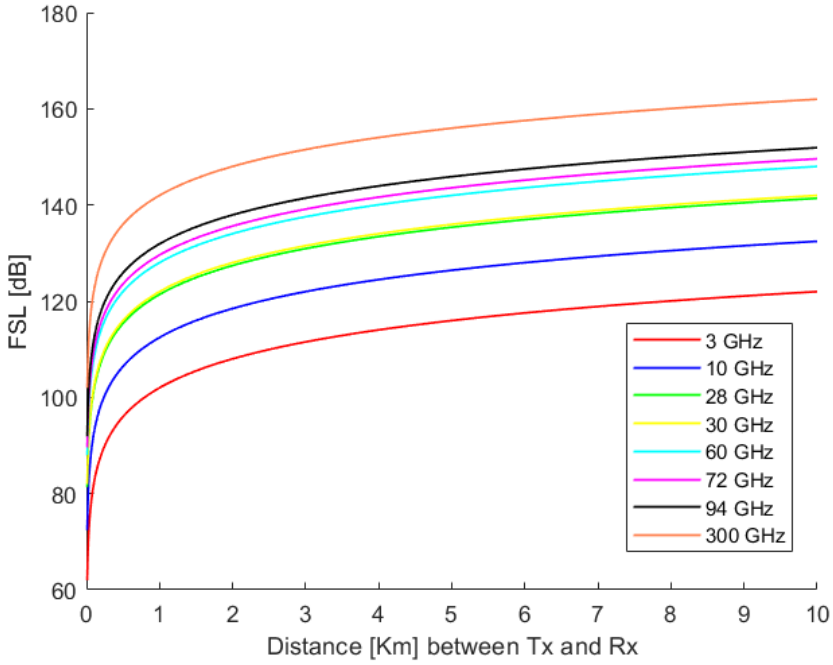

Figure 3.2: Free Space loss over inter-distance (d) for different values of frequency

3.1.2 Atmospheric attenuation

Atmospheric attenuation can also be designated as gaseous attenuation as there are some atmospheric gases that can induce additional loss on propagation. This is due to the absorption of energy from radio waves by gaseous molecules, which vibrate with a strength proportional to the carrier frequency. The most limiting gases are oxygen and water vapor. The absorption capacity of these depend on temperature, pressure, altitude and carrier frequency.

The mean annual reference atmosphere is given by [20]:

- a pressure of 1013.25 hPa;
- a temperature of 15ºC;
- a water vapour density of 7.5 g/m^3 ("Standard" atmosphere) or 0 g/m^3 ("Dry" atmosphere).

This is for sea level, meaning at zero-meter altitude, and it's considered the worst scenario since the air density reaches its maximum, increasing the attenuation. The total gaseous attenuation should be calculated using the recommendation on [21] that presents equation 3.2 where γ_o, γ_w and d represents the specific

attenuation due to oxygen, the specific attenuation due to water vapor and link distance respectively. On equations 3.3 and 3.4 the $N''_{Oxygen}(f)$ and $N''_{WaterVapour}(f)$ represents the imaginary part of the frequency-dependent complex refractivities and are on appendix A.1.

$$A_{[dB]} = (\gamma_o + \gamma_w) d_{[Km]} \tag{3.2}$$

$$\gamma_{o[dB/Km]} = 0.1820 f(N''_{Oxygen}(f)) \tag{3.3}$$

$$\gamma_{w[dB/Km]} = 0.1820 f(N''_{WaterVapour}(f)) \tag{3.4}$$

Figure 3.3 demonstrates that oxygen molecules resonates around the 60 GHz, inducing an additional loss of 15 dB/Km on propagation. Making this frequency not suitable for outdoor communication. On the other hand, around the 183 GHz there is also a peak of attenuation due to water vapour.

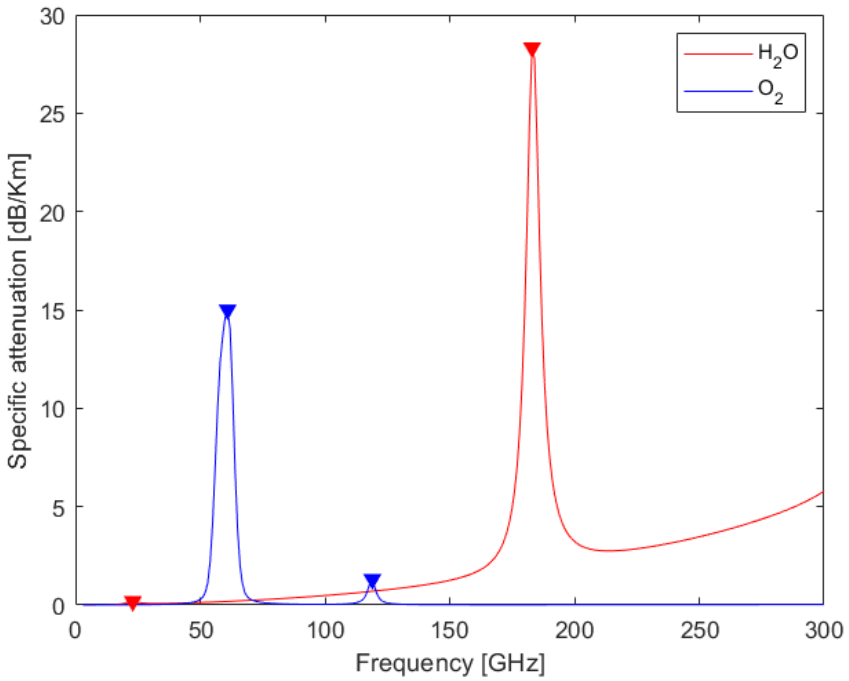

Figure 3.3: Specific attenuation due to oxygen and water vapour over frequency at a sea level altitude

This attenuation can also be calculated for other altitude values, but altitude will influence the other atmosphere values, those are then calculated using the

recommendation in [20] on appendix A.2. Figure 3.4 aims to show the variation of the specifics attenuation for a 300 m altitude. Figure 3.4 points that for higher altitudes the coefficients of attenuation due to atmospheric gases slightly decreases, because the Water-vapour density decreases exponentially with increasing altitude [20], which makes the zero meter scenario the worst case, inducing the highest value of attenuation to consider.

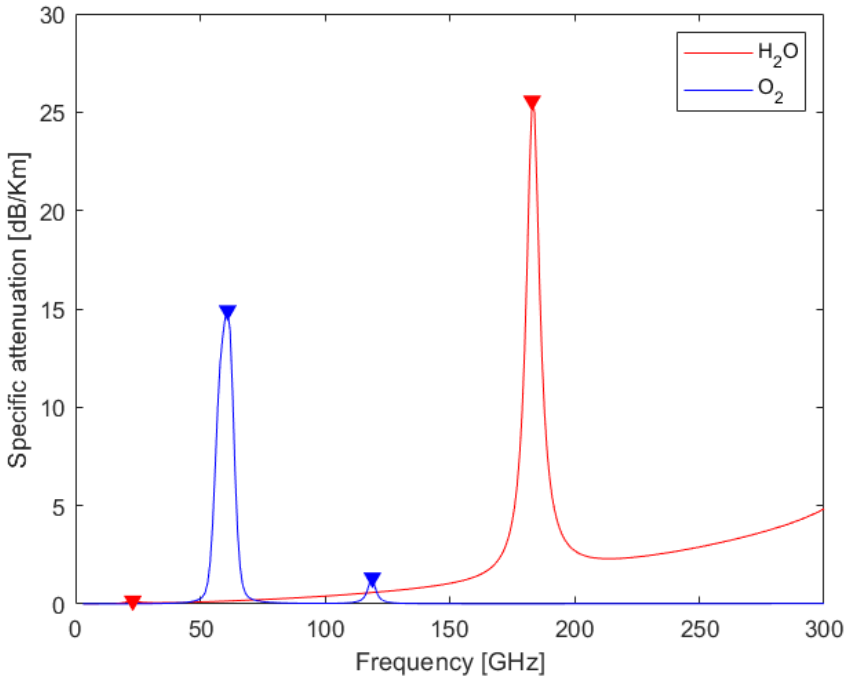

Figure 3.4: Specific attenuation due to oxygen and water vapour over frequency at 300m of altitude

3.1.3 Rain attenuation

The attenuation caused by the rain is a another factor that can not be neglected at mmWaves, due to the comparable sizes of mmWaves' wavelength and the raindrops that have typically a few millimeters as well, makes mmWaves vulnerable to blockage by raindrops.

The rain-induced fading is calculated according to the recommendation in [22], where the rain specific attenuation is given by equation 3.5, where k and α are determined functions of frequency, dependent on the path elevation angle and polarization tilt angle relative to the horizontal, and R is the rain rate.

$$\gamma_{r[dB/Km]} = kR^{\alpha} \tag{3.5}$$

Usually the rain specific attenuation is calculated using $R_{0.01}$, meaning, the rain rate exceeded only 0.01% of the time. According to the map on appendix B, extracted from [23], Portugal is divided in two zones where the $R_{0.01}$ annual average was set between 32 and 42 mm/hr.

According to figure 3.5 is possible to say that attenuation caused by rain has a exponential increase on frequencies below 150 GHz and tends to stabilize for higher frequencies. In Portugal for zones where the annual average rain rate is 42 mm/hr, the signal can loss up to 18 dB/Km for frequencies above 100 GHz.

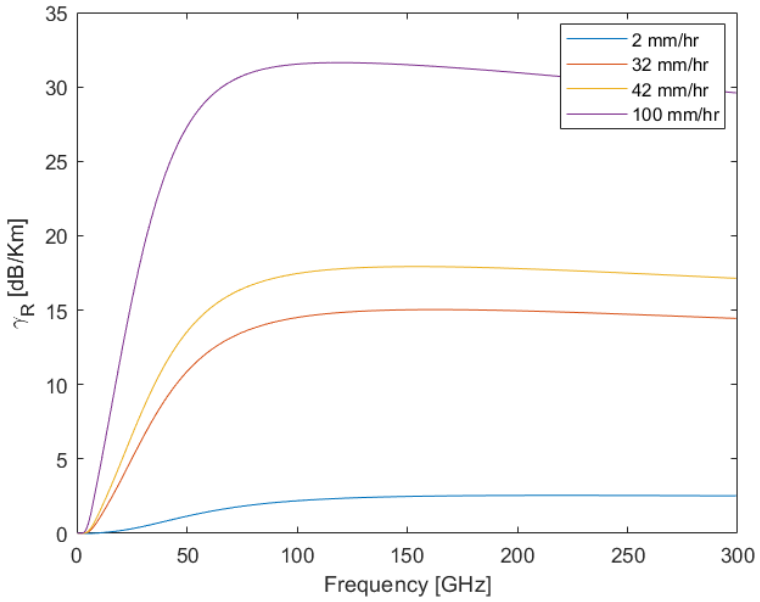

Figure 3.5: Rain specific attenuation in function of frequency

3.1.4 Foliage attenuation

The presence of vegetation is another challenge for millimeter waves as it can ensure another factor of loss for these signals. The attenuation is dependent on the foliage depth, which means that multiple trees will affect the signal in a more severe way then only one tree, on the other hand it can also serve as a source of multipath reflections that can be used to form non line-of-sight (NLoS) links [15].

The loss derived from the presence of vegetation is usually observed in 3 scenarios: a single tree, a line or multiple lines formed by multiple trees or a forest, then the signal can be broke into scattering through medium vegetation such as leaves or branches, into diffraction at the top or edges of trees and finally the signal can also be reflected from ground to the nearby obstacles [15].

Table 3.1 presents some of the existing models to help predict the loss added by foliage. All models are dependent from frequency, f, and the tree depth, d. Some models like Cost235 and FITU-R present different expressions for different foliage states, in leaf and out of leaf which suggests the attenuation can vary on summer and winter, when the trees are fully blossomed or naked. ITU-R model can only predict diffracted components from top and around the vegetation and also the ground reflected component above 1 GHz of frequency, because this model was developed using measurements on Very High Frequency (VHF) and Ultra High Frequency (UHF) [15].

Model	Expression	Frequency range
Weissberger (MED – Modified exponential decay model)	$L(dB) = \begin{cases} 1.33 f^{0.284} d^{0.588}, 14m < d < 400m \\ 0.45 f^{0.284} d, 0m < d < 14m \end{cases}$ f is frequency in GHz , and d is the tree depth in meters	230 MHz to 95 GHz
Cost235	$L(dB) = \begin{cases} 26.6 f^{-0.2} d^{0.5} \text{ , out of leaf} \\ 15.6 f^{-0.009} d^{0.26} \text{ , in leaf} \end{cases}$ f is frequency in MHz , and d is the tree depth in meter and $d <$ 200m	9.6 GHz to 57.6 GHz
FITU-R	$L(dB) = \begin{cases} 0.37 f^{0.18} d^{0.59} \text{ , out of leaf} \\ 0.39 f^{0.39} d^{0.25} \text{ , in leaf} \end{cases}$ f is frequency in MHz , and d is the tree depth in meter and $d <$ 400m	VHF to mmWaves
ITU-R	$L(dB) = 0.2 f^{0.3} d^{0.6}$ f is frequency in MHz , and d is the tree depth in meter and $d <$ 400m	200 MHz to 95 GHz

Table 3.1: Foliage loss models

Figure 3.6 presents the behavior of the models on a frequency range of 3 to 90 GHz for a tree depth of 2.5 m. Is possible to say the FITU-R is the most pessimist model when in leaf stage. The Cost235 model has a lower dependency on frequency. The Weissberger and ITU-R models predicts less attenuation, and the Weissberger as a constant difference of around 1 dB to the FITU-R out-leaf model over frequency.

Is expected that the increase of tree depth indicates a higher attenuation, as shown on Figure 3.7 the tree depth is 200m, which can be considered a forest, the ITU-R estimates higher losses, and the over all behavior of all models indicates a massive loss when millimeter waves cross dense wooded areas, which will be a crucial factor for the communication to be successful.

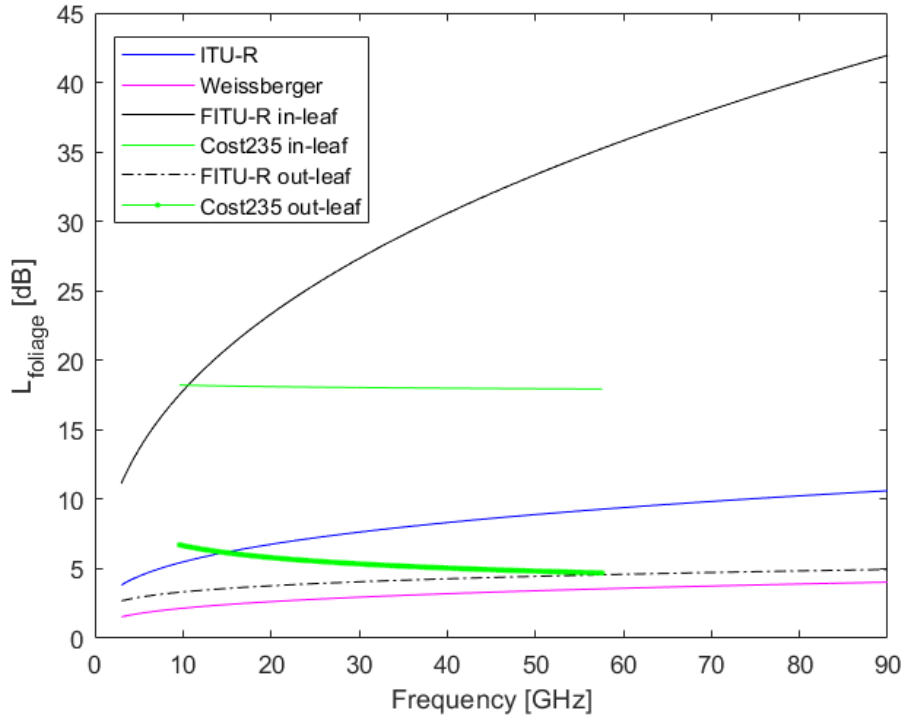

Figure 3.6: Foliage attenuation in order of frequency for 2.5m tree depth

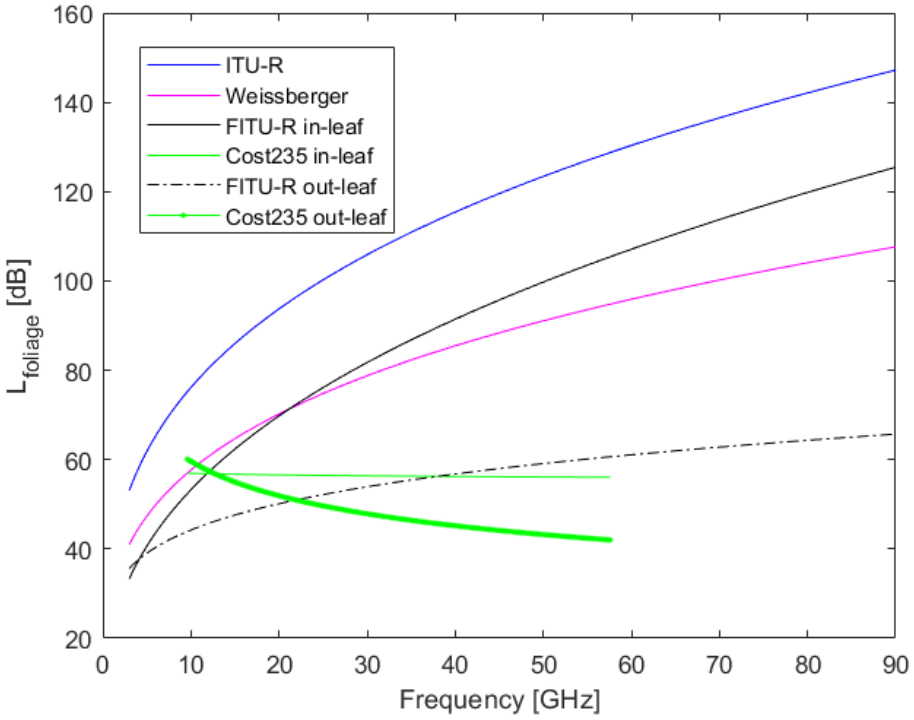

Figure 3.7: Foliage attenuation in order of frequency for 200m tree depth

3.1.5 Material penetration loss

The higher frequencies like millimeter waves are not suitable to pass trough materials, because it will add a new attenuation factor to the signal, so millimeter waves will be highly attenuated in indoor environments due to the presence of room paraphernalia, such as furniture, doors or walls. On the already presented table 2.3 of chapter 2 there are some measurements of different frequency signals passing through typical building materials, showing that a signal of 28 GHz can suffer an additional attenuation of 34.1 dB when penetrating concrete. Also the transfer of propagation environment from outdoor to indoor will induce significantly loss due to the passing through on buildings walls, this is the main reason of the need of having heterogeneous solutions when deploying 5G on these frequencies, to ensure coverage inside buildings from outside base stations.

The penetration loss is difficult to model due to the multiple contributor factors such as type of material, frequency, material thickness, but 3GPP initiative presents a model to account for the penetration loss on external building walls for the Outdoor-to-Indoor (O2I) scenario. 5GCM has also purposed models, that can be found on table 3.2. Where *fc* is the frequency in GHz, and L_{glass}, $L_{concrete}$ and $L_{IRRglass}$ can be found on table 3.3. Figure 3.8 has a representation of the models presented before. The 3GPP high loss model shows a penetration loss of 37.95 dB for 28 GHz.

Initiative	Path loss model [dB]	Standard deviation [dB]
3GPP Low loss model [24]	$PL_{tw} = 5 - 10log_{10}(0.3 \times 10^{-L_{glass}/10} + 0.7 \times 10^{-L_{concrete}/10})$	$\sigma = 4.4$
3GPP High loss model [24]	$PL_{tw} = 5 - 10log_{10}(0.7 \times 10^{-L_{IRRglass}/10} + 0.3 \times 10^{-L_{concrete}/10})$	$\sigma = 6.5$
5GCM Low loss model [24]	$PL_{tw} = 10log_{10}(5 + 0.03f_c^2)$	$\sigma = 4.0$
5GCM High loss model [24]	$PL_{tw} = 10log_{10}(10 + 5f_c^2)$	$\sigma = 6.0$

Table 3.2: O2I models

Material	Penetration Loss [dB]
Standard multi-pane glass	$L_{glass} = 2 + 0.2f_c$
IRR glass	$L_{IRRglass} = 23 + 0.3f_c$
concrete	$L_{concrete} = 5 + 4f_c$
Wood	$L_{wood} = 4.85 + 0.12f_c$

Table 3.3: O2I penetration loss models for different materials

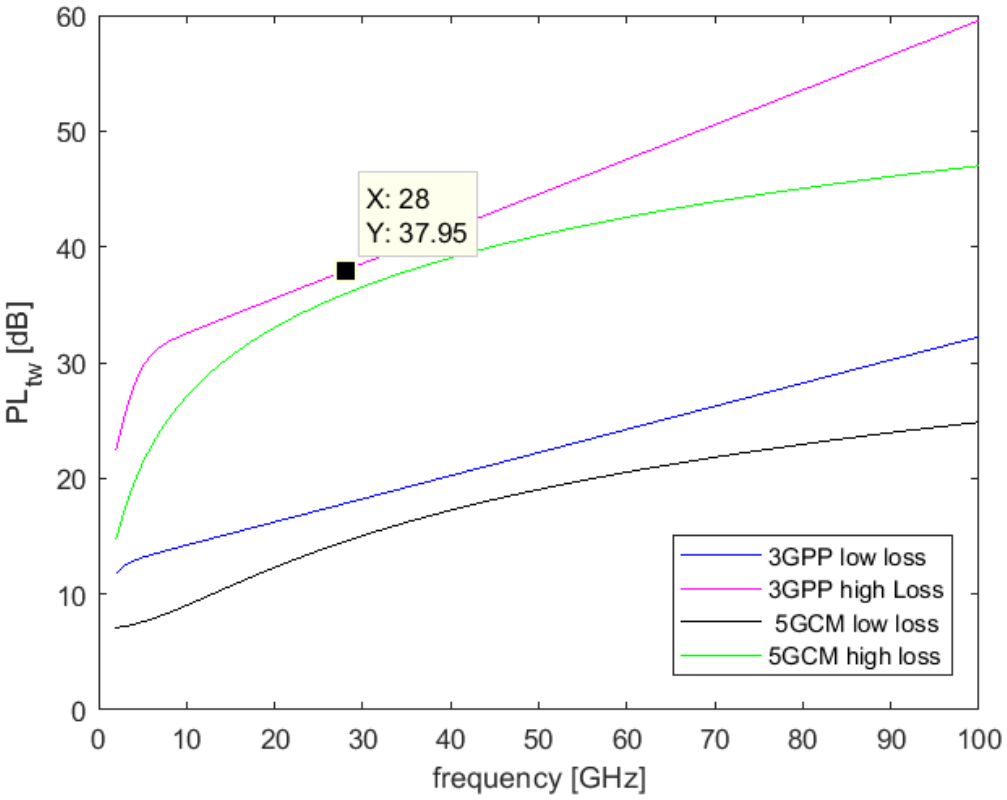

Figure 3.8: Penetration Loss models

3.2 Propagation Models

In the last years a reasonable number of organizations have gathered some measurements and surveys purposing some path loss models for both NLoS and LoS scenarios in urban or rural environment. The main contributors are:

- The 3rd Generation Partnership Project (3GPP TR 38.901) presents the findings of a channel model research for frequencies above the 6 GHz, The documentation should reflect the continuous work therefore being kept up-to-date, becoming the standard for the international industry of 5G deployment. 3GPP is the only party, studied on this chapter, that provides models for every scenario;
- The 5G Channel Model (5GCM) is an ad-hoc group of 15 companies and universities that developed models based on extensive measurements and ray-tracing results so that have helped reinforcing the 3GPP TR 38.900;
- The Mobile and wireless communications Enablers for the Twenty–twenty Information Society (METIS) is a European Union research initiative that developed a map-based channel model, which promise to be flexible and scalable to the 5G computation and accuracy requirements;
- The Millimeter-Wave Based Mobile Radio Access Network for 5G Integrated Communications (mmMAGIC) is also a large project sponsored by the European Union that worked to provide a channel model accurate for the band of frequencies between 6 and 100 GHz.

.

It is important to highlight the basic large-scale path loss models that originated the path loss models referenced in this chapter. There are two major types of large-scale path loss models, the ones that have some anchor based on the physics of transmitted power close to the antenna, which includes the close-in free space reference (CI) path loss model, usually with 1 m of reference distance, and the ones that do a mathematical curve fitting over the data set without any physical anchor to the transmitted power, namely the floating intercept model (FI) also known as ABG model, due to its three parameters α, β and γ.

The CI path model is a frequency dependent model and is based on the Friis' law, by adding a free space constant at 1 m reference inter-distance and given by equation 3.6.

$$PL^{CI}(fc, d_{3D})[dB] = FSPL(f_c, 1m) + 10nlog_{10}(d_{3D}) + \chi_{\sigma}^{CI}$$
$$FSPL(f_c, 1m)[dB] = 32.4 + 20log_{10}(f_C) \tag{3.6}$$

Where χ_{σ}^{CI} is the log normal function with zero mean and σ deviation, representing the shadow fading, n is Path Loss Exponent (PLE). CI model is also a function of the 3D euclidean distance between the transmitter and receiver (d_{3D}), represented in figure 3.9. Should be referred that the CI model has an intrinsic frequency dependence of path loss embedded within the 1 m FSPL value, and it has only one parameter, the PLE, to be optimized and which accounts for losses above 1 m of distance. Furthermore, the CI model is applicable to both single- and multi-frequency cases [25]. The 1 m reference distance is a suggested standard that ties the transmitted power or path loss to a convenient close-in distance of 1 m. By standardizing the a reference distance to 1 m the comparisons of measurements and models becomes simpler and allows faster computation of path loss [25].

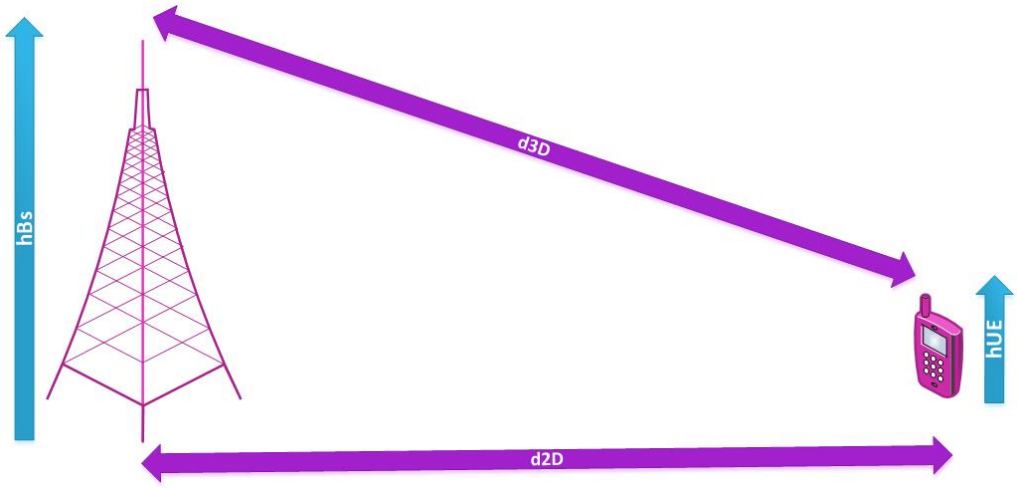

Figure 3.9: inter-distances between Tx and Rx and heights

The the CIF model is an extension of CI model, where the PLE has a frequency-dependent term, on other side if the PLE is a function of the base station height then the model is CIH, both given by equations 3.7 and 3.8.

$$PL^{CIF}(fc, d_{3D})[dB] = 32.4 + 20log_{10}(f_C) + 10n\left[1 + b\left(\frac{f_c - f_0}{f_0}\right)\right] log_{10}(d_{3D}) + \chi_{\sigma}^{CIF} \tag{3.7}$$

$$PL^{CIH}(fc, d_{3D})[dB] = 32.4 + 20log_{10}(f_C) + 10n\left[1 + b\left(\frac{h_{BS} - h_{B0}}{h_{B0}}\right)\right] log_{10}(d_{3D}) + \chi_{\sigma}^{CIH} \tag{3.8}$$

Where b is a optimization parameter, and f_0 represents a average frequency from the data used to optimize the model. The CIH model depends on a reference base station height h_{B0}.

The frequency intercept model (FI) or ABG path loss model is a three parameter model. Those parameters are calculated through a fitting process to reduce the differences found on measured data and the model simulation results. Equation 3.9 represents the model.

$$PL^{ABG}(fc, d_{3D})[dB] = 10\alpha log_{10}(d_{3D}) + \beta + 10\gamma log_{10}(f_C) + \chi_{\sigma}^{ABG} \tag{3.9}$$

Where α and γ represents the model dependencies on frequency and distance, while β indicates a optimized floating offset value.

3.2.1 UMi Scenario

As already referred the models available are defined for different scenarios, when speaking in urban environment this can be divided in the Urban Microcell (UMi) or Urban Macrocell (UMa), as in figure 3.10. UMi scenarios referrers to cell ranges of 200 m maximum, usually with base station locations below rooftops, in areas with high pedestrian density and slow vehicular traffic such as open squares or street canyons.

To predict the probability of the user equipment find a clear path to the base station, some parties have also provided LoS probability models. These models are not frequency dependent, but are functions of the 2D inter-distance between the UE and BS (d_{2D}), and also take in account two curve-fit parameters referred as $d1$ and $d2$. Table 3.4 provides each model that are plotted in figure 3.11.

Through figure 3.11 is possible to say that all LoS probability models, meaning the models that predict the probability of having LoS communication over distance, are very alike and have the same behaviour when increasing the distance between the transmitter and receiver. As most of the models are based on the same equation, the offset between the curves of 3GPP and 5GCM ($d1/d2$ model) are due to the differences between the $d1$ and $d2$ curve-fit parameters.

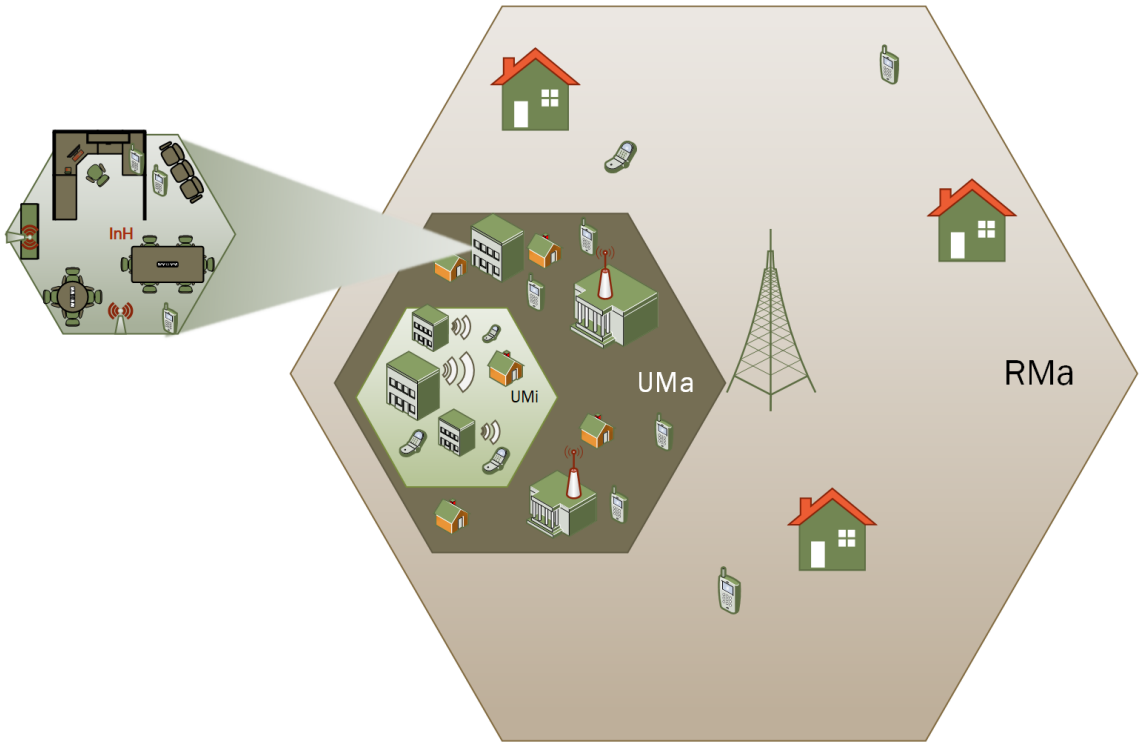

Figure 3.10: Rural and Urban environments

The 5GCM NYU model cross over the other line around the 120 m due to it is square equation. This model used a real database of New York city's downtown, showing a faster decay over distance.

Initiative	Model	Parameters
3GPP TR 38.901 [24]	$P_{LOS}(d_{2D}) = \min(\frac{d1}{d_{2D}}, 1)(1 - e^{\frac{-d_{2D}}{d2}}) + e^{\frac{-d_{2D}}{d2}}$	$d_1 = 18$ m, $d_2 = 36$ m
5GCM NYU (squared model) [26]	$P_{LOS}(d_{2D}) = (\min(\frac{d1}{d_{2D}}, 1)(1 - e^{\frac{-d_{2D}}{d2}}) + e^{\frac{-d_{2D}}{d2}})^2$	$d_1 = 22$ m, $d_2 = 100$ m
5GCM [26]	$P_{LOS}(d_{2D}) = \min(\frac{d1}{d_{2D}}, 1)(1 - e^{\frac{-d_{2D}}{d2}}) + e^{\frac{-d_{2D}}{d2}}$	$d_1 = 20$ m, $d_2 = 39$ m
METIS [27]	$P_{LOS}(d_{2D}) = \min(\frac{d1}{d_{2D}}, 1)(1 - e^{\frac{-d_{2D}}{d2}}) + e^{\frac{-d_{2D}}{d2}}$	$d_1 = 18$ m, $d_2 = 36$ m
mmMAGIC [28]	$P_{LOS}(d_{2D}) = \min(\frac{d1}{d_{2D}}, 1)(1 - e^{\frac{-d_{2D}}{d2}}) + e^{\frac{-d_{2D}}{d2}}$	$d_1 = 18$ m, $d_2 = 36$ m

Table 3.4: UMi LoS probability models

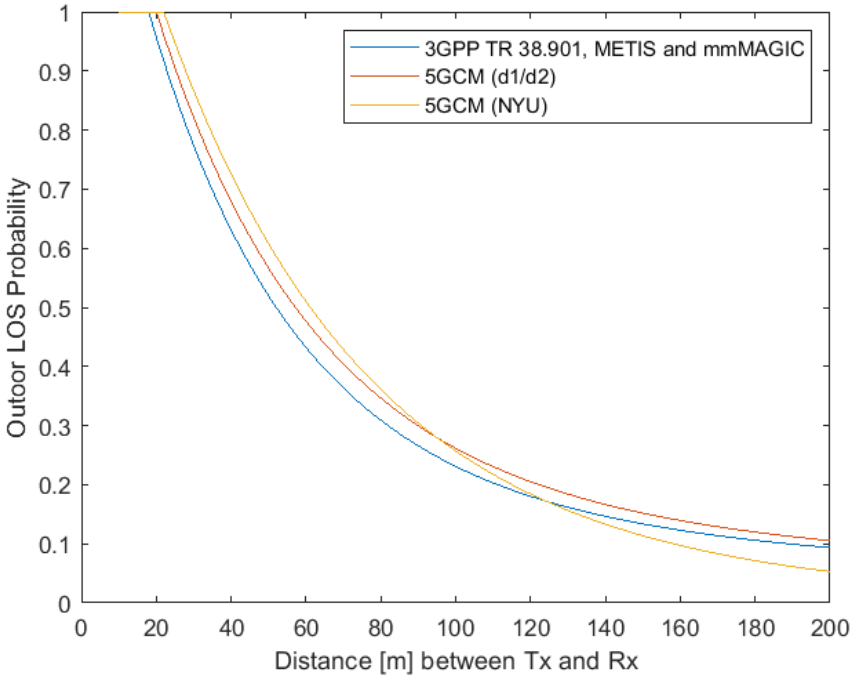

Figure 3.11: UMi LoS probability

The omnidirectional path loss models are represented in table 3.5 for UMi LoS condition.

The 3GPP model is based on measurements on a street canyon configuration, uses the 3D T-R distance and is a breakpoint model at d'_{BP}, in equation 3.10, that is a function of the frequency and of both base station and user equipment heights. This is not yet confirmed by measurements, but some ray-tracing simulations indicates that on UMi scenarios, where cell radius is typically less then 500 m, the breakpoint distance is not necessary because it exceeds the cell radius [29]. Therefore the primary model is a CI based model with a PLE of 2.1, which is very close to the PLE predicted by Friis' law.

The 5GCM presents models for both street canyon and open square configurations, both are CI based models differing on the PLE and variance of the shadow fading. METIS model is similar to the 3GPP presenting a breakpoint model as well, but this model predicts a break even in the UMi typical cell radius. This breakpoint is given by equation 3.11.The model given by mmMAGIC project is a ABG model with $\alpha = 1.92, \beta = 32.9$ and $\gamma = 2.08$.

Initiative	Model	Shadowing fading [dB]	Parameters
3GPP Street Canyon [24]	$PL = \begin{cases} PL_1, & 10 \leqslant d_{2D} \leqslant d'_{BP} \\ PL_2, & d'_{BP} \leqslant d_{2D} \leqslant 5Km \end{cases}$ $PL_1 = 32.4 + 21log_{10}(d_{3D}) + 20log_{10}(f_c)$ $PL_2 = 32.4 + 40log_{10}(d_{3D}) + 20log_{10}(f_c)$ $- 9.5log_{10}\left[(d'_{BP})^2 + (h_{BS} - h_{UE})^2\right]$ where d'_{BP} in eq. 3.10	$\sigma = 4.0$	$0.5 < f_c < 100GHz$ $1.5m \leqslant h_{UE} \leqslant 22.5m$ $h_{BS} = 10m$
5GCM Street Canyon [26]	CI model with 1 m reference distance: $PL = 32.4 + 21log_{10}(d_{3D}) + 20log_{10}(f_c)$	$\sigma = 3.76$	$6 < f_c < 100GHz$
5GCM Open Square [26]	CI model with 1 m reference distance: $PL = 32.4 + 18.5log_{10}(d_{3D}) + 20log_{10}(f_c)$	$\sigma = 4.2$	$6 < f_c < 100GHz$
METIS Street Canyon [27]	$PL = \begin{cases} PL_1, & 10 \leqslant d_{3D} \leqslant d'_{BP} \\ PL_2, & d'_{BP} \leqslant d_{3D} \leqslant 500m \end{cases}$ $PL_1 = 28 + 22log_{10}(d_{3D}) + 20log_{10}(f_C) + PL_0$ $PL_2 = 7.8 + 40log_{10}(d_{3D}) + 2log_{10}(f_c)$ $+ PL_1(d_{BP}) - 18log_{10}(h_{BS}h_{UE})$ where d_{BP} and PL_0 in eq. 3.11 and 3.12	$\sigma = 3.1$	$0.8 < f_c < 60GHz$ $1.5m \leqslant h_{UE} \leqslant 22.5m$ $h_{BS} = 10m$
mmMAGIC Street Canyon [28]	$PL = 19.2log_{10}(d_{3D}) + 32.9 + 20.8log_{10}(f_c)$	$\sigma = 2.0$	$6 < f_c < 100GHz$

Table 3.5: UMi LoS Path Loss models

$$\begin{aligned} d'_{BP} &= 4h'_{BS}h'_{UE} \times f_c \times \frac{10^9}{c} \\ h'_{BS} &= h_{BS} - 1.0 \\ h'_{UE} &= h_{UE} - 1.0 \end{aligned} \tag{3.10}$$

$$d_{BP} = 0.87e^{\frac{-log_{10}(f_c)}{0.65}} \times \frac{4(h_{BS} - 1)(h_{UE} - 1)}{\lambda} \tag{3.11}$$

$$PL_0 = -1.38log_{10}(f_c) + 3.34 \tag{3.12}$$

Figure 3.12 shows the behavior of the path loss models described above for a maximum cell radius of 400 m, or in other words, a maximum of 400 m of 2D distance between the transmitter and receiver and for a carrier frequency of 28 GHz. All the models have a similar behaviour, and the small differences can be explained by the shadow fading variance σ between models. As expected the METIS model has a deviation at about the 157 m mark, where the model changes it's pattern showing a much bigger loss regarding the other models (around 80

dB). The table 3.6 presents all the models for NLoS conditions. The 3GPP entity

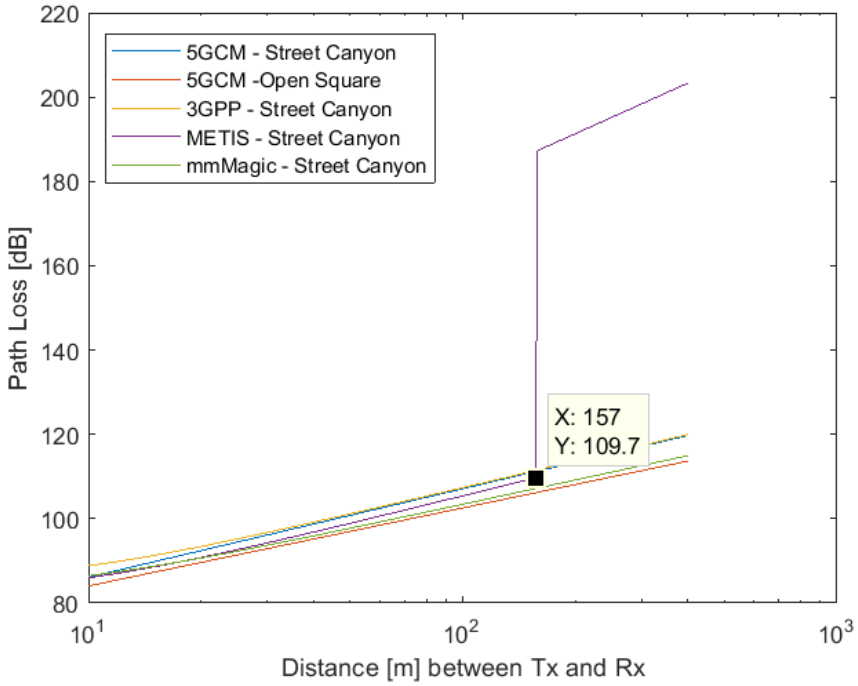

Figure 3.12: Path loss for LoS UMi

presents two options, the first model takes in account their path loss result on Los condition, presented on table 3.5, and considers the actual NLoS path loss the maximum between the LoS and NLoS result, they also present a CI model option for the calculation of NLoS path loss.

The 5GCM party also suggest two options for both street canyon and open square configurations, a CI model and a ABG model. The mmMAGIC project introduces a ABG model again. The METIS project has come to a NLoS model that is only applicable to frequencies between 0.45 and 6 GHz, so it is not applicable to the frequencies range of this work's interest.

The representation of each model is on figure 3.13. It is showed that the mmMAGIC model has a bigger loss prediction pattern than the other model, that can be explained by the β value of 31.0, becoming an offset compared with the other models. The remaining models converge to a similar path loss value when increasing the distance. Only the 5GCM CI model, for the open square configuration, has smaller increase of path loss for bigger distances. that is explained by the smaller PLE value of 2.89.

Initiative	Model	Shadowing fading [dB]	Parameters
3GPP Street Canyon [24]	$PL = \max(PL_{UMi-LoS}(d_{3D}), PL_{UMi-NLos}(d_{3D}))$ $PL_{UMi-NLoS} = 22.4 + 35.3log_{10}(d_{3D}) + 21.3log_{10}(f_c)$ $- 0.3(h_{UE} - 1.5)$ Option: CI model with 1 m reference distance $PL = 32.4 + 31.9log_{10}(d_{3D}) + 20log_{10}(f_c)$	$\sigma = 7.82$ $\sigma = 8.2$	$0.5 < f_c < 100GHz$ $1.5m \leqslant h_{UE} \leqslant 22.5m$ $h_{BS} = 10m$
5GCM Street Canyon [26]	CI model with 1 m reference distance: $PL = 32.4 + 31.7log_{10}(d_{3D}) + 20log_{10}(f_c)$ ABG model: $PL = 22.4 + 35.3log_{10}(d_{3D}) + 21.3log_{10}(f_c)$	$\sigma = 8.09$ $\sigma = 7.82$	$6 < f_c < 100GHz$
5GCM Open Square [26]	CI model with 1 m reference distance: $PL = 32.4 + 28.9log_{10}(d_{3D}) + 20log_{10}(f_c)$ ABG model: $PL = 3.66 + 41.4log_{10}(d_{3D}) + 24.3log_{10}(f_c)$	$\sigma = 7.1$ $\sigma = 7.0$	$6 < f_c < 100GHz$
mmMAGIC Street Canyon [28]	$PL = 45.0log_{10}(d_{3D}) + 31.0 + 20.0log_{10}(f_c)$	$\sigma = 7.82$	$6 < f_c < 100GHz$

Table 3.6: Umi NLoS Path Loss models

The aim of figure 3.14 is to represent a comparison between the NLoS and LoS path loss models of the 3GPP and 5GCM parties for the street canyon configuration, which are represented as magenta and blue traces respectively. As expected the NLoS models predict higher path losses for the same distances then the LoS models, due to the fact that in NLoS condition the main source of received power is from reflected or scattered MPCs (Multipath Components). The orange traces were originated through the calculation of the arithmetic average of the plotted models for both LoS and NLoS conditions.

Through the orange traces of the prior graphic is possible to calculate the average difference of the path loss for the UMi scenario over distance, plotted on figure 3.15. Showing a maximum rounding 33 dB for 400 m of distance, between the transmitter and the receiver. As expected the difference between the NLoS and LoS increase with the distance, because the NLoS path loss has a faster increase due to the increase of obstacles.

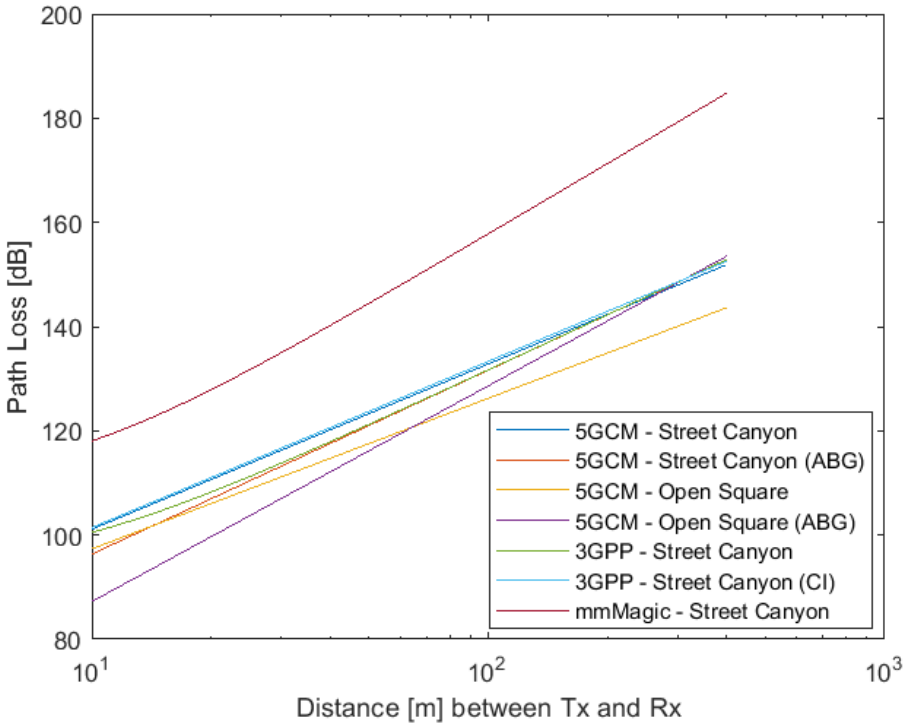

Figure 3.13: Path loss for NLoS UMi

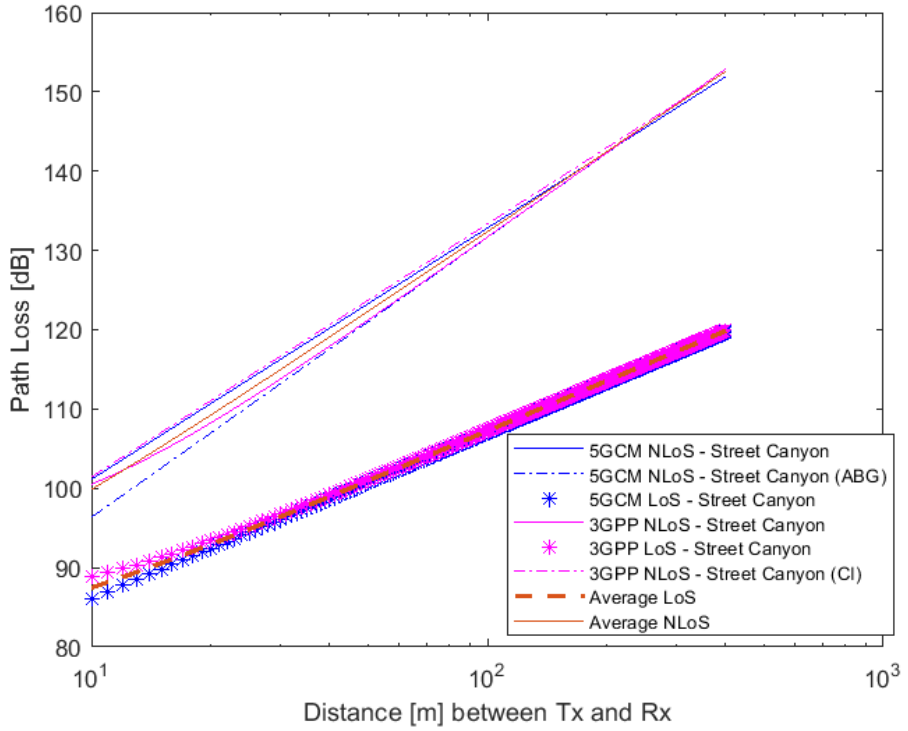

Figure 3.14: Path loss for NLoS Vs LoS on UMi

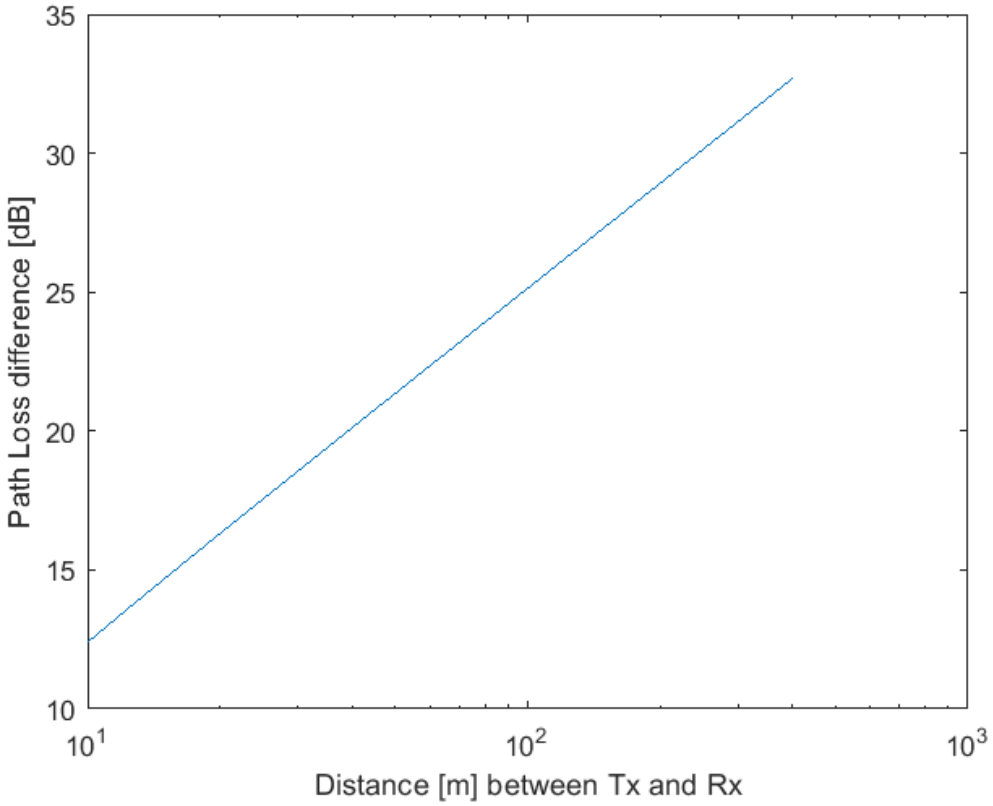

Figure 3.15: Path loss difference between NLoS and LoS on UMi

3.2.2 UMa Scenario

When analysing propagation in a urban environment it also can be in a macrocell typology, the called UMa scenario. The macrocell architecture is defined by having the base stations mounted above the rooftops, typically at heights of 25 to 30 m, and no more then 500 m of cell radius.

In resemblance with the UMi scenario it is also important to study the LoS probaibility of the models presented. LoS probability models are in table 3.7 for UMa scenario, which are very similar with the UMi models, the main difference is the dependency of a height-dependent function C, in equation 3.13, that depends from the user equipment height, this is only applicable when the mobile is at a position higher then 13 m. As in the UMi scenario all LoS probability models are based on the 3GPP's, diverging only on the curve fit parameters. All models are represented in figure 3.16, showing that the 5GCM NYU square model is the one that predicts a lower probability, although all models have similar performances.

Initiative	Model	Parameters
3GPP TR 38.901 [24]	$P_{LOS} = (\min(\frac{d1}{d_{2D}}, 1)(1 - e^{\frac{-d_{2D}}{d2}}) + e^{\frac{-d_{2D}}{d2}})(1 + C(d_{2D}, h_{UE})$	$d_1 = 18$ m, $d_2 = 63$ m
5GCM NYU (squared model) [26]	$P_{LOS} = ((\min(\frac{d1}{d_{2D}}, 1)(1 - e^{\frac{-d_{2D}}{d2}}) + e^{\frac{-d_{2D}}{d2}})(1 + C(d_{2D}, h_{UE})))^2$	$d_1 = 20$ m, $d_2 = 160$ m
5GCM [26]	$P_{LOS} = (\min(\frac{d1}{d_{2D}}, 1)(1 - e^{\frac{-d_{2D}}{d2}}) + e^{\frac{-d_{2D}}{d2}})(1 + C(d_{2D}, h_{UE})$	$d_1 = 20$ m, $d_2 = 66$ m
METIS [27]	$P_{LOS} = (\min(\frac{d1}{d_{2D}}, 1)(1 - e^{\frac{-d_{2D}}{d2}}) + e^{\frac{-d_{2D}}{d2}})(1 + C(d_{2D}, h_{UE})$	$d_1 = 18$ m, $d_2 = 63$ m

Table 3.7: UMa LoS probability models

$$C(d_{2D}, h_{UE}) = \begin{cases} 0, \ h_{UE} < 13m \\ \left(\frac{h_{UE}-13}{10}\right)^{1.5} \times g(d_{2D}), 13m \leqslant h_{UE} \leqslant 23m \end{cases}$$
$$g(d_{2D}) = \begin{cases} 0, \ d_{2D} \leqslant 18m \\ (1.25 \times 10^{-6})(d_{2D})^3(\frac{-d_{2D}}{150}), 18m < d_{2D} \end{cases} \tag{3.13}$$

These models also have similar performance compared with the UMi LoS probability models, on figure 3.11, at 200 m of distance, both sets of models predict 10 % of probability of achieving LoS communication.

The LoS path loss models for the UMa scenario can be found on table 3.8. For

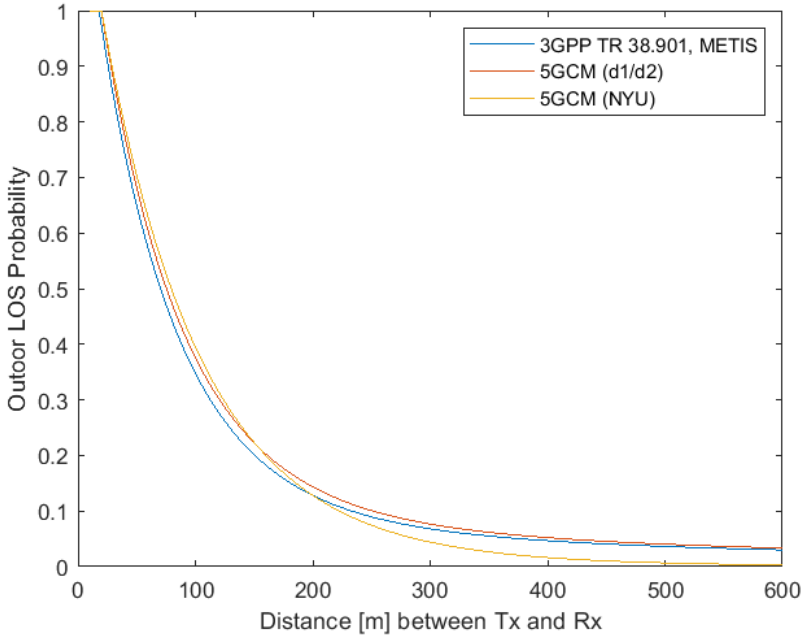

Figure 3.16: UMa LoS probability

this study only the 3GPP and 5GCM models are considered, although the METIS party has adopted the model published by 3GPP TR36.873 [29], it is only applicable to frequencies until 6 GHz, which is below of the range this work is contemplating. The UMa LoS 3GPP model is adapted from the the 3GPP TR36.873 [24]. The 5GCM model is a CI model akin to the UMi LoS model, only lowering its PLE value, which points to less losses over distance [29].

Figure 3.17 presents the evolution of the above two models over distance using a carrier frequency of 28 GHz. As expected the performances look alike.

Initiative	Model	Shadowing fading [dB]	Parameters
3GPP [24]	$PL = \begin{cases} PL_1, & 10 \leqslant d_{2D} \leqslant d'_{BP} \\ PL_2, & d'_{BP} \leqslant d_{2D} \leqslant 5Km \end{cases}$ $PL_1 = 28.0 + 22log_{10}(d_{3D}) + 20log_{10}(f_c)$ $PL_2 = 28.0 + 40log_{10}(d_{3D}) + 20log_{10}(f_c)$ $- 9log_{10}((d'_{BP})^2 + (h_{BS} - h_{UE})^2)$ where d'_{BP} in eq. 3.10	$\sigma = 4.0$	$0.5 < f_c < 100GHz$ $1.5m \leqslant h_{UE} \leqslant 22.5m$ $h_{BS} = 25m$
5GCM [26]	CI model with 1 m reference distance: $PL = 32.4 + 20log_{10}(d_{3D}) + 20log_{10}(f_c)$	$\sigma = 4.1$	$6 < f_c < 100GHz$

Table 3.8: UMa LoS Path Loss models

Table 3.9 contains the NLoS path loss models for UMa scenario, as in UMi scenario the 5GCM project presents two options of models, a CI and ABG model.

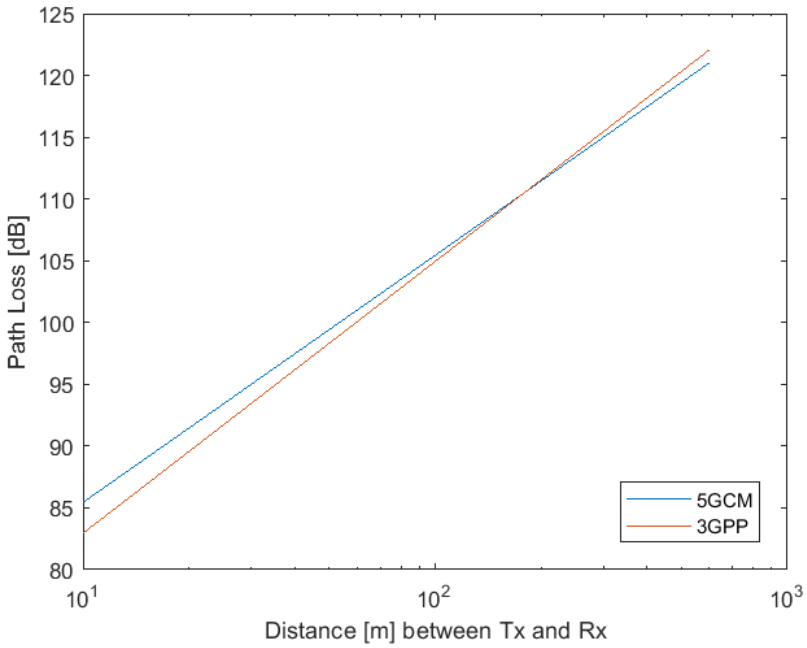

Figure 3.17: Path loss for LoS UMa

The 3GPP also follows the same approach as in UMi, presenting a CI model option. Figure 3.18 represents graphically the models, and as expected, have a similar evolution over distance. On figure 3.19 is a visual comparison between the

Initiative	Model	Shadowing fading [dB]	Parameters
3GPP [24]	$PL = \max(PL_{UMa-LoS}(d_{3D}), PL_{UMa-NLos}(d_{3D}))$ $PL_{UMa-NLoS} = 13.54 + 39.08log_{10}(d_{3D}) + 20log_{10}(f_c)$ $- 0.6(h_{UE} - 1.5)$ Option: CI model with 1 m reference distance $PL = 32.4 + 30log_{10}(d_{3D}) + 20log_{10}(f_c)$	$\sigma = 6.0$ $\sigma = 7.8$	$0.5 < f_c < 100GHz$ $1.5m \leqslant h_{UE} \leqslant 22.5m$ $h_{BS} = 25m$
5GCM [26]	CI model with 1 m reference distance: $PL = 32.4 + 30log_{10}(d_{3D}) + 20log_{10}(f_c)$ ABG model: $PL = 19.2 + 34log_{10}(d_{3D}) + 23log_{10}(f_c)$	$\sigma = 6.8$ $\sigma = 6.5$	$6 < f_c < 100GHz$

Table 3.9: UMa NLoS Path Loss models

5GCM and 3GPP NLoS and LoS models for the UMa scenario, resembling to the UMi scenario it is also presented an average model for each condition, and it is used the same color scheme to represent each class of model. In figure 3.20 the difference between those average behaviors has similar values on the distance limits as in UMi.

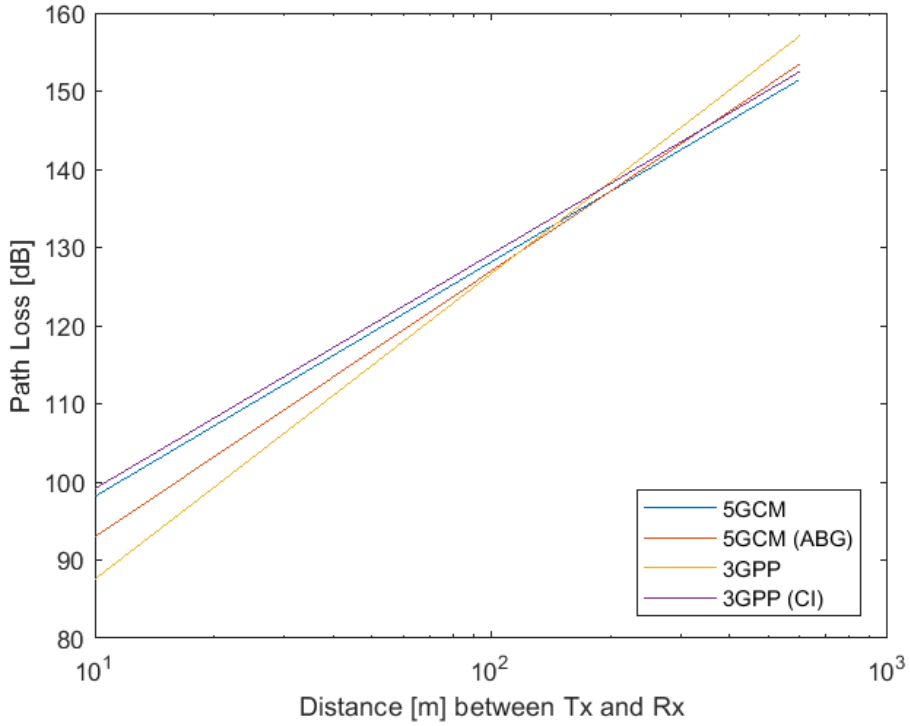

Figure 3.18: Path loss for NLoS UMa

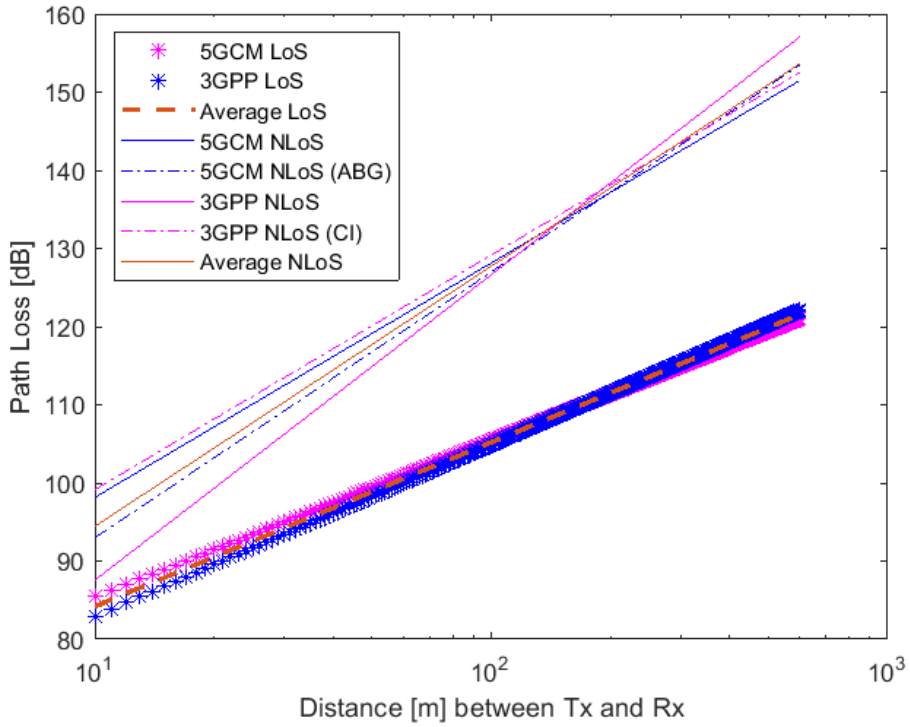

Figure 3.19: Path loss for NLoS Vs LoS on UMa

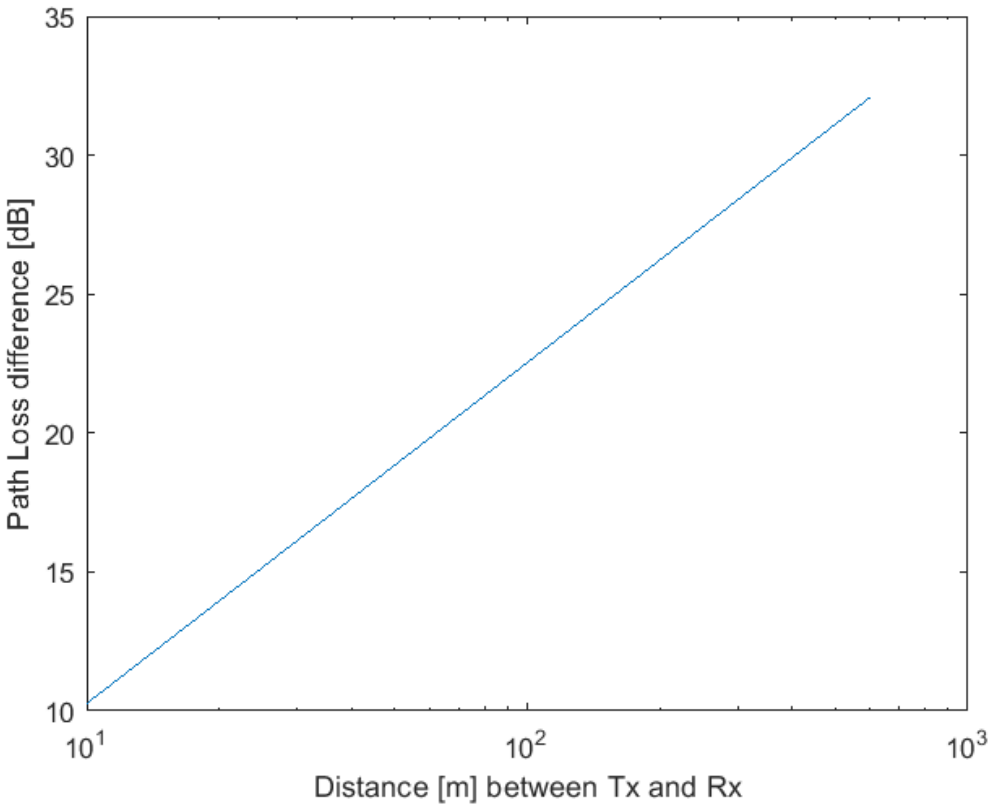

Figure 3.20: Path loss difference between NLoS and LoS on UMa

3.2.3 RMa Scenario

When switching to a rural environment or so called Rural Macrocell (RMa) scenario the base station usually sets at a height range between 10 to 150 m and the distance between the transmitter and receiver can reach at least till 5 Km [29].

Neither mmMAGIC, METIS or 5GCM had come up with a propagation model to the RMa scenario. The 3GPP TR 38.901 RMa path loss model is based on the ITU-R M.2135 model for sub-6 GHz, as the LOS probability model published, equation 3.14 [29]. 3GPP validated their model by a single measurement campaign using a 24 GHz carrier [24].

$$P_{LoS} = \begin{cases} 0, d_{2D} \leqslant 10m \\ e^{\left(-\frac{d_{2D}-10}{1000}\right)}, 10m < d_{2D} \end{cases} \tag{3.14}$$

The authors on [30] have developed a path Loss model for rural areas for the millimeter waves based on 73 GHz measurement campaigns for both LoS and NLoS conditions. They also present two model options of the 3GPP/ITUR model, that can be employed on frequencies above the 500 MHz till 100 GHz [30]. They present a closed-in model option and a CIH model with a PLE dependent on the base station height. They have showed that the RMa path loss can be modeled by a simpler model and achieve identical performances, through Monte Carlo simulations 1) for the 3GPP's default parameters on table 3.10 and 2) for the default parameters but varying the base station height.

RMa LoS default values
$10m < d_{2D} < 10Km$
$h_{BS} = 35m,\ h_{UE} = 1.5m,\ W = 20m,\ h = 5m$
applicability ranges: $5m < h < 50m;\ 5m < W < 50m;$
$10m < h_{BS} < 150m;\ 1m < h_{UE} < 10m$
RMa NLoS default values
$10m < d_{2D} < 5Km$
$h_{BS} = 35m,\ h_{UE} = 1.5m,\ W = 20m,\ h = 5m$
applicability ranges: $5m < h < 50m;\ 5m < W < 50m;$
$10m < h_{BS} < 150m;\ 1m < h_{UE} < 10m$

Table 3.10: 3GPP RMa path loss model default parameters and applicability ranges [24]

The path loss models for LoS condition is presented on table 3.11. The models proposed on [30] are represented as NYU's models.

The W variable on 3GPP original model average street width and parameter h is the average building height. It is possible to say that the 3GPP original model is a break point model, although the break point distance exceeds the LoS d_{2D} limit of 10 Km for the 28 GHz carrier used on this study, which means that 3GPP model is a single-slope model on this frequency.

Initiative	Model	Shadowing fading [dB]
3GPP [24]	$PL = \begin{cases} PL_1, & 10 \leqslant d_{2D} \leqslant d_{BP} \\ PL_2, & d_{BP} \leqslant d_{2D} \leqslant 10Km \end{cases}$ $PL_1 = 20log_{10}(40\pi d_{3D}\frac{fc}{3}) + min(0.03h^{1.72}, 10)log_{10}(d_{3D})$ $- min(0.044h^{1.72}, 14.77) + 0.002log_{10}(h)d_{3D}$ $PL_2 = PL_1(d_{BP}) + 40log_{10}(d_{3D}/d_{BP})$ where d_{BP} in equation 3.15	$\sigma = 4.0$ $\sigma = 6.0$
adapted 3GPP [30]	CI model with 1 m reference distance: $PL = 32.4 + 23.1log_{10}(d_{3D}) + 20log_{10}(f_c)$ CIH model with h_{B0} = 35 m: $PL = 32.4 + 23.1\left(1 - 0.006\left(\frac{h_{BS} - 35}{35}\right)\right) log_{10}(d_{3D}) + 20log_{10}(f_c)$	$\sigma = 5.9$ $\sigma = 5.6$
NYU [30]	CI model with 1 m reference distance: $PL = 32.4 + 21.6log_{10}(d_{3D}) + 20log_{10}(f_c)$ CIH model with h_{B0} = 35 m: $PL = 32.4 + 23.1\left(1 - 0.03\left(\frac{h_{BS} - 35}{35}\right)\right) log_{10}(d_{3D}) + 20log_{10}(f_c)$	$\sigma = 1.7$ $\sigma = 1.7$

Table 3.11: RMa LoS Path Loss models

$$d_{BP} = 2\pi h_{BS} h_{UE} \frac{fc}{c} \tag{3.15}$$

Figure 3.21 presents a graphic comparison of all models using the default values of 3GPP model. It's possible to say the adapted 3GPP CI and CIH models have similar performances. The original 3GPP model is not physically proven to be suitable for frequencies above the 30 GHz, and have some differences regarding the alternative models, due to it's complexity and odd parameters, such as parameters W and h, that does not make sense when talking in rural areas [30]. NYU models are less conservative, predicting lower path loss values.

For the NLoS models there is the same number of options to model the path loss, observable on table 3.12, and plotted on figure 3.22, showing that the NYU CI option predicts lower losses for the same distance, due to the lower PLE of 2.75.

As in the prior scenarios, figure 3.23 presents the same kind of comparison

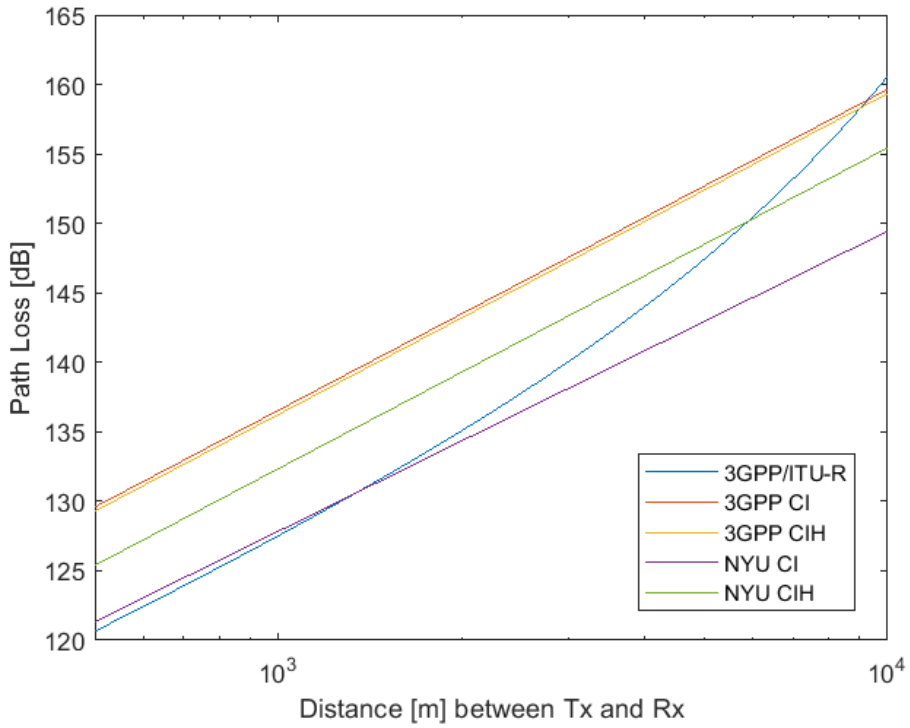

Figure 3.21: Path loss for LoS RMa

between path loss models when in presence or absence of the line of sight. For this graphic only the original 3GPP/ITU-R and NYU suggested models were used, represented in magenta, blue and orange as the others scenarios.

Once again figure 3.24 presents a similar increase pattern for the difference between NLoS and LoS path Loss.

Initiative	Model	Shadowing fading [dB]
3GPP [24]	$PL = \max(PL_{RMa-LOS}, PL_{RMa-NLOS})$ $PL_{RMa-NLOS} = 161.04 - 7.1log_{10}(W) + 7.5log_{10}(h) - (24.37 - 3.7\left(\frac{h}{h_{BS}}\right)^2)log_{10}(h_{BS})$ $+ (43.42 - 3.1log_{10}(h_{BS}))(log_{10}(d_{3D}) - 3) + 20log_{10}(fc)$ $- (3.2(log_{10}(11.75h_{UE}))^2 - 4.97)$	$\sigma = 8.0$
adapted 3GPP [30]	CI model with 1 m reference distance: $PL = 32.4 + 30.4log_{10}(d_{3D}) + 20log_{10}(f_c)$ CIH model with h_{B0} = 35 m: $PL = 32.4 + 30.7\left(1 - 0.06\left(\frac{h_{BS} - 35}{35}\right)\right) log_{10}(d_{3D}) + 20log_{10}(f_c)$	$\sigma = 8.2$ $\sigma = 8.7$
NYU [30]	CI model with 1 m reference distance: $PL = 32.4 + 27.5log_{10}(d_{3D}) + 20log_{10}(f_c)$ CIH model with h_{B0} = 35 m: $PL = 32.4 + 30.7\left(1 - 0.049\left(\frac{h_{BS} - 35}{35}\right)\right) log_{10}(d_{3D}) + 20log_{10}(f_c)$	$\sigma = 6.7$ $\sigma = 6.7$

Table 3.12: RMa NLoS Path Loss models

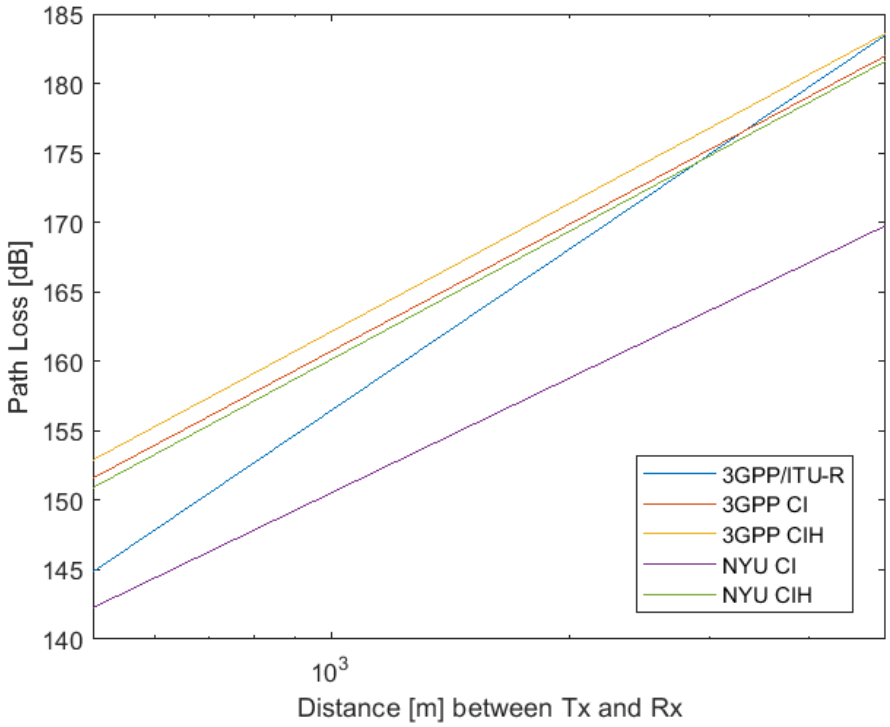

Figure 3.22: Path loss for NLoS RMa

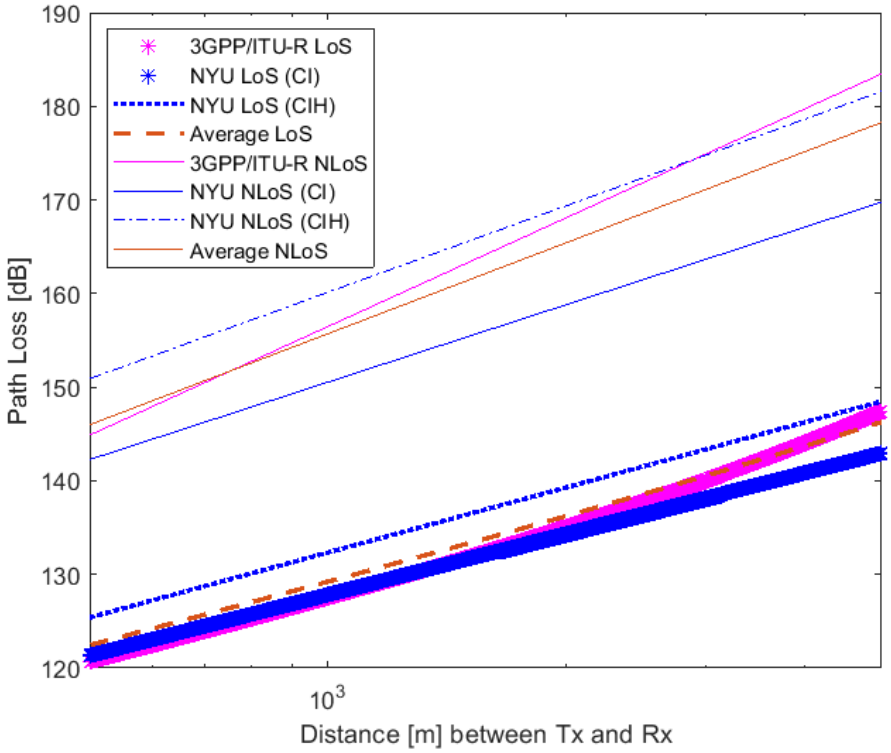

Figure 3.23: Path loss for NLoS Vs LoS RMa

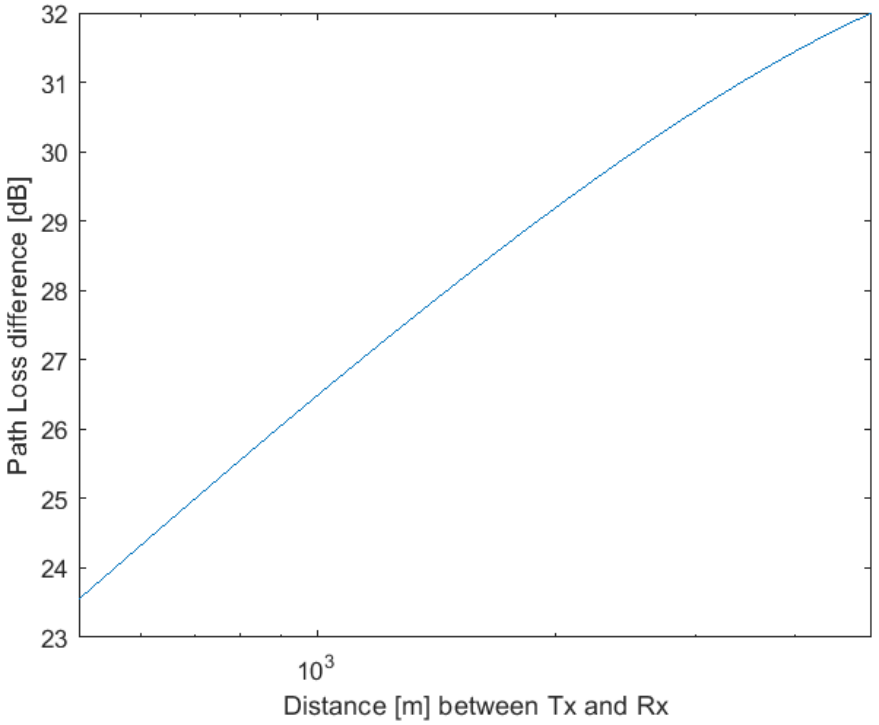

Figure 3.24: Path loss difference between NLoS and LoS RMa

3.2.4 InH Scenario

It is also important to have a view of the propagation of millimeter waves inside doors that is the Indoor Hotspot (InH) scenario.

There are multiple organizations that have been successfully on providing propagation models for the indoor scenario. The 5GCM have proposed single and dual-slope models for both LoS and NLoS conditions, although only the single-slope models are explored in this section, due to its simplicity and the fact that there is no guarantee of benefit when using the dual-slope [24]. They also proposed different models for a shopping mall scenario and for an open office. On release 16 of 3GPP TR 38.901 is also presented an InH model but only for office scenario. The mmMAGIC group have presented InH models for LoS and NLoS condition without specifying the measured scenario. Although METIS have also proposed a model for indoor offices, it is only valid for the 63 GHz frequency, not reflecting interest on this dissertation, so will not be presented.

The LoS models are on table 3.13 where is visible that both models of 5GCM and the one from 3GPP are identical CI models with the same PLE, only varying the shadowing fading. The mmMAGIC has a ABG model. The graphic representation of these models are on figure 3.25, showing a more optimist performance on the mmMAGIC model.

Initiative	Model	Shadowing fading [dB]	Parameters
3GPP Indoor-Office [24]	$PL_{InH-LoS} = 32.4 + 17.3log_{10}(d_{3D}) + 20log_{10}(f_c)$	$\sigma = 3.0$	$0.5 < f_c < 100GHz$ $1m \leqslant d_{3D} \leqslant 100m$
5GCM Indoor-Office [26]	$PL_{InH-LoS} = 32.4 + 17.3log_{10}(d_{3D}) + 20log_{10}(f_c)$	$\sigma = 3.02$	$6 < f_c < 100GHz$
5GCM Shopping-Mall [26]	$PL_{InH-LoS} = 32.4 + 17.3log_{10}(d_{3D}) + 20log_{10}(f_c)$	$\sigma = 2.01$	$6 < f_c < 100GHz$
mmMAGIC [28]	$PL_{InH-LoS} = 33.6 + 13.8log_{10}(d_{3D}) + 20.3log_{10}(f_c)$	$\sigma = 1.18$	$6 < f_c < 100GHz$

Table 3.13: InH LoS Path Loss models

The NLoS InH models are given by the equations on table 3.14. The 5GCM party presents an ABG model and CIF with a frequency reference of 24.2 GHz for the indoor-office model and a frequency reference of 39.5 GHz for the shopping-mall option. The 3GPP have decreased the distance applicability range of the NLoS model compared with the LoS.

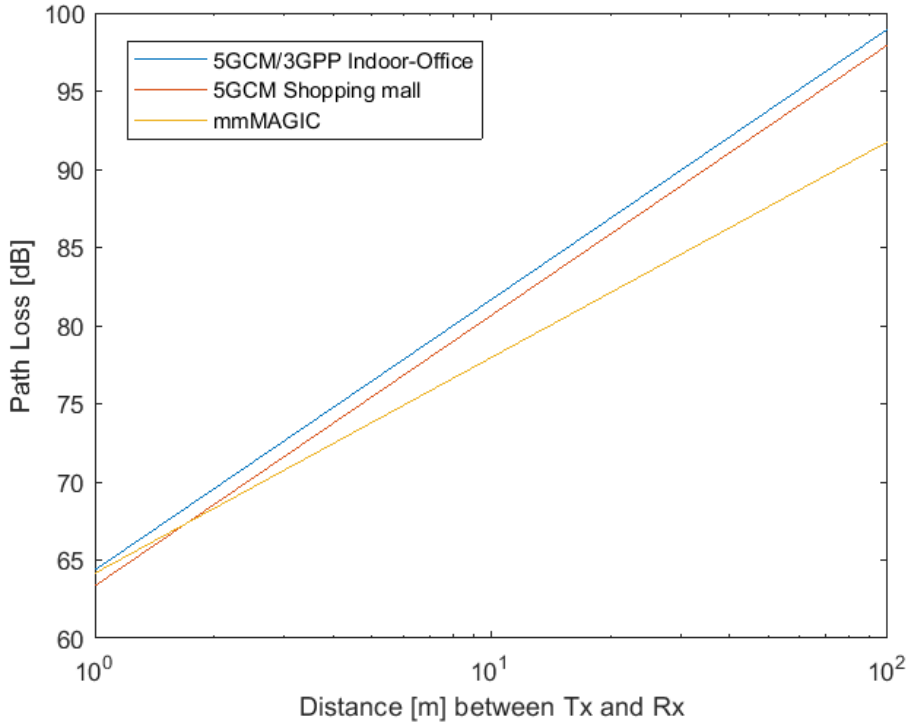

Figure 3.25: Path loss for LoS InH

The performances of each model are represented on figure 3.26 where is possible to observe that most of the models converges to similar path loss values in exception of the 5GCM shopping mall models indicating lower losses for the same distances. Both figure 3.27 and figure 3.28 presents similar performances as in the other scenarios when comparing NLoS and LoS models for the indoor scenario, the average difference among the two condition have the same maximum value. It's worth mentioning that on shorter distances there is no difference between the NLoS and LoS models because when considering the InH the range is no more than 100 m.

Initiative	Model	Shadowing fading [dB]	Parameters
3GPP Indoor-Office [24]	$PL = \max(PL_{InH-LoS}, PL_{InH-NLoS})$ $PL_{InH-NLoS} = 17.3 + 38.3log_{10}(d_{3D}) + 24.9log_{10}(f_c)$ CI model with 1 m reference distance: $PL = 32.4 + 31.9log_{10}(d_{3D}) + 20log_{10}(f_c)$	$\sigma = 8.03$ $\sigma = 8.29$	$0.5 < f_c < 100GHz$ $1m \leqslant d_{3D} \leqslant 86m$
5GCM Indoor-Office [26]	ABG model: $PL = 17.3 + 38.3log_{10}(d_{3D}) + 24.9log_{10}(f_c)$ CIF model: $PL = 32.4 + 31.9\left[1 - 0.06\left(\frac{f_c - 24.2}{24.2}\right)\right]log_{10}(d_{3D}) + 20log_{10}(f_c)$	$\sigma = 8.03$ $\sigma = 8.29$	$6 < f_c < 100GHz$
5GCM Shopping-Mall [26]	ABG model: $PL = 18.09 + 32.1log_{10}(d_{3D}) + 22.4log_{10}(f_c)$ CIF model: $PL = 32.4 + 25.9\left[1 - 0.01\left(\frac{f_c - 39.5}{39.5}\right)\right]log_{10}(d_{3D}) + 20log_{10}(f_c)$	$\sigma = 6.97$ $\sigma = 7.40$	$6 < f_c < 100GHz$
mmMAGIC [28]	$PL = \max(PL_{InH-LoS}, PL_{InH-NLoS})$ $PL_{InH-NLoS} = 15.2 + 36.9log_{10}(d_{3D}) + 26.8log_{10}(f_c))$	$\sigma = 8.03$	$6 < f_c < 100GHz$

Table 3.14: InH NLoS Path Loss models

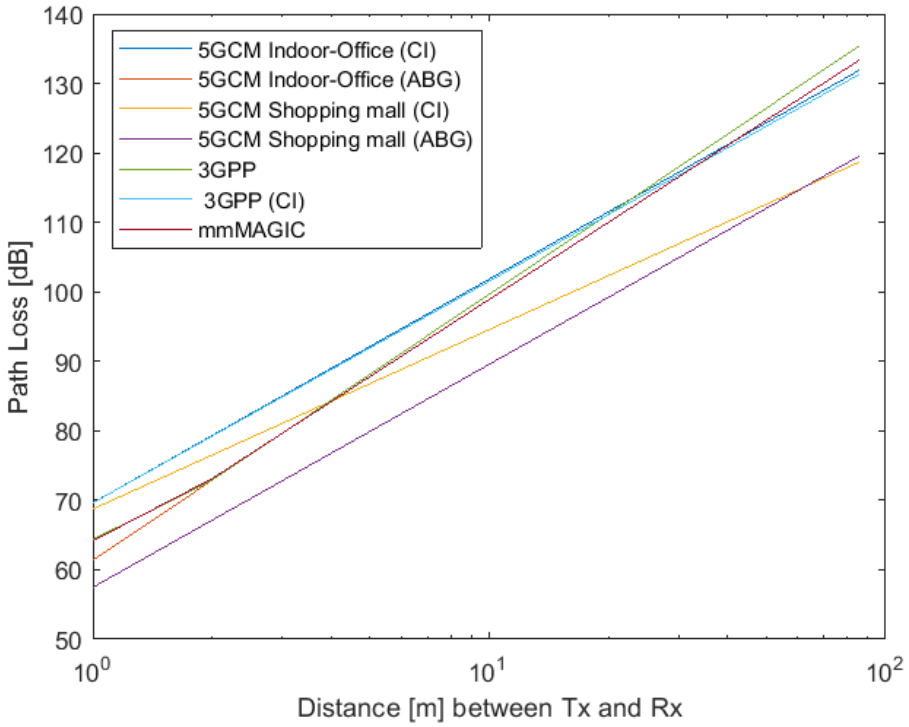

Figure 3.26: Path loss for NLoS InH

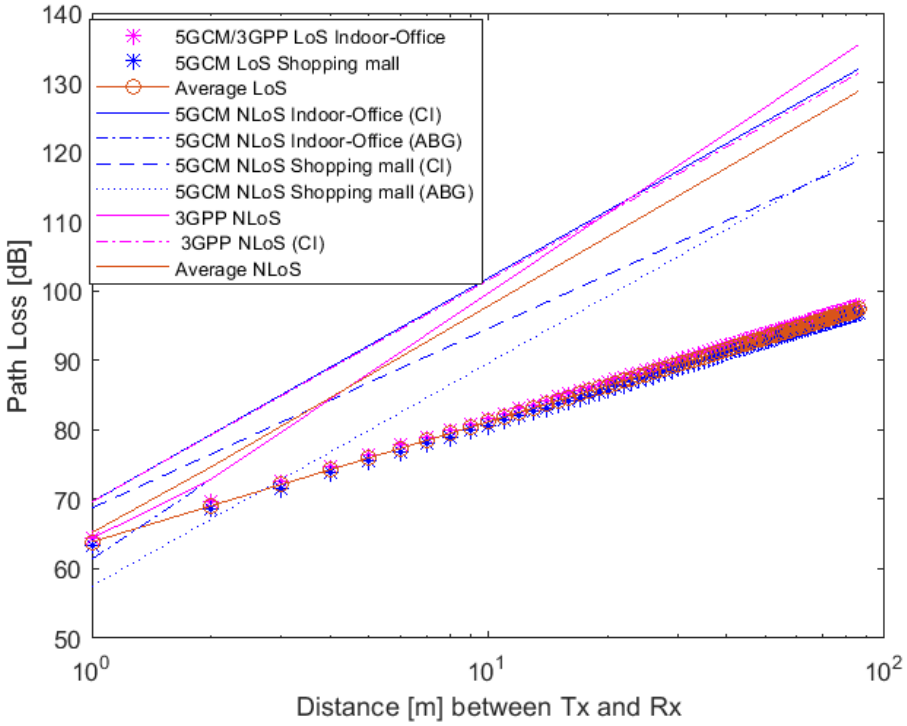

Figure 3.27: Path loss for NLoS Vs LoS InH

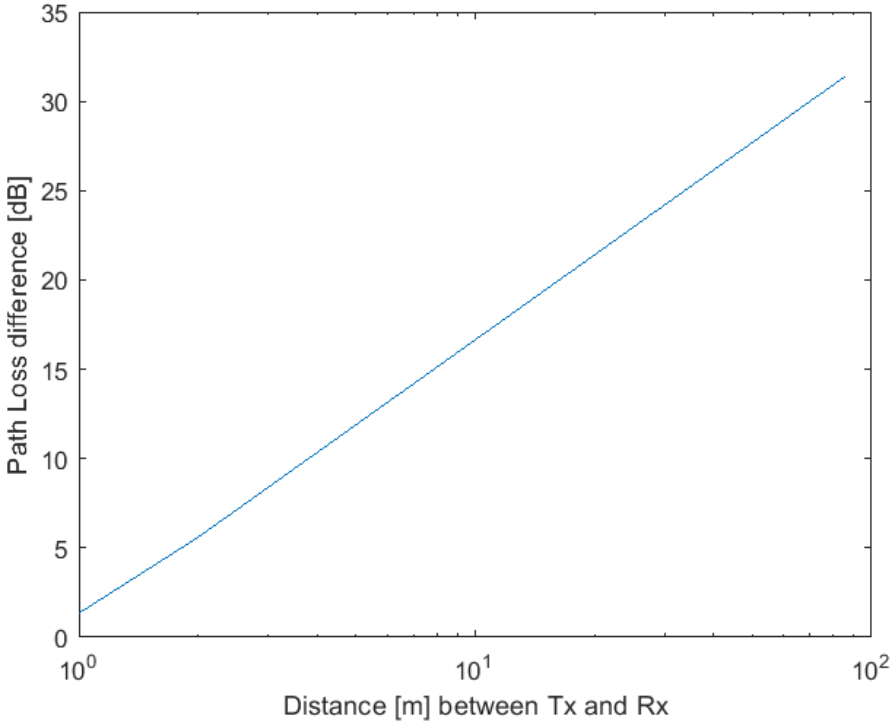

Figure 3.28: Path loss difference between NLoS and LoS InH

3.2.5 Comparison between Scenarios

Finally, this section presents some comparisons between scenarios, like UMi versus UMa and RMa versus UMa.

Figure 3.29 is a representation of the 5GCM models for both NLoS and LoS conditions in UMa and UMi scenarios, considering the UMi street canyon model. It is possible to say that the comparison between NLoS and LoS models shows the same behavior observed in figure 3.14, that due to a obstructed path the loss increases. When comparing between scenarios, it is showed that the UMi models are more conservative, leading to higher losses predictions, this can be explained by the higher position of the BS in UMa case which is benign for LoS probability. The aim of figure 3.30 is to present a comparison between RMa 3GPP's official

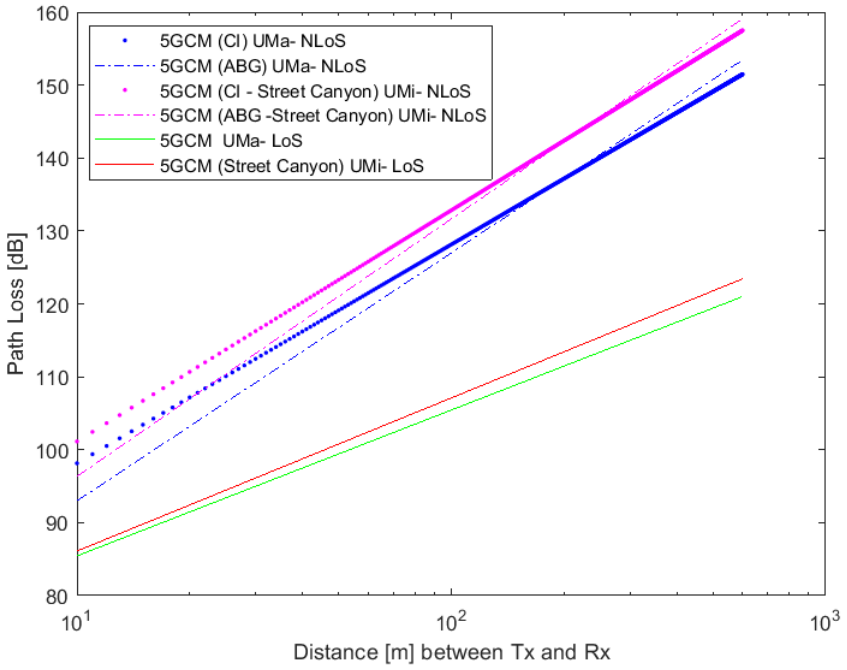

Figure 3.29: Path loss comparison between UMa and UMi

models, UMa 3GPP's models and a statistical model for the 28 GHz and 72 GHz, based on New York city data, presented in [31] that is used on chapter 4 of this these. For this comparison it's only used the 28GHz parameters.

The NYU statistical model follow the equation 3.16, where the parameters can be found on table 3.15.

$$PL_{[dB]} = \alpha + 10\beta log_{10}(d_{[m]}) + X_{\sigma} \tag{3.16}$$

	LoS	NLoS
LoS	$\alpha = 61.4, \beta = 2, \sigma = 5.8dB$	$\alpha = 72.0, \beta = 2.92, \sigma = 8.7dB$

Table 3.15: NYU statistical model parameters for 28 GHz

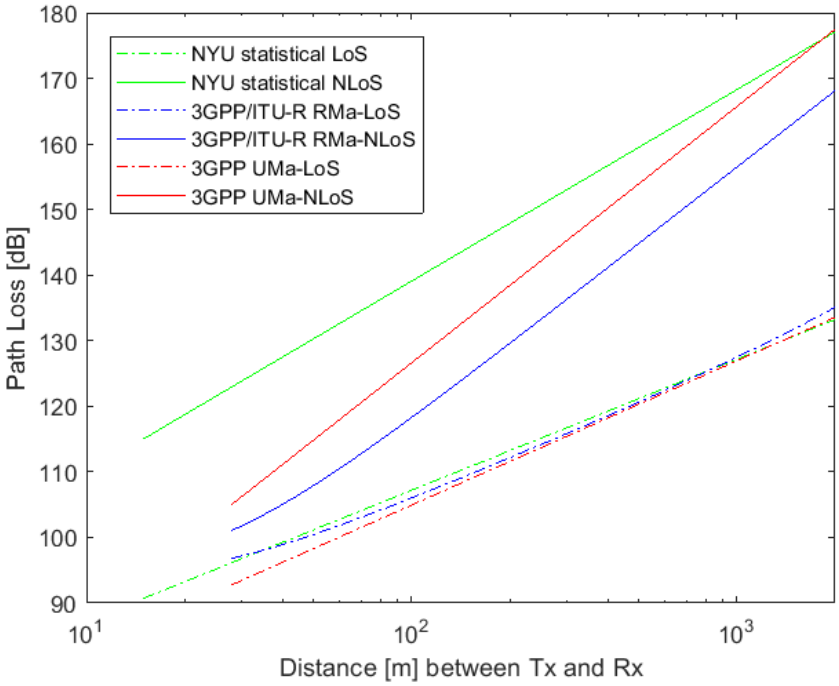

Figure 3.30: Path loss comparison between RMa and UMa

Trough the above figure it is observable that the RMa model for NLoS condition is the most optimist, predicting lower path loss values, which can be explained by the higher positioned base station that leads to a clear view of the receiver and is presumed that when speaking in RMa it is the same of speaking in areas with less building construction meaning less obstacles.

The NYU statistical model is based in New york data, so should be applied to a urban scenario, that is why is the most pessimist prediction, as the 3GPP UMa model.

The LoS performances are very alike.

4

Link Budgets and Antenna Design

The aim of this chapter is to present different system link budgets in order to understand the impact of system' characteristics variations on the achievable channel capacity, such as the use of different transmit power, link distance, bandwidth and frequency. With this calculations is, then, presented a possible solution of antenna array, by simulating the number of elements that would be needed to achieve the system's channel capacity.

4.1 Link Budget Estimations

On this section will be studied four link budgets' proposals, for two different frequencies.

The selection of these frequency bands is related with the frequencies used on 5G. As already referred, the mobile technologies prior to 5G are mostly allocated on the frequency band below the 6 GHz and, as also discussed before, this is causing scarcity of bandwidth, thus table 4.1 shows the additional bands identified during World Radiocomunnication Conference in 2015 (WRC-15), as potential frequencies to be used by IMT, to fulfill the need of frequency availability for the deployment of the 5G. Table 4.1 also present the frequency bands considered for 5G NR.

In order to understand the differences between the multiple frequency bands,

Existing band allocations to the mobile service	Candidate bands for additional allocations to the mobile service
24.25-27.5 GHz	31.8-33.4 GHz
26.5-29.5 GHz	
27.5-28.35 GHz	
37-40.5 GHz	40.5-42.5 GHz
42.5-43.5 GHz	
45.5-47 GHz	47-47.2 GHz
47.2-50.2 GHz	
50.4-52.6 GHz	
66-76 GHz	
81-86 GHz	

Table 4.1: Candidate bands for IMT and 5G NR, [32] [33]

this dissertation focuses on two of them, being the 28 GHz and the 72 GHz, also sustained by several surveys and measurements already conduct like in [34] [35].

Table 4.2 is an example of a link budget done for a mobile communication on uplink and downlink in LoS environment, using a 28 GHz carrier for a maximum cell radius of 500 m and considering a total 0.5 GHz of bandwidth. The transmit power value and both transmit and receive antenna gains are the ones referred in [34]. Hence the transmit power of the base station is 40 dBm with a 25 dBi antenna gain while the mobile equipment transmits 23 dBm with an extra 12 dBi of antenna gain. It is also considered a margin of 20 dB to account for shadowing and extra fading effects [34], should also be referred that this value is used for all link budgets scenarios calculated in this section, although some cases have distinct frequencies, the value is considered the same due to lack of references. It is also wise to consider an extra margin to account for the losses on feeders and jumpers described as implementation losses.

The values of free space loss, received power, thermal noise, SNR, channel capacity and finally the spectral efficiency are calculated using the equations 4.1, 4.3 and 4.4, 4.5, 4.6, 4.7 and 4.8 respectively.

The free space loss on equation 4.2 is derived from the Friis Formula 4.1, where P_t is the transmit power, P_r is the received power, G_t and G_r are the transmit and receiver gains respectively, λ is the wavelength in m and d is the link distance in m .

$$\frac{P_r}{P_t} = G_r G_t \left(\frac{\lambda}{4\pi d}\right)^2 \tag{4.1}$$

MMB link budget analysis	Downlink	Uplink
Carrier frequency (GHz)	28	28
Distance (Km)	0,5	0,5
Bandwidth (GHz)	0,5	0,5
Transmit power (dBm)	40	23
Transmit antenna gain (dBi)	25	12
Other losses (shadowing, fading) (dB)	20	20
Free space propagation loss (dB)	115.4	115.4
Path loss based in NYU model (dB)	121.2	121.2
Receive antenna gain (dBi)	12	25
Implementation loss (dB)	3	3
Received power (dBm)	-67.2	-84.2
Thermal noise PSD (dBm/Hz) at 25 ºC	-174	-174
Noise figure (dB)	7	7
Thermal noise (dBm)	-80	-80
SNR (dB)	12.8	-4.2
Channel capacity (Gbps)	2.17	0.234
Spectral efficiency (bps/Hz)	4.34	0.468

Table 4.2: Link budgets for typical mmWave communications

$$FSL_{[dB]} = 92.44 + 20log_{10}(d_{[Km]}) + 20log_{10}(f_{[GHz]}) \tag{4.2}$$

The received power values of the tables were estimated using the statistical path model for large scale parameters [31], already referred on section 3.2.5 for 28 GHz beam, instead of the free space loss, because this model will account for shadowing effects. The LoS omnidirectional path loss has a log normal shadowing with a zero mean and σ deviation, assuming equations 4.3, where L_o is the extra loss accounted for extra shadowing and fading effects and L_i is the loss due to implementation, finally PL is the path loss, using equation 4.4 assuming the parameters on table 4.3.

$$P_{r[dBm]} = P_t - PL + G_r + G_t - L_o - L_i \tag{4.3}$$

$$PL_{[dB]} = \alpha + 10\beta log_{10}(d_{[m]}) + X_\sigma \tag{4.4}$$

28 GHz	72 GHz
$\alpha = 61.4, \beta = 2, \sigma = 5.8dB$	$\alpha = 69.8, \beta = 2, \sigma = 5.8dB$

Table 4.3: NYU model parameters' values for a LoS communication [31]

The power of Thermal noise can be calculated through equation 4.5.

$$N_{[dBm]} = 10log_{10}\left(\frac{KT}{1_{[mW]}}\right) + F + 10log_{10}(B_{[Hz]}) \tag{4.5}$$

Where $K = 1.38064852 * 10^{-23}$ is the Boltzmann constant, T is the temperature, around 25 ºC but needs to be converted in Kelvin, F is the noise figure in dB and B the bandwidth.

The Signal-to-Noise Ratio (SNR) aims to measure the ratio between the level of received power and the level of the noise associated to it, can be obtained using equation 4.6.

$$SNR_{[dB]} = P_{r[dBm]} - N_{[dBm]} \tag{4.6}$$

To calculate the channel capacity using the Shannon–Hartley theorem represented in equation 4.7, this estimates the maximum data rate the system can achieve.

$$C_{[bps]} = B_{[Hz]} * log_2(1 + 10^{SNR/10}) \tag{4.7}$$

Finally the spectral efficiency can be determined by equation 4.8.

$$S_{eff[bps/Hz]} = \frac{C}{B} \tag{4.8}$$

The differences between uplink and downlink shows that the antenna gains play a big role on the data rate of the communication, using higher gains is possible to reach higher data throughout, as expected to be possible to feed multiple users at the same time. The difference of about 6 dB is due to the shadowing fading deviation of the NYU model, that free space do not account for.

The values on table 4.4 were also calculated using the logic above and static values were based on [31]. It is possible to say that a higher data rate is achievable when using a link of 28 GHz then using a link of 72 GHz, this is mainly due to the differences on the received power, the path loss model already accounts for the environment losses that target higher frequencies. Comparing the downlink case of table 4.2 and the case 1 of table 4.4, that have the same Effective Isotropic Radiated Power (EIRP), is possible to affirm that the channel capacity diminish with the increase of the distance between transmitter and receiver, as expected.

MMB link budget analysis	Case 1	Case 2
Carrier frequency (GHz)	28	72
Distance (Km)	1	1
Bandwidth (GHz)	1	1
Transmit power (dBm)	35	35
Transmit antenna gain (dBi)	30	30
Other losses (shadowing, fading) (dB)	20	20
Free space propagation loss (dB)	121,4	129,6
Path loss based in NYU model (dB)	127.2	135.6
Receive antenna gain (dBi)	15	15
Implementation loss (dB)	5	5
Received power (dBm)	-72.2	-80.6
Thermal noise PSD (dBm/Hz) at 25 ºC	-174	-174
Noise figure (dB)	10	10
Thermal noise (dBm)	-74	-74
SNR (dB)	1.8	-6.6
Channel capacity (Gbps)	1.33	0.285
Spectral efficiency (bps/Hz)	1.33	0.285

Table 4.4: Link budgets for mmWave links using 28 GHz and 72 GHz carriers

Tables 4.5 and 4.6 shows the above scenarios but recalculated for a NLoS environment. The path loss was calculated using the NYU model, applying the parameters on table 4.7, and the 3GPP UMa model [24], assuming $h_{UE} = 1.5$ m, as already studied on section 3.2.2. The received power and following was then calculated using the NYU path loss value.

It is possible to say that the NYU model is more conservative, predicting higher path loss values as already showed on the graphic of figure 3.30. And as expected the difference between the two path loss values decrease with the increase of distances, as observable on table 4.5 the link distance is 500 m and in table 4.6 the distance is 1 Km, meaning in table 4.6 the path loss calculated using the NYU model is more closer to the path loss calculated using the 3GPP, then in table 4.5.

For both scenarios is possible to understand that when in NLoS environment the communications are highly attenuated resulting in lower channel capacities that are far from the desired data rates expected for 5G. However it is worth mentioning that the T-R distances used in these cases are not ideal for NLoS communications, usually this conditions is overcame by set up multiple base stations or a DAS network, to decrease the link distance, therefore the cell size, or other techniques to increase the transmit gain and directivity as beamforming or MIMO systems.

MMB link budget analysis	Downlink	Uplink
Carrier frequency (GHz)	28	28
Distance (Km)	0,5	0,5
Bandwidth (GHz)	0,5	0,5
Transmit power (dBm)	40	23
Transmit antenna gain (dBi)	25	12
Other losses (shadowing, fading) (dB)	20	20
Path loss based in NYU model (dB)	159,5	159,5
Path loss based in 3GPP model (dB)	154	154
Receive antenna gain (dBi)	12	25
Implementation loss (dB)	3	3
Received power (dBm)	-102,5	-119,5
Noise figure (dB)	7	7
Thermal noise (dBm)	-80	-80
SNR (dB)	-25,5	-42,5
Channel capacity (Mbps)	2,03	0,04
Spectral efficiency (bps/Hz)	4,06E-03	8,11E-5

Table 4.5: Link budgets on NLoS environment

MMB link budget analysis	Case 1	Case 2
Carrier frequency (GHz)	28	72
Distance (Km)	1	1
Bandwidth (GHz)	1	1
Transmit power (dBm)	35	35
Transmit antenna gain (dBi)	30	30
Other losses (shadowing, fading) (dB)	20	20
Path loss based in NYU model (dB)	168,3	168,1
Path loss based in 3GPP model (dB)	165,7	173,9
Receive antenna gain (dBi)	15	15
Implementation loss (dB)	5	5
Received power (dBm)	-113,3	-113,1
Thermal noise PSD (dBm/Hz) at 25 ºC	-174	-174
Noise figure (dB)	10	10
Thermal noise (dBm)	-74	-74
SNR (dB)	-39,3	-39,1
Channel capacity (Mbps)	0,17	0,18
Spectral efficiency (bps/Hz)	1,69E-4	1,77E-4

Table 4.6: Link budgets for mmWave links using 28 GHz and 72 GHz carriers in NLoS environments

28 GHz	72 GHz
$\alpha = 72, \beta = 2.92, \sigma = 8.7dB$	$\alpha = 86.6, \beta = 2.45, \sigma = 8.0dB$

Table 4.7: NYU model parameters' values for a NLoS communication [31]

4.2 Antenna Design

The aim of this Section is to provide an estimation of the ideal number of antenna elements that an antenna array should have to achieve a desired data rate. It is presented a study to understand how the increase of frequency used as carrier can induce an increment of the number of elements in an array to achieve the same data rate. It is also studied how the emitted power and distance of the link can influence the antenna gain and therefore the number of elements needed.

4.2.1 Antenna Array

The system for mmWaves should be able to communicate by overpassing the propagation restraints like path loss and scattering effects studied on chapter 3. There are techniques that are used to mitigate those effects such as the use of antenna arrays that will introduce an extra gain, achieved by placing a number of antennas elements and that can assume different geometries.

Antenna arrays can assume different typologies, like linear (Uniform Linear Array (ULA)), which is a one dimension architecture and the elements are equally separated.

There are many aspects of the arrays that can influence the gain and directivity of the beam, such as the distance between elements - d - as shown in figure 4.1.

The Array Factor (AF) of an ULA antenna with N elements is given by equation 4.9, where λ is the wavelength, β the excitation phase of the array, k is the angular wave number, θ and d as in figure 4.1 and a_n is the voltage amplitude of the element n, which in ULA all elements have unitary amplitude $a_n = a_1 = 1$.

$$\begin{aligned} AF &= \sum_{n=1}^{N} a_n e^{j(n)\psi} \\ \psi &= kdcos\theta + \beta \\ k &= \frac{2\pi}{\lambda} \end{aligned} \tag{4.9}$$

If the reference point is the center of the array the AF can be reduced to

equation 4.10 [36], meaning that the maximum value of AF is equal to N.

$$AF = \frac{sin(\frac{N}{2}\psi)}{sin(\frac{1}{2}\psi)} \tag{4.10}$$

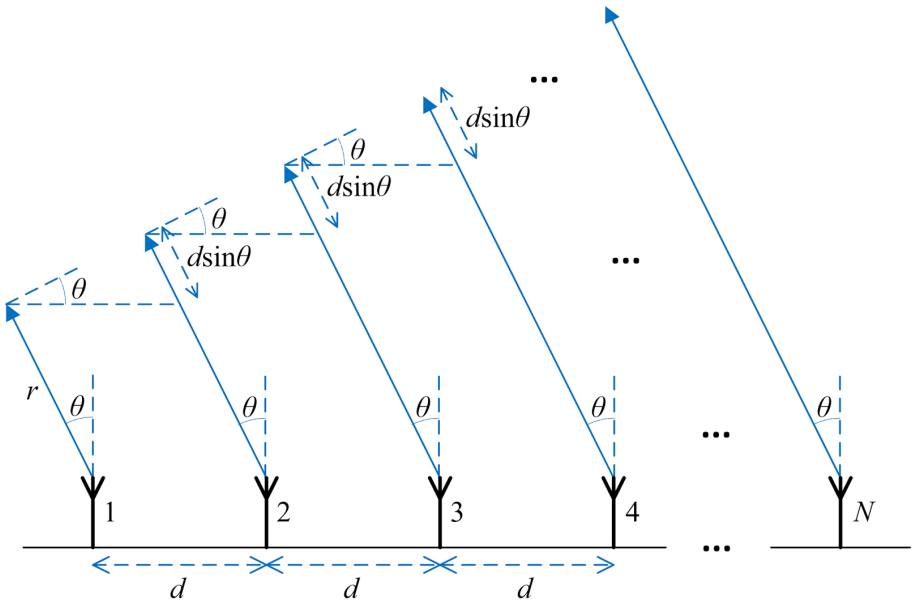

Figure 4.1: Wavefront crossing a linear antenna array having N elements at an angle θ [37]

The excitation phase will influence the direction of nulls, which are where the radiation gain equals to 0 dB, when not normalized. If $\beta = 0$ the first maximum is always at $\theta = 90°$ for $0° \leqslant \theta \leqslant 360°$, for the first maximum to be placed at $\theta = 0°$ then the elements need to be phase separated by $\beta = -kd$, so the excitation phase is a factor that will influence the direction of the radiation pattern as shown in figure 4.2 and higher phased arrays also means wider beams.

The number of elements N also affect the narrowness of the beam besides the gain as shown in figure 4.3. The inter-distance, d, between elements can also narrow the beam and form side lobes on the radiation pattern as figure 4.4 shows.

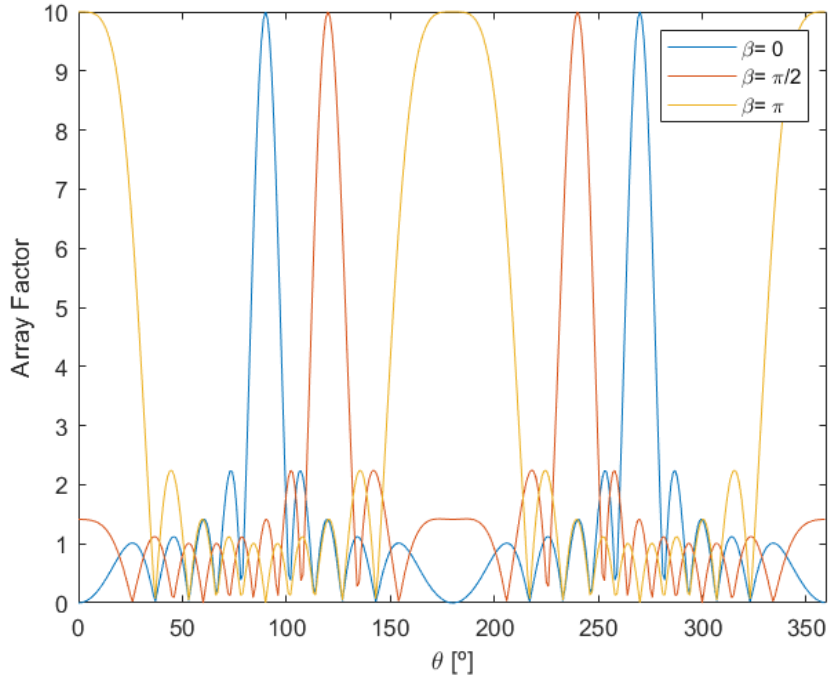

Figure 4.2: Array factor of an ULA with 10 elements and $d = \lambda/2$ for different β values

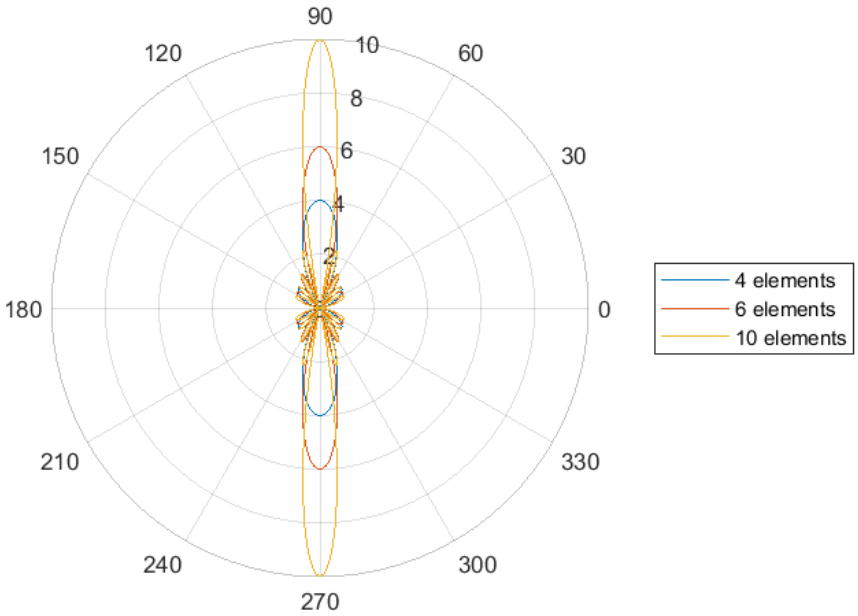

Figure 4.3: Array factor of an ULA with $d = \lambda/2$ for different number of elements

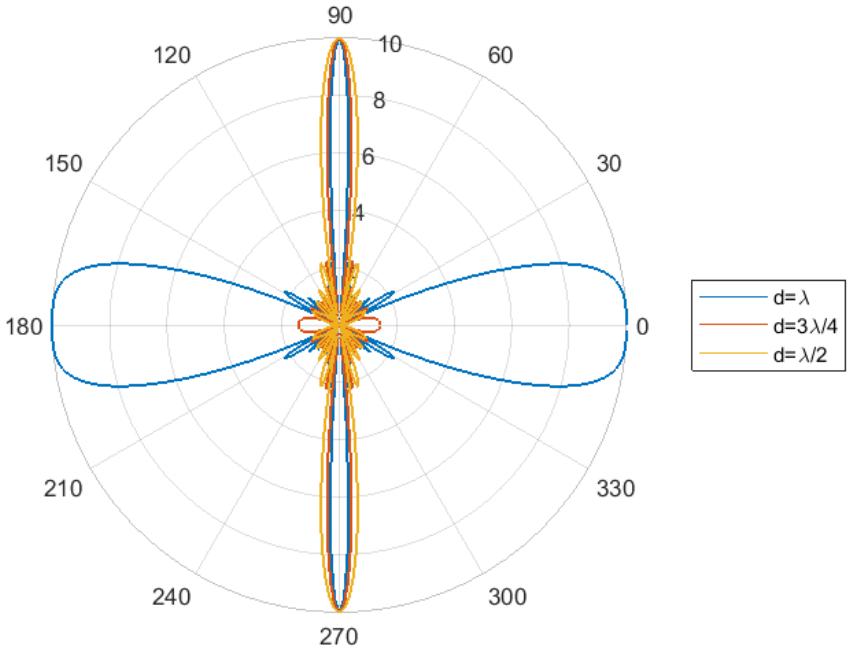

Figure 4.4: Array factor of an ULA with 10 elements different element inter-distance

Although the there are many geometries of arrays, if the array factor is not normalized the maximum of gain is also the number of elements, which can be converted to antenna gain through equation 4.11

$$ArrayGain_{[dB]} = 10log_{10}(\eta AF) = 10log_{10}(\eta N) \tag{4.11}$$

The array gain can also be affected by efficiency (η) of the array to steer the beam only in the desired direction [14], figure 4.5 shows how the array gain increases with the number of elements of the array for different efficiencies values.

Figure 4.5 shows that efficiency can decrease the array gain till 3 dB as expected, when considering half of the capability of steer ($\eta = 0.5$). Also demonstrates that increase of the number of elements will not promote a proportional gain, which means that to increase the gain will be needed much more elements.

Besides ULA there are other geometries for antenna arrays, such as Uniform Planar Array (UPA) and Uniform Circular Array (UCA). The UPA solutions are the most common for cellular applications due to the fact that can accommodate a larger number of elements in the same area [14].

The UPA is a two-dimensional array where AF is given by equations 4.12

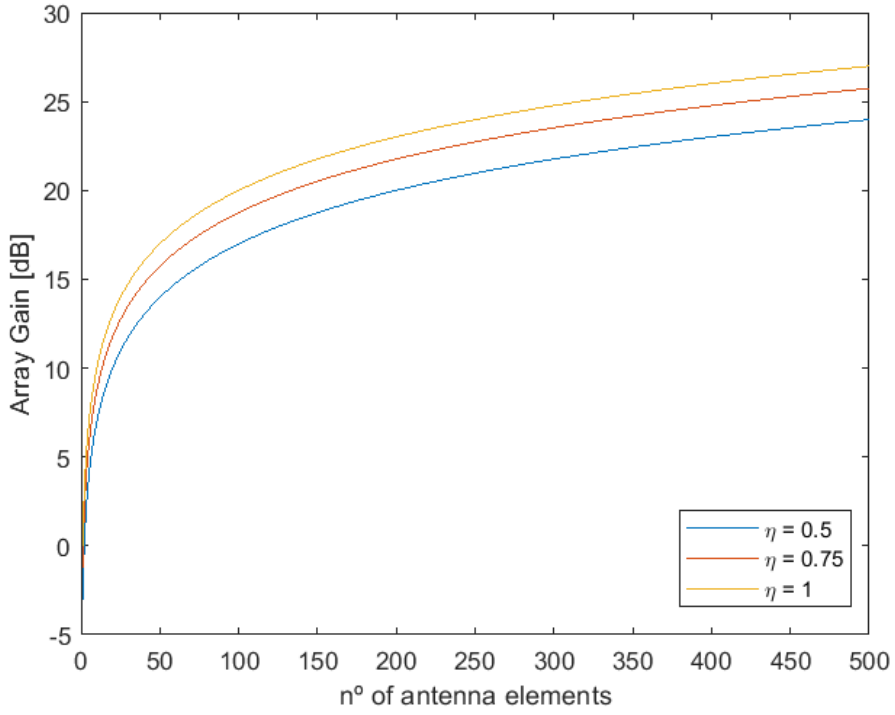

Figure 4.5: Array gain in function of number of antenna elements

and 4.13 according to the geometry in figure 4.6. The maximum gain achieved by this geometry will be $M \times N$.

$$\begin{aligned} AF &= a_0 \sum_{m=1}^{M} e^{j(n-1)\psi_x} \sum_{n=1}^{N} e^{j(n-1)\psi_y} \\ \psi_x &= kd_x sin\theta cos\phi + \beta_x \\ \psi_y &= kd_y sin\theta sin\phi + \beta_y \end{aligned} \tag{4.12}$$

$$AF(\theta,\phi) = \left[\frac{sin(\frac{M}{2}\psi_x)}{sin(\frac{1}{2}\psi_x)} \frac{sin(\frac{N}{2}\psi_y)}{sin(\frac{1}{2}\psi_y)} \right] \tag{4.13}$$

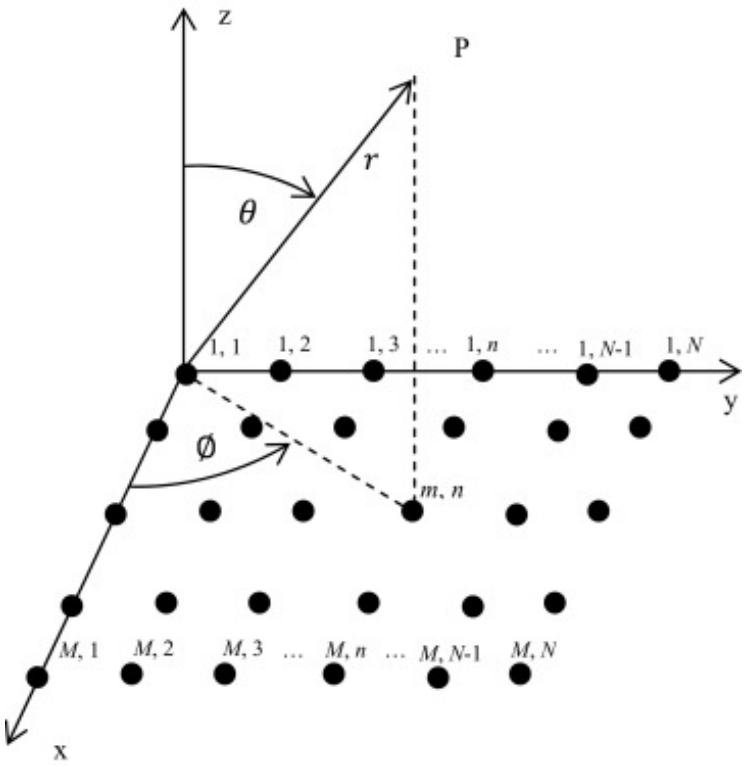

Figure 4.6: UPA geometry [38]

4.2.2 Design considerations

As already studied the mmWaves have major path losses specially when increasing the frequency which can be compensated by larger antenna arrays with high gain and directivity. Is important to understand how the increase of frequency influences the array gain and consequently the number of elements needed to achieve the same data rate.

From the link budgets done on the prior section, namely the downlink case on table 4.2 where the goal is to achieve 2.17 Gbps of data rate. A simulation was done in order to understand how the number of elements the transmit antenna, needed to achieve a suffice gain, will increase along the frequency to reach the same data rate. As the path loss model used on the link budget is empiric and specific for the 28 GHz frequency, the simulation was done assuming the path loss calculated thought the 3GPP model. The total antenna gain is given by equation 4.14,

$$AntennaGain_{[dBi]} = 10log_{10}(\eta) + ElementGain_{[dBi]} + 10log_{10}(AF) \tag{4.14}$$

Figure 4.7 shows how the number of elements increases along frequency to reach 2.2 Gbps of channel capacity, for different transmit powers and different link distances. The reference case is the one where transmit power is 40 dBm and link distance is 500m.

The reference case states that 25 dB are needed on the transmit side, if the element gain is 10 dBi then the array gain needs to achieve 15 dB if considering $\eta = 1$, so inverting equation 4.11, the transmit antenna needs to have around 32 elements. As expected figure 4.7 demonstrates that for the 28 GHz are needed around 32 elements.

The peak around the 60 GHz are due to the oxygen absorption which demonstrates that using a carrier of 60 GHz outdoor implicates larger antenna arrays. When diminishing the transmit power it impacts the SNR and there is an escalation of the number of elements to try to compensate the gain needed to achieve the 2.2 Gbps.

Figure 4.8 also demonstrates the oxygen effect, where the frequency that needs more elements is 60 GHz. This figure also shows how the distance can impact an mmWaves system mainly on higher frequencies, showing that the

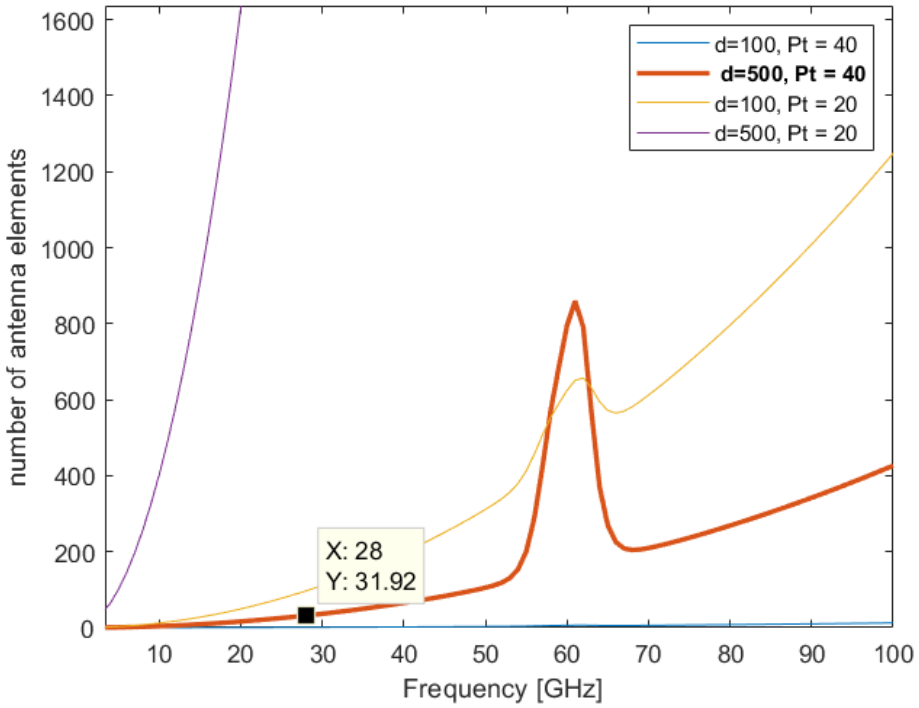

Figure 4.7: Number of antenna elements needed along frequency to achieve 2.2 Gbps

mmWaves communications will benefit from the reduction of the cell radius, resulting on simplifying the transmit antenna on the number of elements.

On figure 4.9 aims to show the evolution on the number of elements for all the cases scenarios of link budgets chapter for the LoS condition, to achieve at least 3.5 Gbps, assuming that the element gain is 10 dBi, only the uplink case considers a element gain of 4 dBi to be applicable to a user equipment.

The above figure helps to understand that the case 2, where the frequency carrier is 72 GHz will need a larger number of elements to achieve the necessary gain to compensate the path loss and provide a 3.5 Gbps of data rate. The difference between downlink scenario and case 1 scenario where the EIRP is the same, sets on the fact of having the double of link distance and also double bandwidth, showing that the proportional increase on bandwidth is not suffice to compensate the extra pass loss related to the larger distance.

Figure 4.10 was produced in order to show how many array elements the base station needs to achieve a data rate until 10 Gbps, assuming the study case of the downlink link budget in LoS condition, where the transmit power is set to 40 dBm, the received gain is considered 12 dB and each transmit element has 10

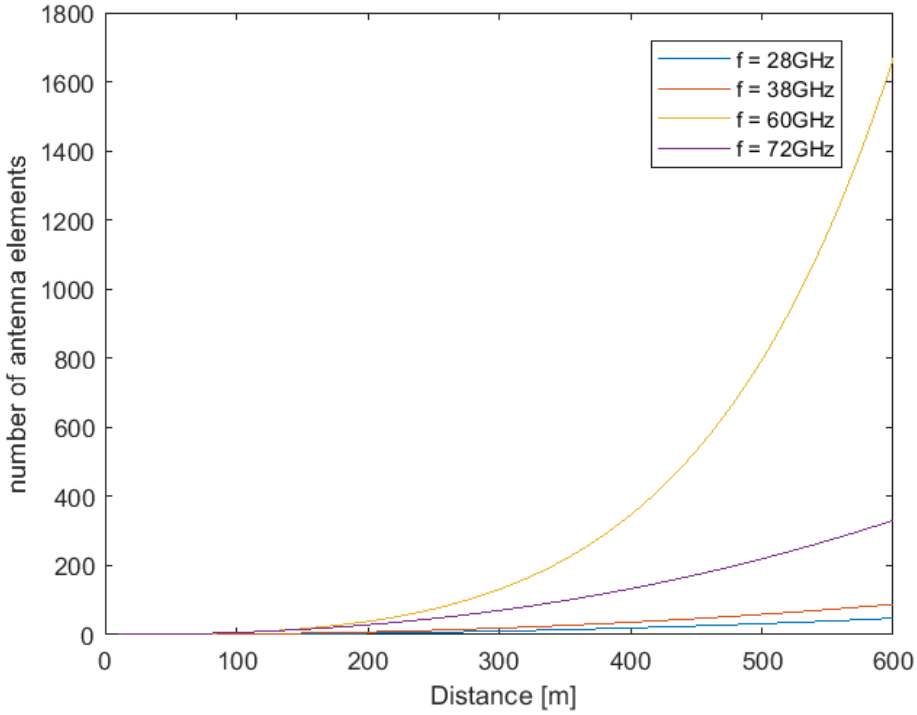

Figure 4.8: Number of antenna elements needed along distance to achieve 2.2 Gbps

dBi of gain, and assuming a total bandwidth of 500 MHz.

At the desired link distance of 500 m and to achieve 10 Gbps, the transmit antenna needs to be built with the aid of almost 1.5 million elements which becomes an impractical solution. Decreasing the cell size will automatically drop the number of elements, although for the 10 Gbps is still needed an extensive array as is possible to observe in the zoomed graphic of figure 4.11.

One of the advantages of employing mmWaves is the availability of contiguous portions of bandwidths which can lead to the use of wider band systems, that can help balancing the number of elements the transmitter needs to obtain higher transfer rates, as shown on figure 4.12. Extending the system bandwidth up to 1 GHz or even to 1.5 GHz can already ensure the possibility of reaching around 10 Gbps with a feasible to implement array, however it means that it would need to allocate a channel with 1.5 GHz of bandwidth to feed a single user equipment. Thus, a system using a bandwidth of 1.5 GHz will need an array built with 415 elements.

The above simulations allow to understand the impact of the variations on the carrier frequency, link distance or bandwidth on the channel capacity. The

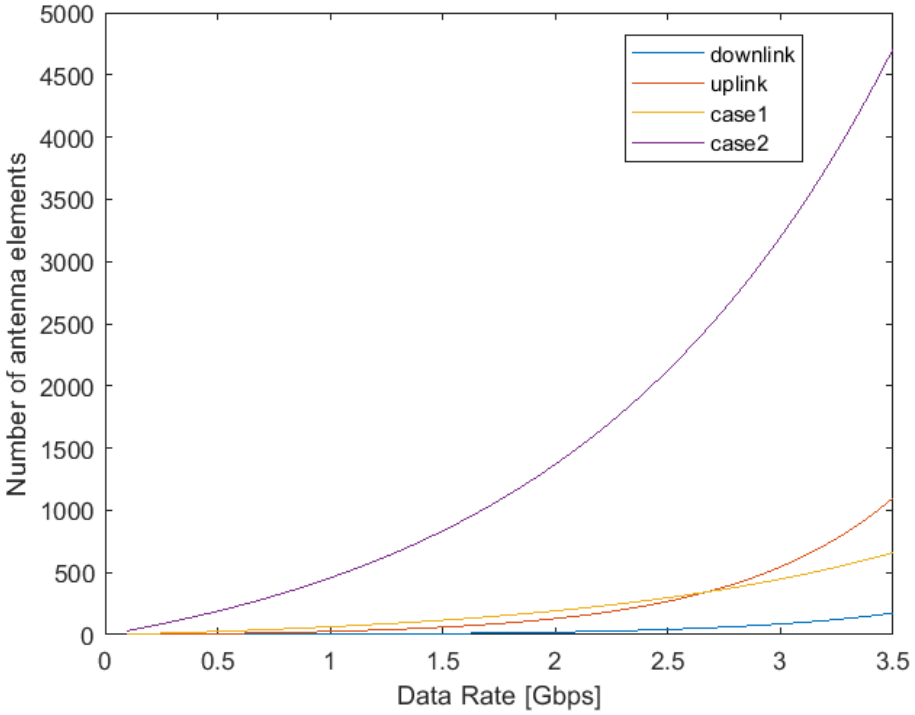

Figure 4.9: Number of antenna elements needed to achieve the data rate for all link budget scenarios

direct inferences is that the increase of frequency means larger path losses and with that larger arrays, regarding the elements number. The same occurs for the increase of link distances, sustaining the idea of needing 5G deployment in smaller cells than the previous generations, never in UMa or RMa scenarios, but in micro, pico or femtocells. On the other hand, the availability of large portions of free bandwidth on mmWaves band, means larger bandwidths to allocate to a channel, granting higher data rates, as possible to see on table 4.1, one of the bands that includes the 28 GHz carrier has a total bandwidth of 3 GHz. The band that includes the 72 GHz has a total bandwidth of 5 GHz

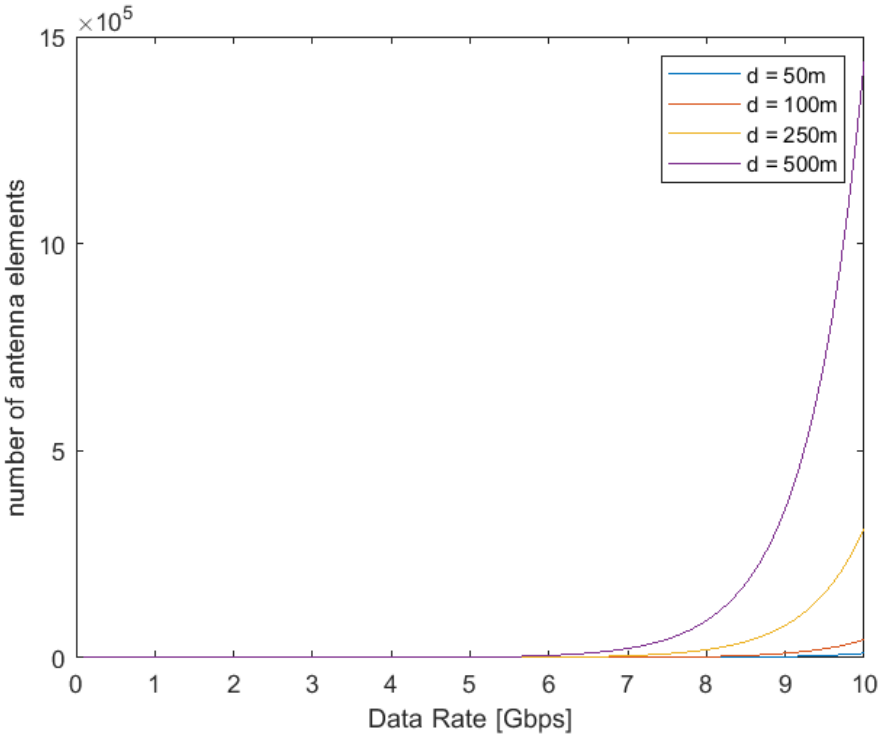

Figure 4.10: Number of antenna elements needed to achieve the data rate

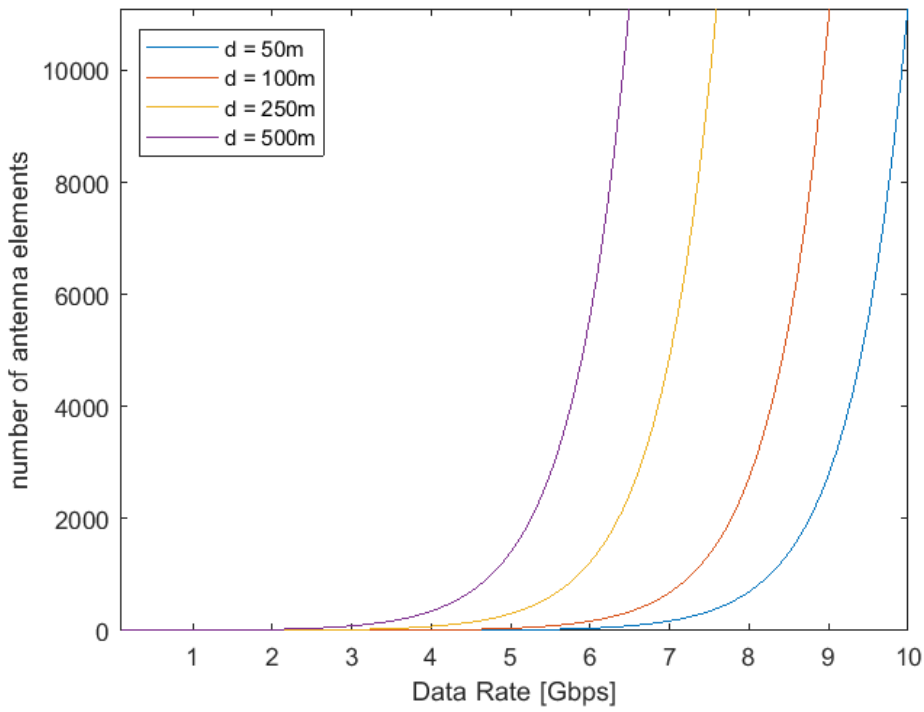

Figure 4.11: Number of antenna elements needed to achieve the data rate (zoomed)

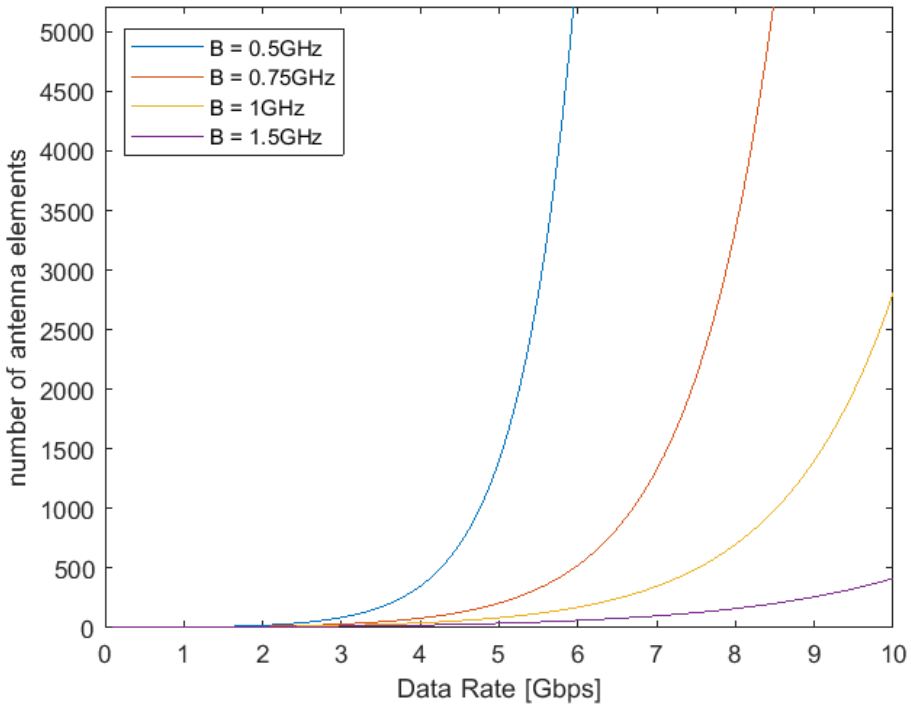

Figure 4.12: Number of antenna elements needed to achieve the data rate (zoomed) with different bandwidths

5

Conclusions and Future Work

The main purpose of this dissertation focus on studying the major challenges that millimeter waves band faces during propagation. Starting with the study of the major contributors of loss, such as free space loss, atmospheric gasses, rain or vegetation presence or even material penetration, in an attempt to predict the behavior of the higher frequencies.

The Friis formula shows that the free space loss increases with the increase of frequency, adding a total of 20 dB of attenuation in a link of 1 Km using a 30 GHz frequency versus a link using a 3 GHz frequency, and assuming a constant gain over frequency. This shows how millimeter waves are much impacted by the air interface than the sub-6 GHz band. The atmospheric gases, meaning the oxygen and water vapour, are also a source of loss on this band, although the impact of this gases are only meaningful on the band between 50 and 70 GHz, with a significant pike on 60 GHz, where oxygen can induce an extra loss of 15 dB/Km. Around 160 to 200 GHz, water vapour can induce almost 30 dB/Km of attenuation. This zones are, thus, not suitable for outdoor propagation. The rain greatly impacts the mmWaves propagation due to the comparable sizes between the mmWaves wavelength and raindrops, making mmWaves not a viable solution for transmissions on zones with high rain annual average rates, like tropic zones. The presence of vegetation also impacts the quality of a millimeter wave signal and the diverse existing models shows that dense wooded and blossomed areas are not ideal for mmWaves to propagate through. Higher frequencies are

also not suitable to go through materials like common building materials such as concrete, glass and wood, because the waves are absorbed instead of being reflected to contribute for the MPCs and ensure NLoS communication. With this said, mmWaves are not the best approach for O2I solutions, neither inside rooms with much furniture.

There are multiple models to predict the overall omnidirectional path loss in different environments - LoS or NLos - and cell categories (UMi, UMa, RMa and InH). The study of the different models allowed to understand that NLoS usually predict almost 35 dB more then LoS models in the cells range limits. When analyzing urban outdoor models, is possible to say that UMi zones are the most loss affected, because although those UMi models are applicable to shorter distance ranges, these also account for more obstacles and crowded zones, predicting higher path losses. When comparing the models between UMa and RMa cells, the same occurs because UMa zones are heavily populated in terms of buildings and obstacles.

With the study of models it was possible to calculate different link budgets, in an attempt to understand how the variation of the radio channel characteristics would affect the channel capacity. It was used UMa distance ranges, between 500 m and 1 Km, so UMa models were employed to calculate the path loss. The frequencies were chosen based on the candidates bands for 5G deployment. The link budgets showed that millimeter waves can achieve multi Gpbs data rates for distances up to 1 Km. In a 500 m communication, using a 28 GHz frequency and having 0.5 GHz of available bandwidth, it is possible to achieve 2.2 Gbps and for 1 Km distance the channel can provide 1.3 Gbps. The link budgets also showed how the EIRP of the terminal can influence the channel capacity by decreasing the SNR. These calculations also showed how the LoS is the most suitable condition for mmWaves communications at least when trying to achieve data rates of Gbps on networks with macrocell architecture.

Through LoS link budgets, it was possible to calculate the number of antenna elements a single array need to have in order to achieve the desired data rate. In a 500 m communication, using a 28 GHz frequency and having 0.5 GHz of available bandwidth, the antenna would need 32 elements to reach a data rate of 2.2 Gbps. If the system need to achieve 10 Gbps, the array would be impractical, because it would need more than 1 million elements. The solution can pass by increasing the channel bandwidth to 1.5 GHz, meaning the array would be built with 415 elements, a number accepted for mmWaves massive MIMO systems. However, the solution would need to allocate 1.5 GHz to a single channel.

With this dissertation it was possible to understand the promising use of mmWaves in 5G when trying to achieve multiple Gbps data rates. However, this work also shows why 5G need heterogeneous networks to cover indoor environments, since millimeter waves are so easily absorbed. Millimeter waves are not suitable for high distance communications and so the need to use these frequencies in small cells contribute for hyper dense deployments, which can benefit zones densely populated that demand high capacities.

5.1 Future Work

This work can, however, be enhanced with the application of massive MIMO to try to boost the channel capacity and understand how it will affect the number of elements needed to achieve higher data rates mostly in NLoS condition. Another approach is the attempt to model the channel to be able to generate large and small-scale characteristics through measurements in different scenarios, in order to have a better understanding of the propagation and have a more rigorous system. It will also lead to the full dimension of an antenna for mmWaves communication.

References

[1] G. Barb and M. Otesteanu, "5G: An Overview on Challenges and Key Solutions", pages 1–4, 2018.

[2] Prabesh Paudel and Abhi Bhattarai, "5G Telecommunication Technology: History, Overview, Requirements and Use Case Scenario in Context of Nepal", 2018.

[3] GSMA, *5g spectrum GSMA Public Policy Position*, Last accessed 24 February 2020, 2019. [Online]. Available: https://www.gsma.com/spectrum/wp-content/uploads/2019/09/5G-Spectrum-Positions.pdf.

[4] ETSI, *Why do we need 5g?*, Last accessed 24 February 2020. [Online]. Available: https://www.etsi.org/technologies/mobile/5g?jjj=1609701010501.

[5] M. Ferreira and P. Pinho, "Propagation at mmWaves Frequencies:Some Considerations ", in *ConfTELE2021*, 2021, pages 1–4.

[6] Mansoor Shafi, Andreas F. Molisch, Peter J. Smith, Thomas Haustein, Peiying Zhu, Prasan De Silva, Fredrik Tufvesson, Anass Benjebbour, and Gerhard Wunder, "5g: A tutorial overview of standards, trials, challenges, deployment, and practice",

[7] S. A. Busari, K. M. S. Huq, S. Mumtaz, L. Dai, and J. Rodriguez, "Millimeter-wave massive mimo communication for future wireless systems: A survey", *IEEE Communications Surveys Tutorials*, vol. 20, no. 2, pages 836–869, 2018. DOI: 10.1109/COMST.2017.2787460.

[8] Last accessed 24 March 2020. [Online]. Available: https://www.mtnconsulting.biz/5g-need-for-harmonized-spectrum/.

[9] Naga Bhushan, Tingfang Ji, Ozge Koymen, John Smee, Joseph Soriaga, Sundar Subramanian, and Yongbin Wei, "5G Air Interface System Design Principles", *IEEE Wireless Communication*, 2017.

[10] Glauco E. Gonçalves, Guto L. Santos, Leylane Ferreira, Élisson da S. Rocha, Lubnnia M. F. de Souza, André L. C. Moreira, Judith Kelner, and Djamel Sadok, "Flying to the clouds: The evolution of the 5g radio access networks", in *The Cloud-to-Thing Continuum: Opportunities and Challenges in Cloud, Fog and Edge Computing*, Theo Lynn, John G. Mooney, Brian Lee, and Patricia Takako Endo, Eds. Cham: Springer International Publishing, 2020, pages 41–60, ISBN: 978-3-030-41110-7. DOI: 10.1007/978-3-030-41110-7_3. [Online]. Available: https://doi.org/10.1007/978-3-030-41110-7_3.

[11] Naser Al-Falahy and Omar Alani, "Millimetre wave frequency band as a candidate spectrum for 5g network architecture: A survey", *Physical Communication*, vol. 32, Nov. 2018. DOI: 10.1016/j.phycom.2018.11.003.

[12] T. S. Rappaport, Y. Xing, G. R. MacCartney Jr., A. F. Molisc, E. Mellios, and J. Zhang, "Overview of millimeter wave communications for fifth-generation (5g) wireless networks-with a focus on propagation models", *IEEE Transactions on Antennas and Propagation, Special Issue on 5G*, Nov. 2017.

[13] T. S. Rappaport, H. Tataria, S. Wu., A. F. Molisc, F. Tufvesson, J. Zhang, M. Shafi, K. Kitao, and S. Sun, "Microwave vs. millimeter-wave propagation channels: Key differences and impact on 5g cellular systems", *IEEE Communications Magazine*, Dec. 2018.

[14] I. A. Hemadeh, K. Satyanarayana, M. El-Hajjar, and L. Hanzo, "Millimeter-wave communications: Physical channel models, design considerations, antenna constructions, and link-budget", *IEEE COMMUNICATIONS SURVEYS & TUTORIALS*, vol. 20, 2018.

[15] H. M. Rahim, C. Y. Leow, and T. Abd. Rahman, "Millimeter wave propagation through foliage: Comparison of models", *2015 IEEE 12th Malaysia International Conference on Communications*, Nov. 2015.

[16] J. Zhang, X. Ge, Q. Li, M. Guizani, and Y. Zhang, "5g millimeter-wave antenna array: Design and challenges", *IEEE Wireless Communications*, 2017.

[17] S. Ghosh and D. Sen, "An inclusive survey on array antenna design for millimeter-wave communications", *IEEE Access*, 2019.

[18] *Mimo techniques and architectures for millimeter wave mobile communications*, Last accessed 14 January 2021. [Online]. Available: https://5gbook.org/2017/02/21/mimo-techniques-and-architectures-for-millimeter-wave-mobile-communications/.

[19] W. Hong, Z. H. Jiang, C. Yu, J. Zhou, P. Chen, Z. Yu, H. Zhang, B. Yang, X. Pang, M. Jiang, Y. Cheng, M. K. T. Al-Nuaimi, Y. Zhang, J. Chen, and S. He, "Multibeam antenna technologies for 5g wireless communications", *IEEE Transactions on Antennas and Propagation*, vol. 65, 2017.

[20] Int. Telecommun. Union, *Reference standard atmospheres - recommendation itu-r p.835-6*, Dec. 2017.

[21] ——, *Attenuation by atmospheric gases and related effects - recommendation itu-r p.676-12*, Aug. 2019.

[22] ——, *Specific attenuation model for rain for use in prediction methods - recommendation itu-r p.838-3*, Mar. 2005.

[23] ——, *Characteristics of precipitation for propagation modelling - recommendation itu-r p.837-7*, Jun. 2017.

[24] "Study on channel model for frequencies from 0.5 to 100 GHz - 3rd generation partnership project (3gpp), tech. rep. tr 38.901 v16.1.0 release 16", Tech. Rep., Dec. 2019.

[25] S. Sun, G. R. MacCartney, and T. S. Rappaport, "Millimeter-wave distance-dependent large-scale propagation measurements and path loss models for outdoor and indoor 5g systems", in *2016 10th European Conference on Antennas and Propagation (EuCAP)*, 2016, pages 1–5. DOI: 10.1109/EuCAP.2016.7481506.

[26] "5G channel model for bands up to 100 GHz", Tech. Rep., Oct. 2016.

[27] "Metis channel models - d1.4", Tech. Rep., Feb. 2015.

[28] "Measurement Results and Final mmMAGIC Channel Models - h2020-ict-671650-mmmagic/d2.2 v2.0", Tech. Rep., May 2017.

[29] T. S. Rappaport, Y. Xing, G. R. MacCartney, A. F. Molisch, E. Mellios, and J. Zhang, "Overview of millimeter wave communications for fifth-generation (5g) wireless networks—with a focus on propagation models", *IEEE Transactions on Antennas and Propagation*, vol. 65, no. 12, pages 6213–6230, 2017.

[30] G. R. MacCartney and T. S. Rappaport, "Rural macrocell path loss models for millimeter wave wireless communications", *IEEE Journal on Selected Areas in Communications*, vol. 35, no. 7, pages 1663–1677, 2017.

[31] M. R. Akdeniz, Y. Liu, M. K. Samimi, S. Sun, S. Rangan, T. S. Rappaport, and E. Erkip, "Millimeter wave channel modeling and cellular capacity evaluation", *IEEE Journal on Selected Areas in Communications*, vol. 32, no. 6, pages 1164–1179, 2014.

[32] 5G PPP, *D5.4: Spectrum for 5g*, Last accessed 24 March 2020, 2017. [Online]. Available: https://5g-ppp.eu/wp-content/uploads/2017/10/Euro-5G-D5.4_Spectrum_for_5G_v1.0.pdf.

[33] Last accessed 20 Dec 2020. [Online]. Available: https://www.qualcomm.com/media/documents/files/spectrum-for-4g-and-5g.pdf.

[34] S. Rajagopal, S. Abu-Surra, Z. Pi, and F. Khan, "Antenna array design for multi-gbps mmwave mobile broadband communication", pages 1–6, 2011.

[35] Z. Pi and F. Khan, "System design and network architecture for a millimeter-wave mobile broadband (mmb) system", pages 1–6, 2011.

[36] Constantine A. Balanis, *Antenna Theory: Analysis and Design*. USA: Wiley-Interscience, 2005, ISBN: 0471714623.

[37] Last accessed 14 August 2020. [Online]. Available: https://2.bp.blogspot.com/-1MWg6vXxykk/WQwVH-HWsjI/AAAAAAAAXF4/_uMCrukWzBYTtpdl0JV009-2b24HCo6_wCLcB/s1600/N-elem_uniform_array_scheme.png.

[38] Yasser Albagory, "Performance of circularly masked planar arrays", *AEU - International Journal of Electronics and Communications*, vol. 70, no. 4, pages 482–490, 2016, ISSN: 1434-8411. DOI: https://doi.org/10.1016/j.aeue.2016.01.015. [Online]. Available: http://www.sciencedirect.com/science/article/pii/S1434841116300309.

Appendix A

A.1

The $N''_{Oxygen}(f)$ and $N''_{WaterVapour}(f)$ coefficients of the specific gaseous attenuation, are given by equation A.1 and A.2, where S_i is the strength of the ith oxygen or water vapour line, F_i is the oxygen or water vapour line shape factor, $N"_D(f)$ is the dry continuum, and the summations extend over all the spectral lines in tables A.1,A.2, A.3 and A.4

$$N''_{Oxygen}(f) = \Sigma_{i(oxygen)} S_i F_i + N''_D(f) \tag{A.1}$$

$$N''_{WaterVapour}(f) = \Sigma_{i(WaterVapour)} S_i F_i \tag{A.2}$$

The strength S_i is on equation A.3, where ρ is the dry air pressure (hPa), the e is the water vapour partial pressure (hPa), θ is given by $300/T$ and T is the temperature in kelvin.

$$\begin{aligned} S_i &= a_1 \times 10^{-7} \rho \theta^3 exp[a_2(1-\theta)] \text{ for oxygen} \\ &= b_1 \times 10^{-1} e \theta^{3.5} exp[b_2(1-\theta)] \text{ for water vapour} \end{aligned} \tag{A.3}$$

The line shape factor F_i is given by equation A.4, where f is signal frequency, the f_i is the oxygen or water vapour line frequency, Δf is the width of the line, on equations A.5 and A.6, and the δ is a correction factor that arises due to interference effects in oxygen lines, on equation A.7

$$F_i = \frac{f}{f_i}\left[\frac{\Delta f - \delta(f_i - f)}{(f_i - f)^2 + \Delta f^2} + \frac{\Delta f - \delta(f_i + f)}{(f_i + f)^2 + \Delta f^2}\right] \tag{A.4}$$

$$\begin{aligned}\Delta f &= a_3 \times 10^{-4}(\rho\theta^{0.8+a_4} + 1.1e\theta) \text{ for oxygen} \\ &= b_3 \times 10^{-4}(\rho\theta^{b_4} + b_5 e\theta^{b_6}) \text{ for water vapour}\end{aligned} \tag{A.5}$$

$$\begin{aligned}\Delta f &= \sqrt{\Delta f^2 + 2.25 \times 10^{-6}} \text{ for oxygen} \\ &= 0.535\Delta f + \sqrt{0.217\Delta f^2 + \frac{2.1316 \times 10^{-12} f_i^2}{\theta}} \text{ for water vapour}\end{aligned} \tag{A.6}$$

$$\begin{aligned}\delta &= (a_5 + a_6\theta) \times 10^{-4}(\rho + e)\theta^{0.8} \text{ for oxygen} \\ &= 0 \text{ for water vapour}\end{aligned} \tag{A.7}$$

The dry air continuum arises from the non-resonant Debye spectrum of oxygen below 10 GHz and a pressure-induced nitrogen attenuation above 100 GHz and is given by equation A.8, where d is the width parameter for the Debye spectrum on equation A.9.

$$N"_D(f) = f\rho\theta^2\left[\frac{6.14 \times 10^{-5}}{d\left[1 + \left(\frac{f}{d}\right)^2\right]} + \frac{1.4 \times 10^{-12}\rho\theta^{1.5}}{1 + 1.9 \times 10^{-12} f^{1.5}}\right] \tag{A.8}$$

$$d = 5.6 \times 10^{-4}(\rho + e)\theta^{0.8} \tag{A.9}$$

Table A.1: Spectroscopic data for oxygen attenuation

f0	*a1*	*a2*	*a3*	*a4*	*a5*	*a6*
50.474214	0.975	9.651	6.690	0.0	2.566	6.850
50.987745	2.529	8.653	7.170	0.0	2.246	6.800
51.503360	6.193	7.709	7.640	0.0	1.947	6.729
52.021429	14.320	6.819	8.110	0.0	1.667	6.640
52.542418	31.240	5.983	8.580	0.0	1.388	6.526
53.066934	64.290	5.201	9.060	0.0	1.349	6.206
53.595775	124.600	4.474	9.550	0.0	2.227	5.085
54.130025	227.300	3.800	9.960	0.0	3.170	3.750
54.671180	389.700	3.182	10.370	0.0	3.558	2.654
55.221384	627.100	2.618	10.890	0.0	2.560	2.952
55.783815	945.300	2.109	11.340	0.0	–1.172	6.135
56.264774	543.400	0.014	17.030	0.0	3.525	–0.978
56.363399	1331.800	1.654	11.890	0.0	–2.378	6.547
56.968211	1746.600	1.255	12.230	0.0	–3.545	6.451
57.612486	2120.100	0.910	12.620	0.0	–5.416	6.056
58.323877	2363.700	0.621	12.950	0.0	–1.932	0.436
58.446588	1442.100	0.083	14.910	0.0	6.768	–1.273
59.164204	2379.900	0.387	13.530	0.0	–6.561	2.309
59.590983	2090.700	0.207	14.080	0.0	6.957	–0.776
60.306056	2103.400	0.207	14.150	0.0	–6.395	0.699
60.434778	2438.000	0.386	13.390	0.0	6.342	–2.825
61.150562	2479.500	0.621	12.920	0.0	1.014	–0.584
61.800158	2275.900	0.910	12.630	0.0	5.014	–6.619
62.411220	1915.400	1.255	12.170	0.0	3.029	–6.759
62.486253	1503.000	0.083	15.130	0.0	–4.499	0.844
62.997984	1490.200	1.654	11.740	0.0	1.856	–6.675
63.568526	1078.000	2.108	11.340	0.0	0.658	–6.139
64.127775	728.700	2.617	10.880	0.0	–3.036	–2.895
64.678910	461.300	3.181	10.380	0.0	–3.968	–2.590
65.224078	274.000	3.800	9.960	0.0	–3.528	–3.680
65.764779	153.000	4.473	9.550	0.0	–2.548	–5.002
66.302096	80.400	5.200	9.060	0.0	–1.660	–6.091
66.836834	39.800	5.982	8.580	0.0	–1.680	–6.393
67.369601	18.560	6.818	8.110	0.0	–1.956	–6.475
67.900868	8.172	7.708	7.640	0.0	–2.216	–6.545
68.431006	3.397	8.652	7.170	0.0	–2.492	–6.600
68.960312	1.334	9.650	6.690	0.0	–2.773	–6.650
118.750334	940.300	0.010	16.640	0.0	–0.439	0.079

Table A.2: Spectroscopic data for oxygen attenuation (continuation)

f0	*a1*	*a2*	*a3*	*a4*	*a5*	*a6*
368.498246	67.400	0.048	16.400	0.0	0.000	0.000
424.763020	637.700	0.044	16.400	0.0	0.000	0.000
487.249273	237.400	0.049	16.000	0.0	0.000	0.000
715.392902	98.100	0.145	16.000	0.0	0.000	0.000
773.839490	572.300	0.141	16.200	0.0	0.000	0.000
834.145546	183.100	0.145	14.700	0.0	0.000	0.000

Table A.3: Spectroscopic data for water vapour attenuation

f0	*b1*	*b2*	*b3*	*b4*	*b5*	*b6*
22.235080	.1079	2.144	26.38	.76	5.087	1.00
67.803960	.0011	8.732	28.58	.69	4.930	.82
119.995940	.0007	8.353	29.48	.70	4.780	.79
183.310087	2.273	.668	29.06	.77	5.022	.85
321.225630	.0470	6.179	24.04	.67	4.398	.54
325.152888	1.514	1.541	28.23	.64	4.893	.74
336.227764	.0010	9.825	26.93	.69	4.740	.61
380.197353	11.67	1.048	28.11	.54	5.063	.89
390.134508	.0045	7.347	21.52	.63	4.810	.55
437.346667	.0632	5.048	18.45	.60	4.230	.48
439.150807	.9098	3.595	20.07	.63	4.483	.52
443.018343	.1920	5.048	15.55	.60	5.083	.50
448.001085	10.41	1.405	25.64	.66	5.028	.67
470.888999	.3254	3.597	21.34	.66	4.506	.65
474.689092	1.260	2.379	23.20	.65	4.804	.64
488.490108	.2529	2.852	25.86	.69	5.201	.72
503.568532	.0372	6.731	16.12	.61	3.980	.43
504.482692	.0124	6.731	16.12	.61	4.010	.45
547.676440	.9785	.158	26.00	.70	4.500	1.00
552.020960	.1840	.158	26.00	.70	4.500	1.00
556.935985	497.0	.159	30.86	.69	4.552	1.00
620.700807	5.015	2.391	24.38	.71	4.856	.68
645.766085	.0067	8.633	18.00	.60	4.000	.50
658.005280	.2732	7.816	32.10	.69	4.140	1.00
752.033113	243.4	.396	30.86	.68	4.352	.84
841.051732	.0134	8.177	15.90	.33	5.760	.45
859.965698	.1325	8.055	30.60	.68	4.090	.84
899.303175	.0547	7.914	29.85	.68	4.530	.90
902.611085	.0386	8.429	28.65	.70	5.100	.95
906.205957	.1836	5.110	24.08	.70	4.700	.53

Table A.4: Spectroscopic data for water vapour attenuation (continuation)

f0	*b1*	*b2*	*b3*	*b4*	*b5*	*b6*
916.171582	8.400	1.441	26.73	.70	5.150	.78
923.112692	.0079	10.293	29.00	.70	5.000	.80
970.315022	9.009	1.919	25.50	.64	4.940	.67
987.926764	134.6	.257	29.85	.68	4.550	.90
1 780.000000	17506.	.952	196.3	2.00	24.15	5.00

A.2

To be able to calculate the pressure and temperature of the atmosphere at 2.5 Km of altitude, there are the need to convert the altitude (geometric height), h, to a geopotential height, h', through equation A.10.

$$h' = \frac{6356.766h}{6356.766 + h} \tag{A.10}$$

At an altitude of 2.5 Km the geopotential height is around 2.499 Km, therefore the pressure $P(h')$ and the temperature $T(h')$ is given by equations A.11 and A.12.

$$P(h') = 1013.25 \left[\frac{288.15}{288.15 - 6.5h'} \right]^{-\frac{34.1632}{6.5}} \tag{A.11}$$

$$T(h') = 288.15 - 6.5h' \tag{A.12}$$

B

Appendix B

A map of R0.01, the annual rainfall rate exceeded for 0.01% of an average year, is shown in figure B.1.

Figure B.1: Rainfall rate exceeded for 0.01% of an average year